This is to certify that the

thesis entitled
"A Study of the Optical Absorption Differences
Spectra Attributed to the S1-S2 Transition
in the Oxygen Evolving Complex of Green Plants"

presented by

Dwight Lillie

has been accepted towards fulfillment
of the requirements for

Ph.D degree in Chemistry

Gerald T. Babcock
Major professor

Date August 3, 1988.

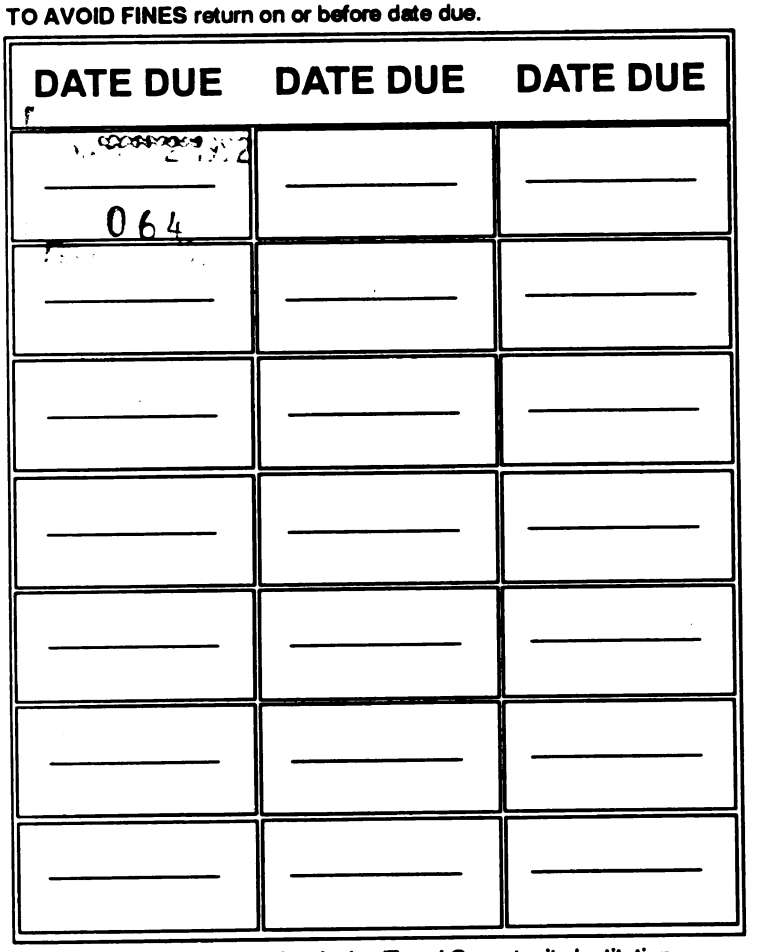

A STUDY OF THE OPTICAL ABSORPTION DIFFERENCE SPECTRA ATTRIBUTED TO THE S1 --> S2 TRANSITION IN THE OXYGEN EVOLVING COMPLEX OF GREEN PLANTS

By

Dwight Henry Lillie

A DISSERTATION

Submitted to
Michigan State University
in partial fulfillment of the requirements
for the degree of

DOCTOR OF PHILOSOPHY

Department of Chemistry

1989

ABSTRACT

A STUDY OF THE OPTICAL ABSORPTION DIFFERENCE SPECTRA ATTRIBUTED TO THE S_1 --> S_2 TRANSITION IN THE OXYGEN EVOLVING COMPLEX OF GREEN PLANTS

By

Dwight Henry Lillie

The optical absorption difference spectrum arising from the S_1 --> S_2 transition of the Oxygen Evolving Complex (OEC) in purified Photosystem II membranes from green plants has been studied under controlled conditions in which the required anion cofactor, Cl^-, has been deleted and reconstituted with a series of monovalent anions, OH^-, Cl^-, Br^-, and NO_3^-. The observed asymmetric absorption difference band, does not undergo the substantial changes expected if it arose from a charge transfer from the anion ligand to the Mn of the OEC, and it is therefore proposed that the absorption band arises from an oxygen ligand to the Mn.

In Dedication to

Gladys Crose,

my grandmother, who passed away the 24th of January, 1988. Her life was a testament of the love she had for her children and grandchildren. I will never forget the lessons she taught me, and in particular the value of hard work and the joy there is to be found in pursuing one's ideals.

ACKNOWLEDGEMENTS

There have been many people who have helped contribute to my completion of this Ph.D. program, and I wish to thank them here.

First, and most of all, I wish to express my deepest thanks and love to my wife, Carolynn. Her patience, understanding, and unselfish love allowed me to accomplish this goal. Our children, Curtis, Erin, and Megan, helped me to remember that there is indeed life after graduate school. I also want to thank my parents, my brother Richard, and my sister Beth, for the encouragement and support I received.

To my mentor and friend, Professor Jerry Babcock, who provided me with an environment to discover a real joy for science and who was willing to allow his students broad latitude in their research, I am indeed grateful.

I relied heavily upon the expertise of the staff in the Electronics, Machine, and Glass Shops. In particular, Marty Rabb, Ron Haas, Scott, and Tom Clarke provided far more assistance and encouragement than required. Their dedication to teaching graduate students the fine points of electronics, "...here, just hold on to this end for a moment while I bring up the power...," guarantees quick studies.

The contributions of another, Dr. Tom Atkinson, who quickly won me to the philosophy, "If you have to do it more than once - I'd rather teach a computer to do it...," cannot be understated. It was only been through his influence and teaching that I was able to produce the software and hardware systems described within as well as to appreciate the inherent advantages of taking backups, "...well, this is trashed - you've got a backup tape, don't you?"

Juan Lopez Garriaga, Chris Bender, Matt Espe, Harold Fonda, Bob Kean, Bill Buttner, Tony Oertling, Pat Callahan, Margie, Carol, and other members of the laboratory - thank you for the friendship, the willingness to pitch in, the late night bull-sessions, and the beer. It was fun, wasn't it...wasn't it??

TABLE OF CONTENTS

LIST OF TABLES

LIST OF FIGURES

ABBREVIATIONS & SYNONYMS

ADC	Analogue to Digital Converter
AIM-65	Evaluation computer system using an 8-bit 6502 microprocessor.
ATP	Adenosine Triphosphate
bit	Smallest piece of information in a number system of base 2
CPU	Central Processing Unit
D	Symbolic identity associated with a kinetic species responsible for Signal II, slow (II_s), and presumed to be of the same type as Z.
DCBQ	2,5 (or 2,6)-Dichloro-p-benzoquinone. Only 2,5-DCBQ was used in the work reported here.
DCMU	3-(3,4 Dichlorophenyl)-1,1 dimethylurea
DEC	Digital Equipment Corporation
DMA	Direct Memory Access
DPC	Diphenylcarbazide
EGTA	Ethyleneglycol-bis-(beta-aminoethyl ether)-N,N,N',N'-tetraacetic Acid
EPR	Electron Paramagnetic Resonance
EXAFS	Extended X-ray Absorption Fine Structure
g4.1	An EPR signal that is centered at g = 4.1 and considered to be one of the conformers of the S^]2\] state of the Oxygen Evolving Complex.
Hepes	N-2-Hydroxylethyl Piperazine-N'-2-Ethanosulfonic Acid.
HLL	High Level Language(s)
IBM	International Business Machines
ISR	Interrupt Service Routine
Kb	Kilobyte, actually 2^{11} or 1024 bytes.
LHC	Light Harvesting Complex

M
M
M
M
M
N
C
C
P
P
P
P
P
Q
R
R
R
Π_4
Π_6
Π_{ff}
SM
task
TCP

Mb	Megabyte, actually 2^{20}.
Mes	4-Morpholineethanesulfonic Acid
MIMD	Multiple Instruction, Multiple Data
MMU	Memory Management Unit
MPU	(see CPU)
NADPH	Nicotinamide Adenoine Dinucleotide Phosphate
OEC	Oxygen Evolving Complex
OS	Operating System
PC	Personal Computer, often used meaning IBM's interpretation of personal computer.
PDP-11	Program Data Processor, 16-bit minicomputer manufactured by DEC.
PMT	Photomultiplier Tube
PPBQ	phenyl-*p*-benzoquinone
PSII	Photosystem II
Q-BUS	The backplane used in the PDP-11 computer systems.
RC	Reaction Center
RSX-11	Real-time System Executive, a multiuser, multitasking operating system for the DEC PDP-11 systems supporting MMU.
RT-11	Real Time operating system, a single user operating system for the DEC PDP-11 systems. There are two versions of the system, RT-11SJ, 'SJ' for single job, and RT-11FB, 'FB' for foreground-background.
II_f	'Signal II, fast.' Fast EPR kinetic signal assigned to Z^+, detected in samples inhbited in the evolution of O_2.
II_s	'Signal II, slow.' Slow EPR kinetic signal associated with D^+.
II_{vf}	'Signal II, very fast.' Very fast EPR kinetic signal assigned to Z^+, detected in samples which can evolve O_2.
SIMD	Single Instruction, Multiple Data
task	Term referring to an executable computer program.
TCP	Task Control Block

Tris

VAX

VMS

Y_D

Y_Z

Z

Tris	Tris(hydroxymethyl)aminomethane
VAX-11	Virtual Machine Architecture, DEC's 32-bit minicomputer.
VMS	Virtual Memory System for the DEC VAX-11 computer family.
Y_D	Symbolic identity which relates the kinetic species, D, with a clearly identified Tyrosine.
Y_Z	Symbolic identity which relates the kinetic species, Z, with an impled chemical identity, Tyrosine.
Z	Symbolic identity for a kinetic species implicated in electron transfer between the Reaction Center and the Oxygen Evolving Complex.

CHAPTER 1

1.1. INTRODUCTION

Photosynthetic organisms couple one electron photochemistry to two and four electron transport, and generate intermediate species with large reductive and oxidative potentials. The reductive equivalents are used initially for the production of 'primary' biochemical energy in the form of ATP (Adenosine Triphosphate) and NADPH (Nicotinamide Adenosine Dinucleotide Phosphate). The oxidative equivalents are toxic waste products from a biochemical viewpoint, and are duly disposed of via a water oxidation process. Water oxidation is a four step process (see Reaction 1.9), and the biochemical catalysis site, otherwise known as the Oxygen Evolving Complex (OEC), must be able to acquire and stabilize four oxidative equivalents until dioxygen is stably formed and evolved. Upon the evolution of oxygen, the storage site is reset for another four electron process. The site implicated for catalysis is a tetranuclear cluster of manganese atoms, the structure of which is not yet known. Several polypeptide and ionic cofactors have been identified as being responsible for establishing and maintaining the local environment(s) necessary for oxygen evolution. Largely thought to be intractable, the catalysis site has recently been proving to be amenable to biochemical and biophysical techniques. This has been driven by the development of biological preparations that have become increasingly resolved in terms of their composition and purity.

1.2. PHOTOSYNTHESIS: AN OVERVIEW

1.2.1. Basic Equation

Photosynthesis refers to the light to chemical energy conversion processes found in plants (eukaryotic organisms) and also in photosynthetic bacteria (prokaryotic organisms). The net sum of all relevant processes in higher plants can be represented as:

$$6CO_2 + 6H_2O \rightarrow C_6H_{12}O_6 + 6O_2 \qquad (1.1)$$

Early in this century photosynthesis was described in a similar fashion. Centuries had been required to reach this point, and many more years remained before the reactions underlying this equation could be properly ferreted out and placed into context. Blackman (1905), with little in the way of experimental evidence, first hypothesized that photosynthesis involved two set of reactions. One set consisted of a series of light dependent reactions that yielded photochemical products for use by the second set. This second set of reactions contained no direct dependence upon light other than the photochemical products, and were thus referred to as the dark reactions. These suggestions made by Blackman; however, remained largely speculation until Van Niel, in the 1920s and 1930s, began systematic investigations that firmly laid the foundations for Equation 1.1 and the subsequent work of Hill that supported the idea of light and dark dependent reactions.

1.2.2. Van Niel's Hypothesis

In 1941 Van Niel (1941) noted that, after comparing hydrogen donors for bacteria and higher plants, molecular oxygen released from plants must arise from water and not from carbon dioxide, as widely believed. In the case of

bacte

place

plants

1 2 3

1 2 3

reacti

chara

isolat

has lo

demo

tissue

signi

respo

strong

produ

molec

be ex

1 2 3

"Mi

Some

bacteria, which can not oxidize water, succinate or hydrogen sulfide was used in place of water as the reducing substrate. The underlying process in bacteria and plants was presumed the same and could be generalized to:

$$H_2A + CO_2 \text{ ---> } (CH_2O) + H_2 + 2A \qquad (1.2)$$

1.2.3. Determination of the Substrate for Evolved Oxygen

1.2.3.1 The Hill Reaction

Confirming the existence and independence of two separate sets of reactions, Hill (1939) demonstrated oxygen evolution from 'osmotically shocked' chloroplasts, subcellular components containing the photosynthetic machinery isolated from leaves, given addition of an external oxidant. These chloroplasts had lost the ability to assimilate carbon dioxide, and so the original purpose of demonstrating complete photosynthesis in a subcellular component of plant tissue was defeated; however, the retention of oxygen evolution proved more significant. Not only did this establish the independence of two sets of reactions responsible for oxygen evolution and carbon dioxide assimilation, but also it strongly indicated that water, not carbon dioxide, was the substrate in the production of oxygen. These experiments, demonstrating the production of molecular oxygen, and the reduction of an exogenous reductant, have come to be known as the 'Hill-Reaction.'

1.2.3.2 Controversy Between CO_2 and H_2O

The concept of water oxidation at this time was not novel. Ruben *et al.* 1941) illuminated *Chlorella* in oxygen labeled water and observed that the content of the oxygen evolved was likewise labeled, and it was also shown that

the content of the labeled oxygen evolved was independent of the content of oxygen labeled carbonate. This was objected to on the grounds of oxygen exchange by Warburg (1964). He had found in 1960 that bicarbonate was required for oxygen evolution (Warburg and Luttgens, 1960). This exchange is apparently facilitated by low pH and carbonic anhydrase, conditions not well controlled in the original experiments of Ruben *et al.* (1941).

It has only been recently that similar isotopic experiments (Stamler and Radmer, 1975) using ^{18}O-labelled water in algae acceptably confirmed this observation. In these experiments the algae samples showed no carbonic anhydrase activity and the pH was regulated to minimize mixing. Ironically, later experiments by Radmer (discussed later) regarding intermediates in the water oxidation process have also fallen prey to the same type of objections.

1.2.4. The Z-scheme

It was not until the 1960s that this evidence could be interpreted properly, which is not to say that the research carried on in the intervening years was fruitless. Those intervening years laid the groundwork necessary for acceptance of a new concept. Hill and Bendall (1960) proposed that the light dependent reactions, those established as responsible for water oxidation, consisted of two separate photochemical reaction centers operating in series driving photosynthetic electron transport, and represented, in a fashion similar to Figure 1.3, the 'Z-scheme.'

Duysens *et al.* (1961) further extended the distinguishability of the reaction centers by using light of selective wavelengths to control the oxidation and reduction of the cytochrome that is in the electron transport chain between the two photosystems (see Figure 1.3). Long wavelength light selectively excited Photosystem I and led to the oxidation of cytochrome. Short wavelength light

see
of
dim

1.3.

par
com
Ele
tra
ele
com
pc
tra
co

exc
Ass
has be
es
ori
top

ori
tra

selectively excited Photosystem II (PSII) and led to the reduction of the oxidized cytochrome. Addition of inhibitors such as DCMU (3-(3,4 Dichlorophenyl)-1,1 dimethylurea), blocked reduction by Photosystem II.

1.3. Current Model: Electron Transport

It has now been fairly well established that electron transport in higher plants from H_2O to $NDAP^+$ involved three membrane protein complexes. These complexes interact with each other via small carriers in a serial fashion. Electrons are extracted from H_2O by the Photosystem II complex and transported to the b_6-f complex by a plastoquinone carrier. Plastocyanin carries electrons from the b_6-f complex to the Photosystem I complex. The Photosystem I complex in turn reduces $NADP^+$. The molecular components making up these complexes, when they are known, plotted against their respective redox midpoint potentials resemble a 'Z' as shown in Figure 1.3 and this diagram of the electron transport chain has become known as the 'Z-scheme.' As the molecular components transport electrons they alternately undergo reduction and oxidation.

Since the 1960s the Z-scheme has remained relatively unchanged except for the addition of new components as they have been identified. Association of sections of the electron transport chain with biochemical structures has been made, and an orientation with respect to membrane topology has been established. Figure 1.3 represents a considerable improvement in detail over the original. Figure 1.4 displays the Z-scheme components in a model membrane topology.

Chloroplasts possess a definite 'inside' and 'outside' orientation. This orientation allows the free energy released during photosynthetic electron transfer, in the form of a buildup of the free proton concentration, $[H^+]$, in the

inner aqueous enclosure, to be partially conserved by the phosphorylation of ADP to ATP, catalyzed by the ATP synthase.

To complete the picture we shall continue to flesh out the scheme, but the chronological detailing will be dropped, and the emphasis will lie with Photosystem II, the system coupled to the OEC. A more detailed historical account can be found by Rabinowitch (1945) and Hill (1972).

1.3.1. The Reaction Center

The reaction centers in Photosystems I and II are responsible for light gathering and initial quasi-stable charge separation. Associated with each reaction center is a core set of 50 chlorophylls, and somewhat more loosely is a larger set of 200 to 250 chlorophylls in a protein pigment complex called the light harvesting complex (LHC) or the antenna complex. These chlorophylls are coupled electronically to each other and to the reaction center to form a potential sink at the reaction center. Light absorption by the LHC results in a coherent exciton packet that is funneled into the reaction center for photochemistry. A fairly detailed physical description of such antenna complexes has been provided by Knox (1977); also see Pearlstein (1982) and Parson and Ke (1982) for somewhat more recent treatments.

The reaction center of higher plants is presumably a chlorophyll dimer 'special pair' that is electronically coupled to chemical groups directly, and indirectly facilitates initial electron transfer from the excited state manifold(s) of the special pair. In green plants and algae there are two such reaction centers and are referred to as P_{680} and P_{700} respectively for Photosystems II and I. The 'P' stands for pigment and the subscripted numbers reflect the absorption maximum for the pigment (Clayton, 1980). A structural analogy between green plants and bacteria may be drawn from crystallographic data from the bacterium

Rhodopseudomonas viridis (Deisenhofer, *et al.*, 1984. See Figure 1.5). In the bacterial case, the special pair, known as P_{870}, consists of two bacteriochlorophylls forming an electronic dimer. Nearby, on each side, forming two branches, are two other bacteriochlorophylls. Continuing down the branches are two more bacteriopheophytins, and terminating the branches are two quinones. These branches are referred to as M and L branches of the reaction center, and possess a general C_2 symmetry. Despite the structural symmetry of the two branches there is evidence that suggests the L branch is preferred over the M branch for electron transfer by a factor greater than 5 (Breton *et al.*, 1986). Recent theoretical calculations have shown that the location of polar groups are sufficient to enforce this observed unidirectionality of electron transfer (Michel-Beyerle, 1988).

While this structural analogy between higher plants and bacteria appears to be generally valid, it is not without problems. The special pair in bacteria lies perpendicular to the inside membrane surface. In green plants, however, there is experimental support for the special pair to be positioned parallel to the membrane surface (see Rutherford, 1985 and Breton and Vermeglio, 1982).

The initial charge separation results in the formation of an oxidized pigment, P^+. Pheophytin, in the case of green plants, or bacteriopheophytin, in the case of bacteria, is reduced in a time scale of 10^{-12}s. In turn, it is oxidized and the primary quinone acceptor is reduced in a time scale of 10^{-9}s. P^+ can either be reduced by its normal physiological donor, Z, and the reduced quinone acceptor will be oxidized or P^+ can undergo a back reaction with the reduced quinone acceptor. The first scenario is preferred in untreated systems. Alteration of one or more of the components in the electron transport chain can shift towards a preference for the back reaction. As an example, deactivation of the Oxygen Evolving Complex shown in Figure 1.3, results in an increased lifetime of

Z^+, the physiological donor to P_{680}. If Z is still oxidized when P_{680}^+ is next oxidized then only the back reaction with the acceptor is reasonable. P_{680}^+ has been difficult to study because of the multiplicity of kinetic phases that it exhibits. In untreated systems it becomes reduced in tens of nanoseconds. In treated systems it develops several micro- and milli-second decay times.

1.3.2. Reducing Side of Photosystem II

The secondary electron acceptor of Photosystem II, the primary acceptor being pheophytin (plants) or bacteriopheophytin (bacteria), is a plastoquinone, referred to commonly as Qa. Figure 1.5 shows its bacterial analogue as being the terminal quinone of the L branch. Upon reduction, the charge separation spans the width of the membrane, ~40Å.

Qa is located in a covalently bonded site and in close proximity is another quinone binding site, Qb. The Qb site, unlike Qa, is labile for quinones in the plastoquinone (oxidized) and plastohydroquinone (reduced) forms, see Figure 1.6. It is in fact lost during isolation as demonstrated in Figure 1.5. An iron in the Fe(II) state supports, and, as discussed below, mediates electron transport between Qa and Qb by altering the equilibrium distribution.

The interaction between Qa and Qb serves as the interface between one electron photochemistry and two electron transport chemistry. Two turnovers are required as shown in Reactions 1.3 and 1.4 before the Qb site is recharged, Reaction 1.5. Note that the second turnover is only possible when the reaction center is 'open', Qb is reduced and Qa oxidized.

$$QaQb \xrightarrow{h\nu} Qa^-Qb \quad <==> \quad QaQb^- \qquad (1.3)$$

$$QaQb^- \xrightarrow{h\nu} Qa^-Qb^- \quad ---> \quad QaQb^{2-} \qquad (1.4)$$

co
abs
bee
tra
ma
Lan
1.3.2
Qa ic
dem
meas
J et a
Cp2-
the co
stabi
prese
Bayes
stabi
1.3.3
bandpa
uncerta

$$QaQb^{2-} \xrightarrow{2H^+} QaQbH_2 \xrightarrow{PQ} QaQb + PQH_2 \qquad (1.5)$$

As will be discussed in more detail in Chapter 4, it is this binary cycle coupled with the contribution of anionic radicals in the near UV and in the blue absorption region that have led to disagreements over procedures that have been used to account for and remove absorption difference spectral contributions that arise solely from the reducing side. Anionic radicals have absorption maxima in the near UV at 320 nm and in the blue at 440-450 nm (Bensasson and Land, 1973).

1.3.2.1 Iron Mediation of Reducing Side Electron Transport.

It was originally thought that iron removal blocked electron transport from Qa to Qb, Parson (1978) and Blankenship and Parson (1978). It has been demonstrated, however, that removal of the iron only appears to reduce the measured efficiency of electron transfer between Qa and Qb by 37% (Debus, R. J. *et al.*, 1986). Reconstitution with divalent transition metals such as Mn^{2+}, Co^{2+}, Ni^{2+}, Cu^{2+}, and Zn^{2+} as well as Fe^{2+} can restore rates to within 10% of the control rates. An interesting aspect of the work of Debus *et al.* (1986) is the stability of the Qa semiquinone with respect to the fully reduced form in the presence and absence of the supporting divalent transition metals. The role played by the metal appears to stabilize the charge separation indirectly by stabilizing the semiquinone form.

1.3.3. The Secondary Donor, Z

Until recently the number of components directly involved in the electron transfer pathway between the OEC and the oxidized reaction center has been uncertain. Since the mid-70s there has been reliable spectroscopic detection of

the redox reactions of the reaction center and its donor(s). The interpretation, though, has been conflicting and has led to differing models. A fairly complete summarization of the plausible models was done by Bouges-Bocquet (1980).

Experiments reported recently, time resolved EPR spectra (Hoganson and Babcock, 1988a), *in vivo* deuteration (Barry and Babcock, 1987), and time resolved optical UV spectra (Gerken *et al.*, 1988), appear to confirm the presence of only one intermediate involved in direct electron transport between the Oxygen Evolving Complex and the reaction center.

1.3.3.1 Spectroscopic and Kinetic Characterization of Z.

Signal II, an EPR signal with an isotropic g = 2.00, was observed as early as 1956 by Commoner *et al.* (1956). Babcock and Sauer (1973) and Babcock *et al.* (1976) associated this Signal II with the Z^+ species, the donor to P_{680}. Since then it has been generally recognized that there are three forms of Signal II, and two distinct molecular species giving rise to the Signal IIs. Signal II_s is a long-lived, slowly decaying signal, and is considered to arise from a molecular species referred to as D^+.

Signal II_f, 'f' meaning 'fast', arising from Z^+, is the direct donor to P_{680} in preparations in which the capability to evolve oxygen has been inhibited. Signal II_f, first observed in thylakoids depleted of manganese (Babcock and Sauer, 1975), has been observed to closely parallel the reduction of P_{680}^+ in the similarly treated samples (Boska *et al.*, 1983, and Weiss and Renger, 1986).

Signal II_{vf}, 'vf' meaning 'very fast', arising from Z^+, is the direct donor to P_{680} in preparations retaining their oxygen evolving capacity. It was reported by Blankenship *et al.* (1975) and Babcock *et al.* (1976). The original characterization of II_{vf} contained a low resolution time resolved spectrum using spinach thylakoids. In preparations that have not been inhibited in oxygen

evolution the primary reductant phases of P_{680}^+ occur in the nanosecond time regime (Mauzerall, 1972, and Van Best and Mathis, 1978), and they report that the rise time of Signal II_{vf} closely parallels the reduction time. Recently the time resolved spectrum of II_{vf} has been reproduced by Hoganson and Babcock (1988b), and their results confirm the similarity between II_f and II_{vf}.

1.3.3.2 Electron Transfer Models for Z

The most widely accepted model places only one component between the OEC and the reaction center:

$$\text{OEC} \quad \text{---}> \quad \text{Z} \quad \text{---}> \quad P_{680} \qquad (1.6)$$

Witt and co-workers (see Schlodder *et al.*, 1984, and Brettel *et al.*, 1984), have argued strongly, largely on the basis of the observed multiple kinetic phases in their optical measurements, for multiple species arranged in serial or parallel fashion:

$$\text{OEC} \text{---}> \quad \text{D1} \quad \text{---}> \quad \text{D2} \quad \text{---}> \quad \text{Z} \text{---}> \quad P_{680} \qquad (1.7)$$

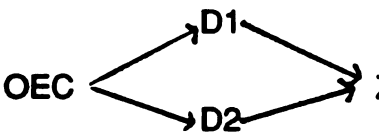

$$\text{---}> \quad P_{680} \qquad (1.8)$$

Where 'D1' and 'D2' are respectively for donor 1 and donor 2. Witt's group has recently recanted these models (Gerken *et al.*, 1988), however, in light of the EPR evidence published by Hoganson and Babcock (1988a) and direct evidence of the chemical identity of an intermediate (Barry and Babcock, 1987, and Debus *et al.*, 1988)

As of yet there is only spectroscopic evidence for the one donor species, Z, linking the OEC to the reaction center, whether it is the primary reductant to P_{680} has yet to be shown. It has been recently reported, however, by Witt's group (Gerken *et al.*, 1987) that the primary donor to P_{680}^+ has been detected optically in uninhibited oxygen evolving samples. The reported extinction coefficients of 6000-8000 $\underline{M}^{-1}cm^{-1}$ at 260 nm agree with those reported for optically detected Z^+ in inhibited samples by Dekker (1984a).

1.3.3.3 Problems with Chemical Identity of Z

Early extraction and reconstitution experiments of isotopically labelled plastoquinone by Kohl and Wood (1969) were correlated with the subsequent loss of Signal II_S, the EPR signal originating from D^+, and led to the tentative conclusion that D^+ (and hence Z^+) was a plastoquinone cation. Other evidence supported this as well. Wood and Bendall (1976) reported a high positive midpoint potential for a QH_2^+/QH_2 redox couple, O'Malley and Babcock (1984) and O'Malley *et al.* (1984) analyzed experimental EPR Signal II data, EPR model compound data, and performed computer simulations of the EPR spectra. This all reasonably supported the plastoquinone hypothesis based on calculated ring spin densities. Optical evidence from Diner and de Vitry (1984) and Dekker *et al.* (1984a) all suggested that D and Z was a quinone.

Unfortunately, several severe problems remained with this hypothesis that could not easily be reconciled. (1) The experimental g_{iso}, 2.0046, was consistently too high for *in vitro* cation plastoquinones, the g-value ranges for these are 2.0034 to 2.0038 (Sullivan and Bolton, 1968). (2) The conditions required for model simulation of Signal II, 12$\underline{N}$ sulfuric acid, was considered by many to be too severe for biological systems to provide. (3) The experiments of Kohl and Wood (1969) could not be reproduced in any other laboratory, and (4)

quantification experiments of plastoquinone levels by de Vitry *et al.* (1986), were unable to find enough plastoquinone-9 in Photosystem II particles isolated from *Chlamydomonas reinhardtii* to account for D and Z being plastoquinones. This was confirmed by Takahashi and Katoh (1986).

1.3.3.4 Tyrosine as Z

Definitive identification of Signal II_S, D^+, as a tyrosine on the D2 polypeptide has been reported by Barry and Babcock (1987). Two sets of *in vivo* deuteration experiments were involved. First, the methyl group of quinones were deuterated. Mass spectral data provided proof of the deuteration and the EPR spectra showed no discernible change in D^+. The second set of experiments deuterated tyrosine. Again, mass spectral data provided proof of deuteration, and the EPR spectra showed a reduction in linewidth as would be expected if the characteristic Signal II spectra were indeed arising from tyrosine.

Debus and Barry (Debus *et al.*, 1988) were able to precisely locate the position of D by reasoning from the facts that D^+ is a tyrosine, spectral evidence indicating Z^+ is the same molecular species, and that Z may be located on the D1 polypeptide and D is located on D2 (iodination experiments by Takahashi *et al.*, 1986, and Ikeuchi and Inoue, 1987). Trebst (1986) had published the amino acid sequence and suggested folding patterns for the D1 and D2 polypeptides; examination revealed two conserved tyrosines. Change of Tyr-160 on D2 to phenylalanine by using site directed mutagenesis resulted in photosynthetic growth but no characteristic Signal II_S. Assuming the symmetry hypothesis holds up, then a corresponding residue on D1, Tyr-161, is Z.

As a side note, this recent identification of D and (possibly) Z as tyrosines has prompted Hoganson and Babcock (1988a) to modify the nomenclature conventions regarding Signal II. The single letter abbreviation of

tyros

and

D an

folde

whet

1.4.

1966

O_2 e

supp

was

exis

rese

with

that

mar

com

ed to

EPR

than

1.4

end

com

tyrosine is 'Y,' and is now used as the primary identifier. The subscripts 's', 'vf', and 'f' are dropped. References to Z and Z^+ become Y_Z and $Y_Z{}^+$. References to D and D^+ become Y_D and $Y_D{}^+$. The spectral references to II_{vf} and II_f are now folded into Y_Z, and depends upon the context of the discussion to determine whether it is uninhibited or inhibited conditions.

1.4. The Oxygen Evolving Complex (OEC)

As early as 1969 phenomological evidence had been gathered by Joliot (1968) and Kok *et al.* (1970) that gave rise to an elegant and abstract model of O_2 evolution. This model is represented in Figure 1.1, and an example of supporting experimental evidence is given Figure 1.2. Until 1981 the situation was frustrating because the S-state model proposed by Kok suggests the existence of discrete, intermediate states in the process of oxidizing water, and researchers were faced with problem of the apparent inability of the OEC to withstand direct attempts to modify its behavour without complete dissolution.

At present, however, biochemical techniques have been made available that not only provide more highly refined samples, but also allow selective manipulation of the environment surrounding the OEC in terms of polypeptide composition and ionic cofactors. This refinement in biochemical techniques have led to better interpretation of information returned by the physical probes, such as EPR, XAFS, and optical spectroscopy, in terms of the states of the OEC rather than merely whether the system was evolving oxygen.

1.4.1. Phenomological Data: The Kok Model.

As stated before the OEC is the site for four electron chemistry with the end result being the oxidation of two water molecules. The major function of this complex is the removal of waste oxidative equivalents. The early experiments of

Joliot (1968) and Joliot *et al.* (1969), examined O_2 yield as a function of short saturating flashes of light with a modulated O_2 electrode, and provided the first quantitative linkage between discrete photoacts and O_2 evolution. This allows the half reaction to be written as a function of photons absorbed:

$$2H_2O \xrightarrow{h\nu} O_2 + 4H^+ + 4e^- \qquad (1.9)$$

Subsequent work by Kok *et al.* (1970) led to the S-state model (Figure 1.3) and provided a basis for explaining the periodicity and damping observed by both Joliot and Kok as depicted in Figure 1.4.

Two observations were key: 1) In dark adapted samples, only three flashes of light were required for maximal O_2 yield, and the next maxima occurred four flashes later; 2) Model simulations (Forbush *et al.*, 1971) required inclusion of parameters allowing for double turnovers and for misses; i.e, one flash of light could result in no S-state advance, a single S-state advance, or a double S-state advance. Including only one or the other resulted in not only damping but a phase shifting of the O_2 yield that was not experimentally observed. The first observation led to the idea of an equilibrium distribution between S_1 and S_0 with the S_0:S_1 ratio being 1:3. This has since been modified after studies on long dark adapted material (hours) revealed that the ratio was closer to 0:1 (Vermas *et al.*, 1984). This dark auto-oxidation has been correlated with the decrease in Y_D (Signal II_s), and it has been suggested that D^+ is reduced by S_0 in the dark over a long period of time (Zimmermann and Rutherford, 1985).

1.4.2. Cofactor Requirements for Oxygen Evolution.

It is difficult to discuss the cofactors that seem to be required on an individual basis because of the interdependency. Table 1.1 lists the known factors that have been established as being required for O_2 evolution. Those directly involved are the extrinsic polypeptides and the ionic species. Of these, manganese is the only one for which there is still an absolute requirement; i.e., manganese can neither be removed or replaced without inhibition. The accepted stoichiometry of four manganese per reaction center and as the site for catalysis has been established by the work of Cheniae and Martin (1970), Ghanotakis and Yocum (1985 and 1986), and Ikeuchi *et al.* (1985) in thylakoids, Photosystem II membranes, and in Photosystem II core preparations.

The extrinsic polypeptides, 17, 23, and 33 kDa, are included only because they are endogenous cofactors. Salt washing with high, non-physiological concentrations of NaCl removes the 17 and 23 and inhibits O_2 evolution, but higher than physiological concentrations of Ca^{2+} and Cl^- largely removes the inhibition (see Ghanotakis and Yocum, 1985). Likewise, salt washing with $CaCl_2$ removes all three polypeptides, and requires a six-fold increase in the Cl^- concentration to sustain O_2 evolution (Kuwabara *et al.*, 1985). The Mn cannot as yet be released without irreversible inhibition.

1.4.3. Spectroscopic Evidence of Manganese Involvement.

1.4.3.1 Multiline - EPR

Perhaps the best understood spectroscopic characterization of the manganese ensemble are the EPR detectable signals arising from the S_2 state. First observed in 1980 (Dismukes and Siderer, 1980), it was shown by Dismukes and Siderer (1981) that a multiline EPR signal, consisting of at least 16 lines and

centered at g = 2.0, could be generated in oxygen competent thylakoids by flashing a dark adapted sample, thereby generating the S_2 state, and then freezing quickly to 77 K. This suggested that this multiline signal arose from the S_2 configuration of the OEC. This observation was supported by others (Hansson and Andreasson, 1982, and Brudvig *et al.*, 1983a,b).

Spectral simulations of the multiline by Dismukes *et al.* (1982) suggested either two dimers, Mn_2(III,IV) or a tetramer, Mn_4(III)$_3$,IV). Hansson and co-workers (Hansson and Andreasson, 1982, and Andreasson *et al.*, 1983) found a better simulation using a binuclear Mn_2(II,III) model.

Confusing the issue has been the observation of the so-called g = 4.1 signal (referred to hereafter as the g4.1). Dark adaptation followed by treatment with (DCMU), an inhibitor at the Qb site, and illumination between 130 - 160K should populate the S_2 state of the OEC (de Paula *et al.*, 1985). Instead of the expected multiline an EPR signal at g = 4.1 was found. Warming the sample to 200K resulted in the disappearance of the g4.1 and the appearance of the multiline. Several have suggested this provided evidence for another intermediate between the OEC and Z (Casey and Sauer, 1984 and Zimmermann and Rutherford, 1984).

Today, it is generally accepted that the EPR spectroscopic properties of manganese in the S_2 state are dependent upon temperature. Studies by Brudvig and co-workers (de Paula and Brudvig, 1985, de Paula *et al.*, 1986) and Rutherford and co-workers (Zimmermann and Rutherford, 1986) have demonstrated that the g4.1 and the multiline signals arose from different configurations of the S_2 state. These configurations can be expressed in an equilibrium as depicted in Figure 1.7. This variability can be accounted for in temperature dependent structural alterations that alter exchange couplings.

In terms of understanding the OEC, characterization of the S_2 state through the EPR multiline and g4.1 signals has been the singularly most important event in the 1980s. The reader is referred to reviews by Babcock (1987) and Brudvig (1986), and also to the Ph.D. theses of de Paula (1986) and Beck (1988).

1.4.3.2 X-Ray Studies

EXAFS (Extended X-ray Absorption Fine Structure) has been used to determine the ligand environment around the manganese in samples poised in the S_1, S_2, and S_3 states. In the resting, S_1, state, a Mn-Mn distance of 2.7Å has been determined (Yachandra *et al.*, 1986). A second Mn-Mn distance of 3.3Å has also been reported (Guiles *et al.*, 1987). In addition, a *u*-oxo bridge at 1.8Å and a terminal oxygen or nitrogen ligation shell at 2.0 - 2.1Å has been identified as well; however, Cl^-, as a ligand, has not been found.

Lack of Cl^- as a ligand is significant. As mentioned in the earlier section discussing required cofactors for steady state oxygen evolution requires a negatively charged ion such as Cl^-, Br^-, or NO_3^-, Cl^- being endogenous. Sandusky and Yocum (1983), through competitive inhibition studies, have suggested that Cl- serves as a bridging ligand between two manganese centers.

From the EPR studies, the model best supporting the available data is a mixed valence tetramer (de Paula, 1986). The EXAFS data indicate the presence of a *u*-oxo bridged manganese dimer. Thus, it has been proposed that the manganese complex is in the form of a 'cubane'-like structure, Mn_4O_4, and undergoes transitions as in Figure 1.8. (Brudvig and Crabtree, 1986).

1.4.3.3 Optical Studies

UV absorption spectroscopy has been used to detect absorption changes associated with S-state advancement by several groups (Velthuys, 1980, Dekker *et al.*, 1984b, Saygin and Witt, 1985 and 1987, Lavergne, 1986 and 1987, and Renger and Weiss, 1983 and 1986). Considerable disagreement exists regarding interpretation. Dekker *et al.* (1984b), after complex data deconvolution that involves the removal of contributions from Qa, Qb (or other acceptor quinones), and Z, reported the changes for the S_0 --> S_1, S_1 --> S_2, and S_2 --> S_3 to be identical and probably arising from successive Mn(III) --> Mn(IV) transitions.

This finding contradicts that of Velthuys, and has since been challenged by Lavergne (Lavergne, 1986 and 1987) and Witt's group (Saygin and Witt, 1985) as well. These three groups claim there are no detected absorption changes on the S_0 --> S_1 and S_2 --> S_3. It appears the source of disagreements arise because of the difficulty in deconvolving unwanted contributions from the experimental data. Both Lavergne and Witt's group point out that deconvolving the S-state transitions, normally dependent upon the relative S_1/S_0 distributions and the hit and miss parameters, does not yield unique solutions.

Dekker and Witt (Kretschmann *et al.*, 1987) have since issued a paper agreeing that the S_0 -->S_1 transition is a factor of three less than originally reported by Dekker *et al.* (1984b) and probably corresponds to a Mn(II) --> Mn(III) change. They also agree that the S_1 --> S_2, and S_2 --> S_3 changes are identical and probably correspond to Mn(III) --> Mn(IV) changes.

1.5. Focus of This Thesis

It is apparent that Cl^- plays a significant role in the evolution of O_2. It is also apparent that the existing data concerning this role are inconclusive. As a

result we decided to study the optical transitions in the near UV associated with the S-states of the Oxygen Evolving Complex in green plants using Photosystem II preparations. It was anticipated that the time resolved optical spectrometer designed for study of the electrochromic shift and proton release patterns in chloroplasts (Lillie, 1984) would prove to be adequate after having its wavelength range extended into the UV and modification of the data acquisition and computer interfaces.

Chapter Two discusses the improvements made to the spectrometer. These changes resulted in an extension of the operation wavelength range to the UV and near UV. Both the bandwidth and the minimum detected absorption change ranges were extended as well.

Chapter Three discusses the improvements of the support and functionality that were provided by the interfaced computer system. These changes extended the type of experiments possible from repetitive single channel collection to include repetitive multiple channel collection and conditional event occurrences dependent upon shot and channel numbers.

Chapter Four discusses experiments performed on the reducing side of Photosystem II. Only one other group has reported in as great of detail the absorption changes undergone by the reducing side.

Chapter Five discusses experiments on the S-state transitions. These experiments were conducted upon untreated and treated Photosystem II systems. The treated systems were those in which the Oxygen Evolving Complex was reversibly inhibited.

Appendix A contains the user documentation for the Flash Absorption Spectrometer and its Computer Interface (FASCI). This was a separately prepared document for users and is included here for completeness.

TABLE 1.1

Cofactors Implicated in Oxygen Evolution

Cofactors implicated in oxygen evolution. Proposed functions are derived from Babcock (1987) and Murata and Miyao (1987), and are the "well-accepted" views. Alternative viewpoints exist for assigning polypeptide functions for D1, D2, Qb, and Mn; for a review see Babcock (1987).

Cofactor	Function
PSII Core Complex	
47 kDa	Chl-binding
43	
34	Mn-binding, D2 (reaction center)
32	Qb, D1 (reaction center)
20	
9	b-559
4	"
Light-Harvesting Polypeptides	
22-28 kDa	Chl-a and b binding
Extrinsic Polypeptides	
33 kDa	Mn-stabilization.
23	Ca^{2+}, Cl^-
17	Ca^{2+}, Cl^-
Ionic Species	
Mn^{+n}, (n = 2,3, or 4)	H_2O site
Ca^{2+}	
Cl^-	

FIGURE 1.1

The Kok S-state Model.

The Kok model is abstract and postulates that there are five oxidative storage states, but is unable to make any statement concerning how the oxidative equivalents are actually stored or even what comprises the storage center. Here, S_n, $n = \{0,1,...,4\}$, represents the five oxidative states of the Oxygen Evolving Complex. 'Z' is the electron carrier between the OEC and the reaction center, P_{680} as discussed in the text.

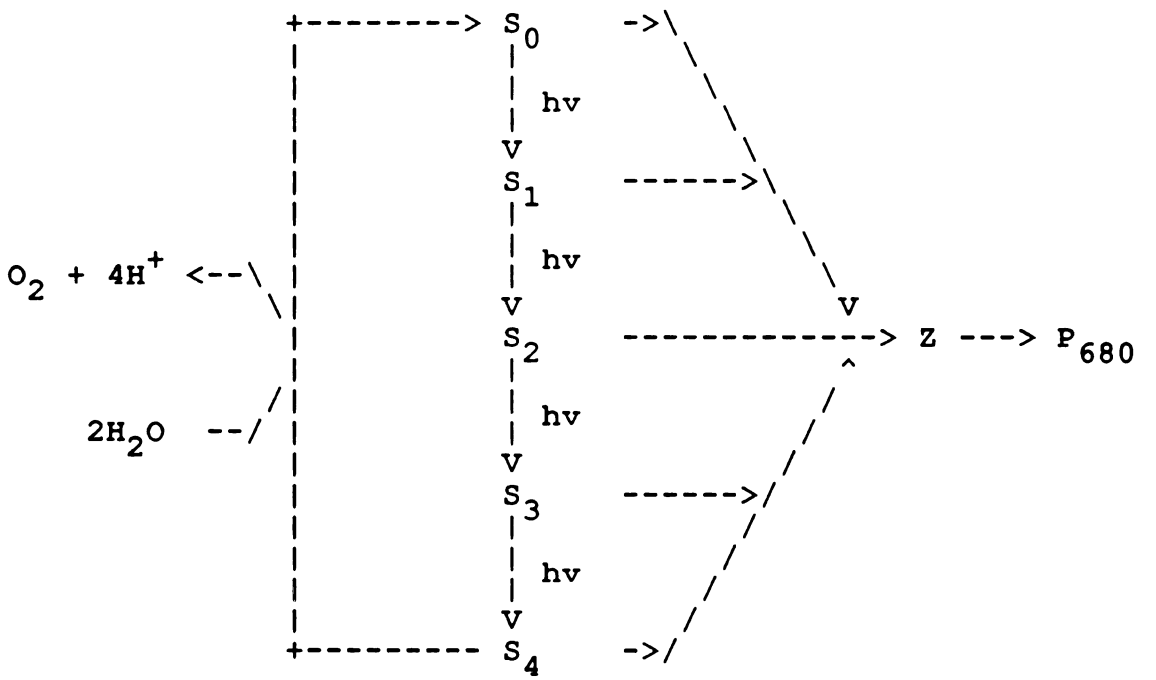
S0
hv
S1
hv
S2
hv
S3
hv
S4
O2 + 4H+
2H2O
Z
P680

FIGURE 1.2

Oxygen Yield as a Function of Flash Number

The oxygen flash yield in isolated chloroplasts after a dark adaptation as a function of flash number (Buttner, 1984). Kok *et al.* (1970) were able to fit the damped, period four oscillations to a model by assuming a fraction of centers did not undergo a transition and that another fraction of centers underwent two transitions per flash. Computer modeling predicts the dark adapted distribution of S_0:S_1 to be 1:3.

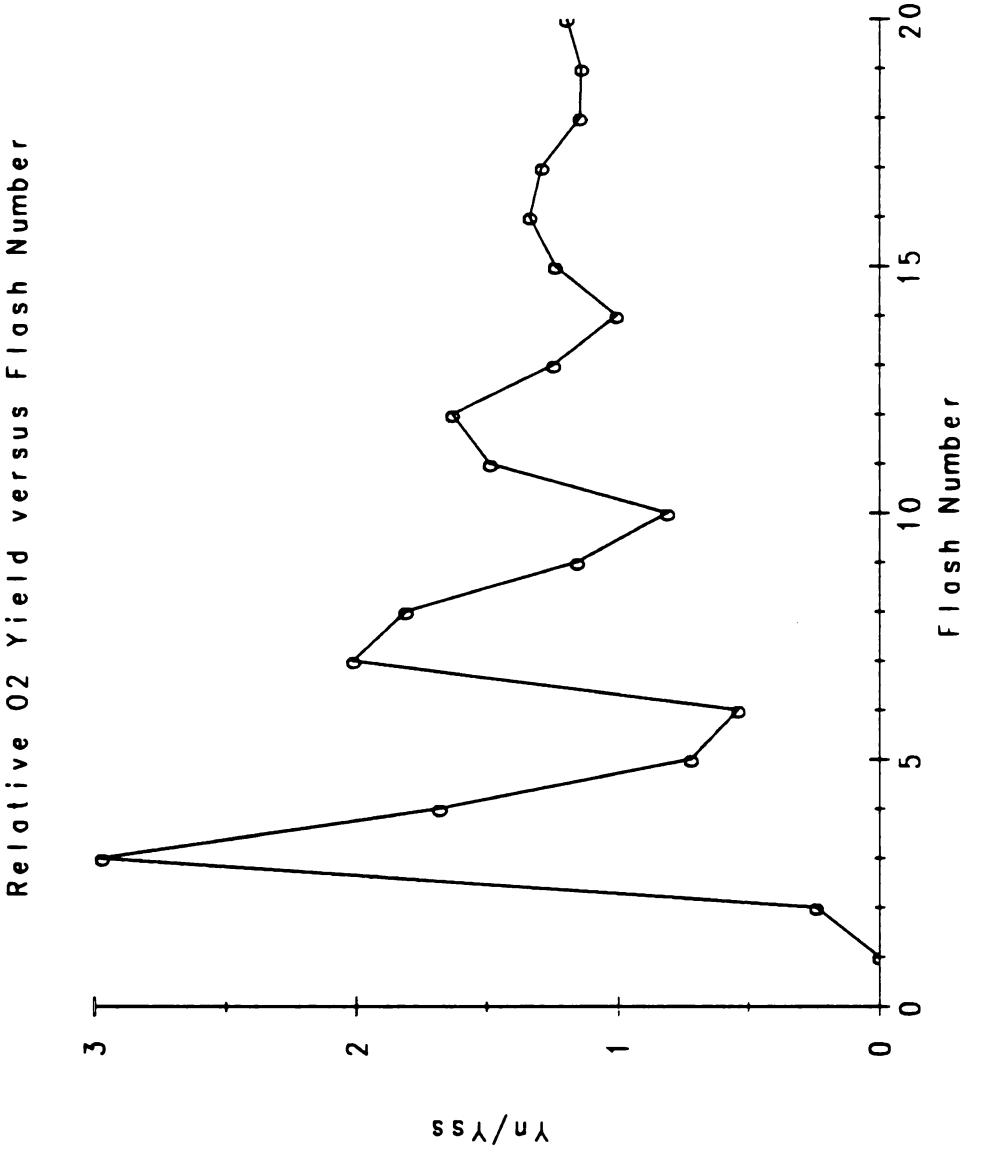
Relative O2 Yield versus Flash Number
Yn/Yss
0
1
2
3
0
5
10
15
20
Flash Number

FIGURE 1.3

The Z-scheme

The Z-scheme is a schematic representation of linear photosynthetic electron transport in plants. The individual components are plotted along the ordinate according to their known or estimated midpoint potentials (adapted from Buttner, 1984).

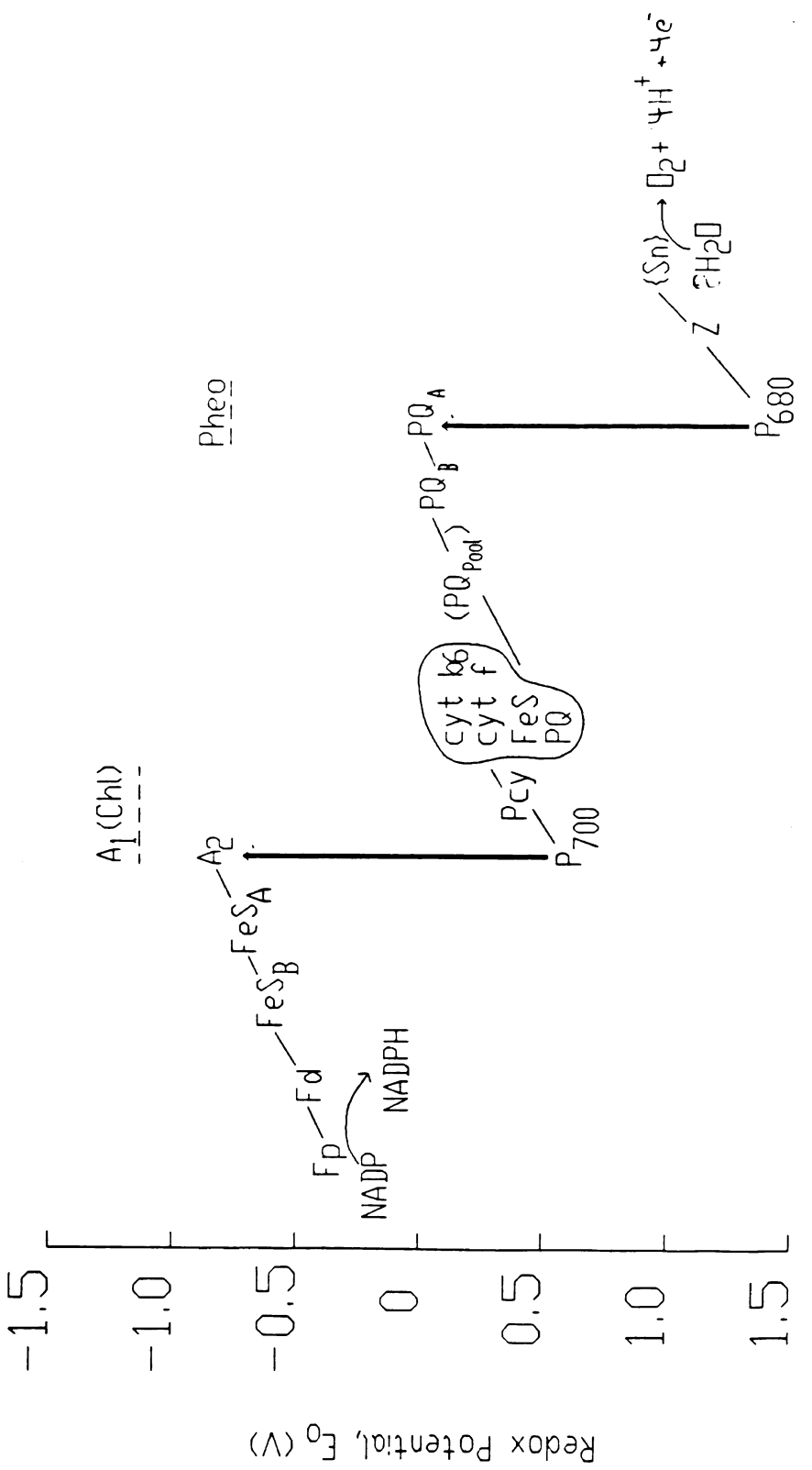
Redox Potential, E_o (V)
-1.5
-1.0
-0.5
0
0.5
1.0
1.5
A_1(Chl)
Pheo
A_2
FeS_A
FeS_B
Fd
Fp
NADP
NADPH
Pcy
P_{700}
cyt b6
cyt f
FeS
PQ
(PQ_{pool})
PQ_B
PQ_A
Z
(Sn)
$2H_2O$
$O_2 + 4H^+ + 4e^-$
P_{680}

FIGURE 1.4

Membrane Topology Corresponding to the Z-scheme

The components involved in the Z-scheme are depicted here in their approximate locations relative to the membrane's orientation. Unlike other topological schemes, sizes and contours of the protein complexes have not been articulated. Instead, an attempt has only been made to show relationships and approximate electron transfer component locations. These components as well as the protein complexes are discussed in the text.

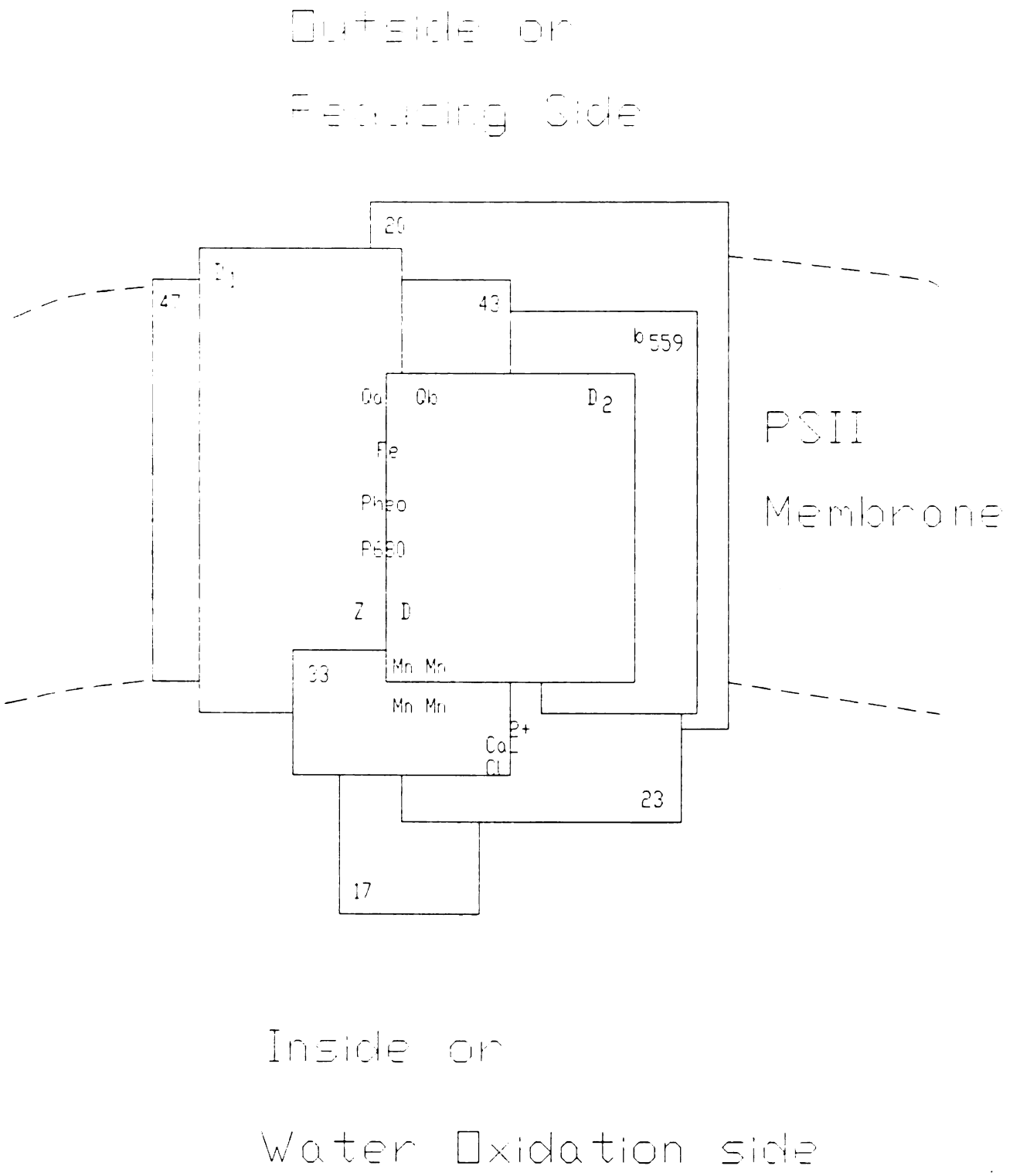
Outside or
Reducing Side
20
D1
47
43
b559
Qa
Qb
D2
Fe
Pheo
P680
Z
D
33
Mn Mn
Mn Mn
Ca
Cl
2+
23
17
PSII
Membrane
Inside or
Water Oxidation side

FIGURE 1.5

Crystal Structure of Bacterial Reaction Center

Overview of the structure of *Rhodopseudomonas viridis* (reproduced from Michel-Beyerle *et al.*, 1987). Numbers in figure represent center to center distances in 0.1 nm. 'P' is the reaction center formed from two Bacteriochlorophyll*b* s with an interplanar distance of 0.3 nm. 'B_M' and 'B_L' are bacteriochlorophyll-*b*'s in the M and L subunits. 'BP_M' and 'H' are bacteriopheophytin-*b*'s in the M and L subunits. 'MQ' is the acceptor, a metaquinone in bacterial reaction centers. Each branch is terminated by a quinone; however, the one in the M branch is lost during isolation.

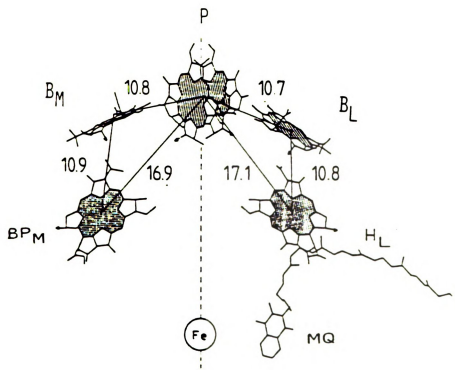
P
B_M
10.8
10.7
B_L
10.9
16.9
17.1
10.8
BP_M
H_L
Fe
MQ

FIGURE 1.6

Structure and Redox Chemistry of Quinones in Photosystem II.

It is important to understand this chemistry and in particular the equilibrium states. Absorption bands in the UV and near UV of the quinone and semiquinone disappear in the doubly reduced states (Chapter 4)

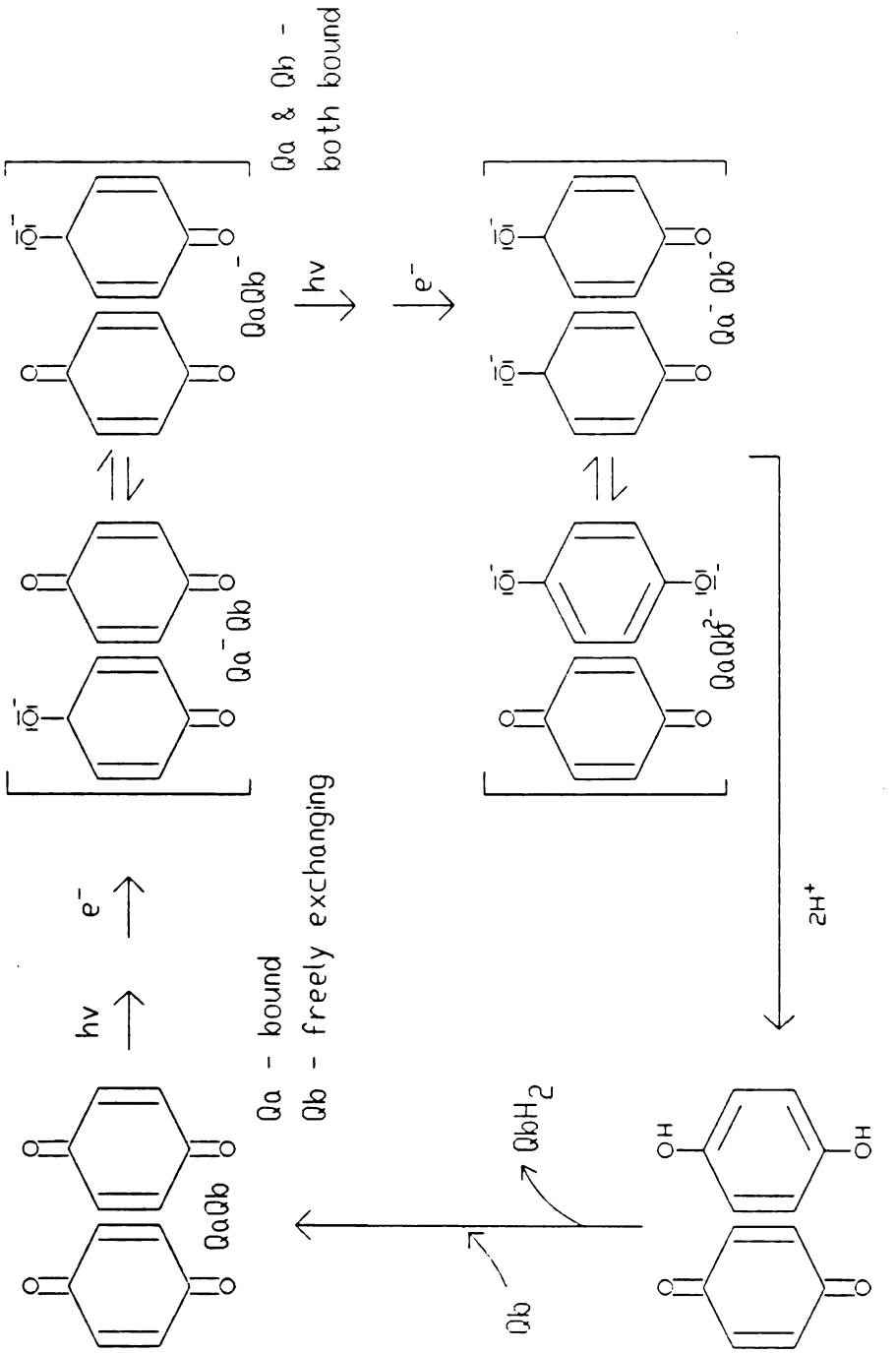
QaQb
hv
e⁻
Qa - bound
Qb - freely exchanging
Qa⁻Qb
QaQb⁻
hv
e⁻
Qa & Qb -
both bound
Qb
QbH2
2H+
QaQb2-
Qa⁻Qb⁻

FIGURE 1.7

Multiline Configurations

Proposed model for multiline and g = 4.1 signals. The proposal is that the ligand substitution reactions influence the equilibrium between the two configurations which give rise to the g = 4.1 and the multiline signals. (adapted from Beck, 1988b).

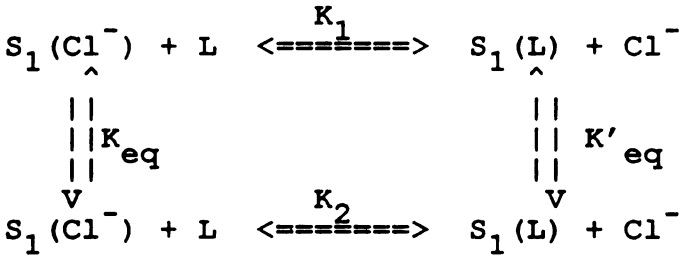
$S_1(Cl^-) + L \xrightleftharpoons{K_1} S_1(L) + Cl^-$
K_{eq}
K'_{eq}
$S_1(Cl^-) + L \xrightleftharpoons{K_2} S_1(L) + Cl^-$

FIGURE 1.8

Cubane structure proposed for the OEC.

Brudvig and Crabtree (1986) have proposed this model in light of the evidence from the EPR studies on the S_2 state, EXAFS data, and optical evidence. This particular model has been of particular interest because the physical evidence backing it is more definitive than for other models that have been suggested (see for example Kambara and Govindjee, 1985, or Spencer *et al.*, 1986).

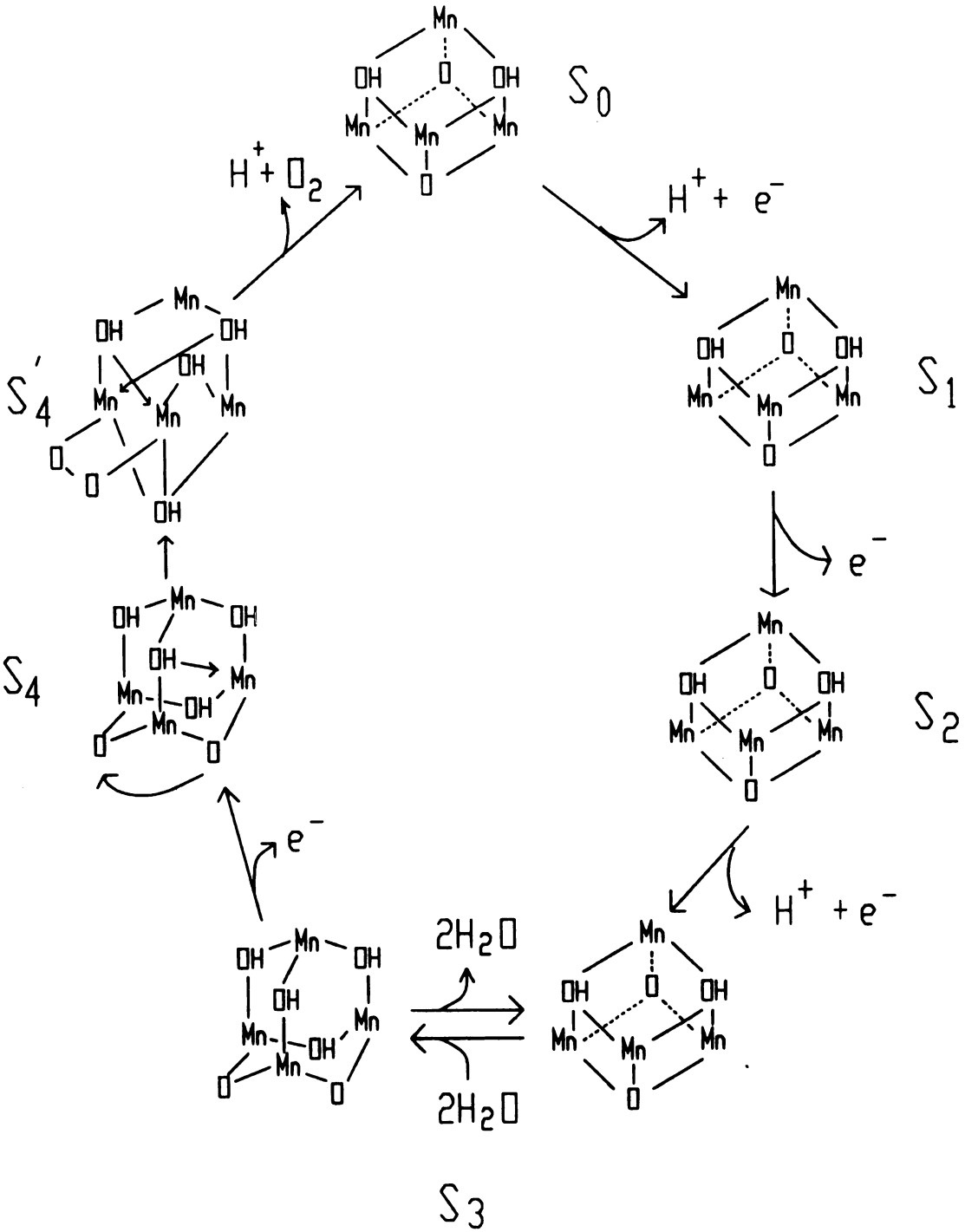
S0
S1
S2
S3
S4
S'4
H+ + O2
H+ + e−
e−
H+ + e−
e−
2H2O
2H2O
Mn
OH
O

REFERENCES

Babcock, G. T. (1987). "New Comprehensive Biochemistry: Photosynthesis," 125-158, (Amesz, J., ed.), Elsevier, Amsterdam.

Babcock, G. T., Blankenship, R. E., and Sauer, K. (1976). FEBS Letters, 61, 286-289.

Babcock, G. T. and Sauer, K. (1975). Biochimica et Biophysica Acta, 376, 315-328.

Babcock, G. T. and Sauer, K. (1973). Biochimica et Biophysica Acta, 325, 483.

Barry, B. A. and Babcock, G. T. (1987). Proceedings of the National Academy of Sciences, USA, 84, 7099-7103.

Beck, W. F. (1988). "Ligand-Exchange and Oxido-Reduction Reactions of Water Analogs with the Manganese Tetramer Complex of Photosystem II," 264, Ph.D. Thesis, Yale University.

Bensasson, R. and Land, E. J. (1973). Biochimica et Biophysica Acta, 325, 175-181.

Blackman, F. F., (1905). Annu. Rev. Bot., 19, 281-295.

Blankenship, R. E. and Parson, W. W. (1978). Annual Reviews of Biochemistry, 545, 635-653.

Blankenship, R. E., Babcock, G. T., and Sauer, K. (1975). Biochmica et Biophysica Acta, 387, 165.

Boska, M., Sauer, K., Butter, W., and Babcock, G. T., (1983). Biochimica et Biophysica Acta, 722, 327-330.

Bouges-Bocquet, B., (1980). Biochimica et Biophysica Acta, 594, 85-103.

Breton, J., Martin, J.-L., Petrich, J., Migus, A., and Antonetti, 26. (1986). FEBS Letters, 209, 37-43.

Breton, J. and Vermeglio, A. (1982). "Energy Conversion in Plants and Bacteria", Volume 1, 153-194, (Govindjee ed.), Academic Press, New York.

Brettel, K., Schlodder, E., and Witt, H. T. (1984). Biochimica et Biophysica Acta, 766, 403-415.

Brudvig, G. .W., Casey, J. L., and Sauer, K. (1983a). Biochimica et Biophysica Acta, 723, 361-371.

Brudvig, G. W., Casey, J. L., and Sauer, K. (1983b). "The Oxygen Evolving System of Photosynthesis", 159-164, (Inoue, Y., Crofts, A. R., Govindgee, Murata, N., Renger, G., and Satoh, K., eds), Academic Press, Tokyo.

Brudvig, G. W. (1986). Journal of Bioenergetics and Biomembranes, 19, 91-103.

Brudvig, G. W. and Crabtree, R. H. (1986). Proceedings of the National Academy of Sciences, USA, 831, 4586-4588.

Buttner, W. J. (1984). Ph.D. Thesis, Michigan State University.

Casey, J. L. and Sauer, K. (1984). Biochimica et Biophysica Acta, 767, 21-28.

Cheniae, G. M., and Martin, I. F. (1970). Biochimica et Biophysica Acta, 197, 219-239.

Clayton, R. K. (1980). "Photosynthesis: Physical Mechanisms and Chemical Patterns," 88-110, Cambridge University Press, Cambridge.

Commoner, V., Heise, J. J., and Townsend, J. (1956). Proceedings of the National Academy of Sciences, USA, 42, 710-718.

Debus, R. J., Barry, B. A., Babcock, G. T., and McIntosh, L. (1988). Proceedings of the National Academy of Sciences, USA, 85, 427-430.

Debus, R. J., Feher, G., and Okamura, M. Y. (1986). Biochemistry, 25, 2276-2287.

Deisenhofer, J., Epp, O., Miki, K., Huber, R. and Michel, H. (1984). Journal of Molecular Biology, 180, 385-398.

Dekker, J. P., Van Gorkom, H. .J., Brok, M., Ouwehand, L., (1984a). Biochimica et Biophysica Acta, 764, 301-309.

Dekker, J. P., Van Gorkom, H. .J., Wensink, J., and Ouwehand, L., (1984b). Biochimica et Biophysica Acta, 767, 1-9.

de Paula, J. C. and Brudvig, G. W. (1985) Journal of the American Chemical Society, 107, 2643-2648.

de Paula, J. C., Beck, W. F., and Brudvig, G. W. (1986) Journal of the American Chemical Society, 108, 4002-4009.

de Paula, J. C. (1986). Ph.D. Thesis, Yale University.

de Vitry, C., Carles, C., and Diner, B. A. (1986). FEBS Letters, 196, 203-206.

Diner, B. A. and de Vitry, C. (1984). "Advances In Photosynthesis Research," Volume 1, (Junk, W., ed.) Martinus Nijhoff Publishers, Dordrecht, The Netherlands.

Dismukes, G. C., Ferris, K., and Watnick, P. (1982). Photobiochemistry and Photobiophysics, 3, 243-256.

Dismukes, G. C. and Siderer, Y. (1980). FEBS Letters, **121**, 78-80.

Dismukes, G. C. and Siderer, Y. (1981). Proceedings of the National Academy of the Sciences, USA, **78**, 274-278.

Duysens, L. N. M., Amesz, J., and Kamp, B. M., (1961). Nature, **190**, 510-511.

Forbush, B., Kok, B., McGloin, M. P. (1971). Photochemistry and Photobiology, **14**, 307-321.

Gerken, S., Brettel, K., Schlodder, E., and Witt, H. T., (1988). FEBS Letters, **223**, 69-74.

Gerken, S., Brettel, K., Schlodder, E., and Witt, H. T., (1987). FEBS Letters, **223**, 376-380.

Ghanotakis, D. F. and Yocum, C. F. (1986). FEBS Letters, **197**, 244-248

Ghanotakis, D. F. and Yocum, C. F. (1985). Photosynthesis Research, **7**, 97-114.

Guiles, R. D., Yachandra, V. K., McDermott, A. E., Britt, R. D., Dexheimer, S. L., Sauer, K., and Klein, M. P. (1987). "Progress in Photosynthesis Research," Volume 1, (Biggins, J., ed.), 561-564, Martinus Nijhoff Publishers, Dordrecht, The Netherlands.

Hansson, O. and Andreasson, L.-E., (1982). Biochmica et Biophysica Acta, **679**, 261-268.

Andreasson, L.-E., Hansson, O., and Vanngard, T. (1983). Chemica Scripta, **21**, 71-74.

Hill, R. (1939). Proceedings of the Royal Society, London, **127**, 192-210.

Hill, R. and Bendall, F., (1960). Nature, **186**, 136-137.

Hill, R. (1972). "Proceedings of the 2nd International Congress of Photosynthesis Research," Vol 1, (Forti, G., Avron, M., Melandri, B.A., eds.), Junk, The Hague.

Hoganson, C. W. and Babcock, G. T. (1988a). Biochemistry, **27**, 5845-55.

Hoganson, C. W. and Babcock, G. T. (1988b). Biochmica et Biophysica Acta, in press.

Ikeuchi, M. and Inoue, Y. (1987). FEBS Letters, **210**, 71-76.

Ikeuchi, M., Yuasa, M., and Inoue, Y. (1985). FEBS Letters, **185**, 316-322.

Joliot, P. (1968). Photochemistry and Photobiology, **8**, 451-463.

Joliot, P., Barbieri, G., and Chabaud, R. (1969). Photochemistry and Photobiology, **10**, 309-329.

Knox, R. S. (1977). "Primary Processes of Photosynthesis", Volume 2, 55-97, (Barber, J., ed.), Elsevier/North-Holland Biomedical Press, Amsterdam, The Netherlands.

Kohl, D. H. and Wood, P. M., (1969). Plant Physiology, 44, 1439-1445.

Kok, B., Forbush, B., and McGloin, M. (1970). Photochemistry and Photobiology, 11, 457-475.

Kretschmann, H., Dekker, J. P., Saygin, O., and Witt, H. T. (1987). Biochimica et Biophysica Acta, 932, 358-361.

Kuwabara, T., Miyao, M., Murata, T., and Murata, N. (1985). Biochimica et Biophysica Acta, 806, 283-289.

Lavergne, J. (1986). Photochemistry and Photobiology, 43, 311-317.

Lavergne, J. (1987). Biochimica et Biophysica Acta, 894, 91-107.

Lillie, D. (1984) M.S. Thesis, Michigan State University.

Mauzerall, D. (1972) Proceedings of the National Academy of the Sciences, USA, 69, 1358-1362.

Michel-Beyerle, M. E., Plato, M., Deisenhofer, J., Michel, H., Bixon, M. and Jortner, J. (1988). Biochimica et Biophysica Acta, 932, 52-70.

Murata, N. and Miyao, M. (1987). "Progress in Photosynthesis Research," Volume 1, (Biggins, J., ed.), 453-461, Martinus Nijhoff Publishers, Dordrecht, The Netherlands.

O'Malley, P. J. and Babcock, G. T. (1984). Biochimica et Biophysica Acta, 765, 370-379.

O'Malley, P. J., Babcock, G. T., and Prince, R. C. (1984). Biochimica et Biophysica Acta, 766, 283-288.

Parson, W. W. (1978). "The Photosynthetic Bacteria", 455-469, (Clayton, R. K. and Sistrom, W. R., eds.), Plenum, New York.

Parson, W. W., Ke, B. (1982). "Energy Conversion in Plants and Bacteria", Volume 1, 330-385, (Govindjee ed.), Academic Press, New York.

Pearlstein, R. M. (1982). "Energy Conversion in Plants and Bacteria", Volume 1, 293-330, (Govindjee ed.), Academic Press, New York.

Rabinowitch, E. I. (1945). "Photosynthesis and Related Processes," Vol I", Interscience, N.Y.

Renger, G. and Weiss, W. (1983). Biochimica et Biophysica Acta, 722, 1-11.

Renger, G. and Weiss, W. (1986). Biochimica et Biophysica Acta, 850, 184-196.

Rutherford, A. W. (1985). Biochmica et Biophysica Acta, 807, 189.

Ruben, S., Randall, M., Kamen, M., and Hyde, J. L., (1941). Journal of the American Chemical Society, 63, 877-890.

Sandusky, P. O., Yocum, C. F. (1983). FEBS Letters, 162, 339-343.

Saygin, O. and Witt, H. T. (1985). Photochemistry and Photobiophysics, 10, 71-82.

Sayin, O. and Witt, H. T. (1987). Biochimica et Biophysica Acta, 893, 452-469.

Schlodder, E., Brettel, K., and Witt, H. T., (1984). Biochimica et Biophysica Acta, 808, 123-131.

Sullivan, P. D. and Bolton, J. R. (1968). Journal of the American Chemical Society, 90, 5366-5370.

Takahashi, Y. and Katoh, S. (1986). Biochimica et Biophysica Acta, 848, 183-192.

Takahashi, Y., Takahashi, M.-A., and Satoh, K. (1986). FEBS Letters, 208, 347-351.

Trebst, A. (1986). Z. Naturforsch, 41c, 240-245.

Van Best, J. A. and Mathis, P. (1978). Biochmica et Biophysica Acta, 505, 178-188.

Van Niel, C. B. (1941). Advances in Enzymology, 1, 263-328.

Velthuys, B. R. (1980). Annual Reviews in Plant Physiology, 31, 545-567.

Warburg, O. and Luttgens, W. (1960) Z. Naturforsch, B: Inorganic Chemistry, Organic Chemistry, Biochemistry, Biophysics, Biology, 15B, 367-369.

Warburg, O. (1964). Annual Reviews of Biochemistry, 33, 1-14.

Weiss, W. and Renger, G. (1986). Biochimica et Biophysica Acta, 850, 173-183.

Wood, P. M. and Bendall, D. S. (1976). European Journal of Biochemistry, 861, 337-344.

Yachandra, V. K., Guiles, R. D., McDermott, A., Britt, R. D., Dexheimer, S. L., Sauer, K., and Klein, M. P. (1986). Biochimica et Biophysica Acta, 850, 324-332.

Zimmermann, J. L. and Rutherford, A. W. (1984). &Biochimica et Biophysica Acta, 767, 160-167.

Zimmermann, J. L. and Rutherford, A. W. (1985). Physiol. Veg., 23, 425-434.

Zimmermann, J. L. and Rutherford, A. W. (1986). Biochemistry, 25, 4609-4615.

wa

fo

orig

use

the p

chlor

exper

PS-II.

Junge

found in

observe

associat

of 10^{-4} to

changes,

In

implement

the experim

CHAPTER 2

SPECTROMETER DEVELOPMENT

2.1. INTRODUCTION

It was stated earlier that the primary instrumental technique to be used was fast absorption spectroscopy. The spectrometer described here and in the following chapter represents a considerable extension and reworking of the original design (Lillie, 1984). The prototype was of a single beam design and used for experiments examining some aspects of the electrochromic shift and of the proton release patterns related to Photosystem II that had been observed in chloroplasts. Additionally, it was to serve as a testbed from which to begin experiments on the primary acceptor, Qa, and the oxygen evolving complex of PS-II. A review of the electrochromic shift and proton release can be found by Junge and Jackson (1982).

The absorption changes associated with the electrochromic shift are found in the blue green region (450 to 550 nm), and the amplitudes of the observed changes are on the order of 10^{-3}. The magnitude of the changes associated with the OEC in the UV and near-UV (250 to 350 nm) are on the order of 10^{-4} to 10^{-5}. Our original design was unable to resolve these absorption changes, and we were forced to re-examine the design of the spectrometer.

In this chapter we will explore the experimental requirements and the implemented design for non-computer components. Design issues arising from the experimental requirements that affect the implementation of the computer

support such as hardware interfacing and software are discussed in the following chapter. Specific discussion of the analogue to digital converters is also delayed until the following chapter, though there may be some general comments here

2.2. EXPERIMENTAL REQUIREMENTS

Careful thought and attention to detail are required to bring an instrumental setup to an operating condition such that the focus is upon the problem at hand instead of focusing on simply being able to perform an experiment. The following section, among other topics, highlights subtle but important considerations we had to take into account during the building and testing of this experimental apparatus.

2.2.1. Information to be Measured.

In general, the information sought is the response of a chemical system in time after an excitation. The response is measured by changes in light transmission of a 'probe' beam at a given wavelength relative to the transmission of the probe at the same wavelength before excitation. The excitation in this case takes the form of a short pulse of intense light perpendicular to the probe beam. This excitation is tuned to a wavelength optimal for inducing photo-chemistry and minimal attenuation of the exciting pulse.

2.2.2. Sample Attenuation of Exciting Pulse

Organic and inorganic photolytic experiments are somewhat similar to the description just given in terms of the information sought and the method used for obtaining it. An important difference is with respect to the chromophore's concentration. The concentration in the photolytic experiments can usually be adjusted to give easily detectable changes in the light intensity. Biological

conditions are such that the chromophore's concentration often cannot be adjusted above the micro- to nano- molar range without aggregation and optical density then becoming limiting factors.

The high optical density of the sample creates a problem as it attenuates the exciting pulse of light as it passes through the sample. Consider Figure 4.8, a spectrum of a Photosystem II membrane preparation. The strong absorption bands in the 650 to 690 nm range are due to chlorophylls from both the light harvesting complex and the reaction center. Use of an exciting light in this wavelength range would optimize excitation, but the light itself would be strongly attenuated and would not uniformly excite across the cross-section of the sample exposed to the probe light. Use of a wavelength region not strongly absorbed by the sample would decrease the amount of attenuation and allow for a more uniform sample exposure; however, the probability for excitation is lessened.

2.2.3. Signal Discrimination

The absorption change for many of the photosynthetic components in the electron transport chain ranges from 10^{-5} to 10^{-3}. The intensity of the detected signal can be related to the concentration of the chromophore by Beer's Law. The differential Beer's Law equation is:

$$-dI/I = aCdx \qquad (2.1)$$

where 'I' is the intensity of the beam before absorption, 'dI' is the fraction transmitted over the distance 'dx' through which the beam passes, 'C' is the concentration of molecules undergoing absorption, and 'a' is a constant of the molecules specifying the probability for absorption. The integrated form is:

$$I = I_0 e^{-aCx} \qquad (2.2)$$

2

ph

pr

the

an

exc

2.2.5

photo

depen

quater

Photos

or, rearranging,

$$A = -\log(I/I_0) = aCx. \qquad (2.3)$$

'I_0' is the intensity of the measuring light before its absorption by the sample, and 'I' is the intensity after absorption. 'A,' then, is the absolute absorption of the sample. If the absolute absorption changes by 10^{-5}, then this corresponds to a change in the I/I_0 ratio by about 0.002% in the intensity of the measuring light after absorption. It is the ability to resolve the changes in I from the ratio, I/I_0, that is important. Increased sensitivity to small changes in probe light intensity also results in an increase in sensitivity to the exciting light. The differences in intensity between the probe and the exciting light will be orders of magnitude, thus complicating discrimination.

2.2.4. Photochemistry Induced by the Probe Light.

The probe beam itself can interact with the sample and perform photochemistry. Figure 4.6 is a plot of the time of exposure of the sample to the probe beam before excitation versus the maximal absorption change at 320 nm, the maxima for monitoring the change associated with Qa^-/Qa. This directly puts an upper limit on the length of exposure of the sample to the probe before excitation. This upper limit has other implications discussed in the next section.

2.2.5. Sample Dependencies on Flash Number.

We also know that the separate electron transfer components in photosynthetic systems can display non-synchronous damped periodic dependencies on number and frequency of excitation. The binary and quaternary oscillations of the reducing and oxidizing sides respectively of Photosystem II were discussed in Chapter One. At the onset, from a resting

state, the periodic reactions on both sides will be synchronous. The accumulation of 'misses' on the oxidizing side will allow the two to shift out of phase with respect to one another. Thus giving rise to the origin of the non-synchronous behaviour.

Experiments aimed at elucidating kinetic or spectral information dependent on these periodicities need to have a sample transport mechanism for the introduction of controlled samples into the excitation chamber for measurement. Also needed are enough data collection channels for update, analysis, and storage to characterize the periodicities.

2.2.6. Other Characteristics

Device timing and the ability to have multiple, separate, sequential data collection sessions is important here as well. As an example, consider an experiment aimed at collecting absorbance changes from the oxygen evolving complex. If we are interested in the optical changes that occur as a result of storage of each oxidizing equivalent and their eventual simultaneous release, the changes of at least four successive excitations will have to be recorded separately.

Figure 2.7 depicts the events that occur per flash, these are known as *inter*sequence events. Figure 2.8 depicts the events that occur between successive flashes for a sequence group of four, these are known as *intra*-sequence events. A sequence is defined as a group of pulses that go through one data collection cycle. In the example given in Figure 2.8 the four successive sequences will define a single iteration. Sixteen such iterations, for a total of 64 flashes, were required to provide the signal to noise resolution as shown here.

The time from opening the shutter to the beginning of recording data is deliberately kept to less than 5 ms because of the photochemistry induced by the

measuring beam (see Figure 4.6), and this implies that the detector system and electronics must be stabilized to a relatively flat baseline within that time period. The linearity of the baseline is important because of the lack of a reference that could be used to correct fluctuations caused by instability in the arc, electronics, or sample.

Once recording has begun, the probe light source must be stable, either through feedback control or an accurate reference, as all optical changes are recorded relative to the baseline established immediately before excitation.

2.3. IMPLEMENTATION

As a result of these deliberations, we settled on an extensive set of modifications and enhancements to the original spectrometer and computer system. The rest of this chapter deals with modifications of the spectrometer (Figure 2.1) and the following chapter discusses the computer system modifications.

2.3.1. Monochromator and Probe Beam Source

Attenuation of the probe beam was severe below 350 nm when a 100 watt tungsten-halogen lamp was used as the probe source. We were able to resolve this by using a xenon arc lamp housing and power supply (A-1000 water-cooled holder and LPS-200 power supply, Photon Technology, Inc.). A 75 watt Osram xenon lamp was used for illumination. Compared to a lamp using a filament, xenon arc lamps have a stability problem as the arc tends to wander around the surface of the electrode tips. The Osram lamp used is of a special design and features a very small surface area with strongly tapered electrode tips. This tends to localize the arc into one position so that arc movement is minimized.

The light output from the arc lamp passes through a beam-splitter that diverts a fraction of the light to an optical feedback unit that regulates the current the power supply provides to the lamp. Following the beam splitter is an electro-mechanical shutter (Uniblitz, model 100B, Advanced Electro-mechanical Engineering; Rochester, NY) and the entrance slit to the monochromator (H-20 monochromator with either a 600 or 1200 gr/mm ion-etched concave holographic grating, Jobin-Yvon, Instruments S.A.; Metuchen, NJ). The shutter is isolation mounted separately on the spectrometer platform.

The original concave holographic gratings (made commercially by Instruments S.A.) generally have a higher spectral purity, though, the efficiency is lower than with a more conventional Czerny-Turner type. A grating optimized for the UV was acquired because of recent advances in the manufacturing technology. An ion-etching process performed on the Master grating supposedly results in a higher efficiency; though, we have not been able to quantitatively demonstrate this.

2.3.2. Sample Compartment

The sample compartment is positioned between the monochromator and the detector housing. Adjustable slit positions on both sides provide for a variety of entrance pathways relative to the sample cell position for excitation. Typically we excited perpendicular to the probe beam, but other groups have used excitation onto the same side of the sample cell as the probe. As the pathlength along this axis is shorter than along the other path the attenuation of the exciting beam should be less. Examination of Figure 4.3, a plot of input excitation energy versus detected response shows that 20% of maximum intensity has essentially achieved 100% response.

Built into the wall holding the face of the detector housing is a mechanical shutter. This allows us to position components inside of the compartment without exposing the detector.

The sample cell holders are removable, and are designed for use with a variety of cell-types. Currently, we have cells suitable for single sample, multiple flash experiments as well as multiple sample flow-type experiments. One is currently being designed for variable temperature work. A small rail inside allows us to position focusing optics for optimal throughput.

2.3.3. Excitation

Sample excitation is provided by a pulsed dye laser (model DL-1100 Phase-R Corporation; New Durham, NH), a xenon flashlamp pumped laser rated at a maximum power output of 250 mJ/pulse at a repetition rate of 0.25 Hz with a pulse width of 500 ns at 640 nm (0.5 Megawatts, MW). In practice a more realistic power output range was between 50 - 70 mJ/pulse (0.1 - 0.14 MW). A repetition rate of 1 Hz could be sustained but only for short periods of time due to a high degradation rate of the dye.

This type of laser is well known for emitting considerable radiation in the radio-frequency range as well as in the visible. Therefore, it is kept in a Faraday cage as designed by Rabb, Yerkes (1979), and Buttner (1983) to minimize electronic interference. Electrical interference from its firing is over in less than 100 ns.

2.3.4. Detector(s)

Devices normally used for the conversion of light into electrical signals are photomultipliers, phototubes, and photodiodes. All rely on a light sensitive surface to produce an electric current; however, the composition of the surfaces,

e

e

in

the

pho

tha

phot

field

the la

curren

drop b

release

voltage

the spectral sensitivity, methods for amplifying the photoelectric current, and the response times differ considerably. The reader is referred to Malmstadt *et al.* (1981) for general information on energy transducers. Specific information on PMTs and photodiodes can be obtained from individual manufacturers. It is important to realize that two PMTs, each made by a different manufacturer, may be completely unsuitable given differences in the materials used. These differences will show up in mean and maximum anode currents, amplication per stage, and maximum radiant intensity. An example of this is EMI-9558 (Gencom) and R622 (Hammamatsu). The Hammamatsu tube is cited as being a replacement for the EMI-9558, and it does appear to have an identical S-20 response. The difference arises in the peak anode current. The EMI tube is rated at 1mA whereas the R622 is rated only for 100 *u*A.

Photomultipliers (PMTs) and phototubes use a photocathodic surface to emit photoelectrons in response to an interaction of incident radiant energy with electrons in the photocathode material; i.e., photoemission. The photoelectrons in phototubes are collected directly onto the anode by a potential drop between the photocathode and anode with virtually no amplification. In PMTs the photoelectrons are accelerated and focused by an electric field to strike a dynode that in turn emits secondary electrons in response to the impact of the photoelectrons. These secondary electrons are in turn accelerated by an electric field toward the next dynode. This process is repeated until the electrons from the last dynode are collected by the anode, and leave the PMT as an electric current.

The electric field responsible for the acceleration is created by a potential drop between each successive element. The number of secondary electrons released per impact is a function of the photocathode material and the potential voltage drop between successive electrodes. Typically the amplification

experienced ranges from two to four depending upon the potential drop; there is an upper limit to the drop supplied.

Photodiodes rely on the light sensitivity of pn semiconductor junctions to generate a reverse-biased current. They do not possess the inherent amplification nor the spectral range of PMTs; however, photodiodes are capable of responding in the sub-nanosecond time scale, an order of magnitude or more faster than the response of PMTs. Often they are packaged with an internal amplifier to obtain better amplification while keeping the fast response.

Our detection system was designed for two detectors to be used depending upon the wavelength region of interest. Below 750 nm an EMI-9558QB photomultiplier tube (EMI-9558QB, 11-stage venetian blind, S-20 response, EMI Gencom, Inc., Plainview, NY) was used, and above 750 nm an FND-100H photodiode (EG&G Photon Devices, Salem, MA) was used. The mounts for each detector were made so that the housing could accomodate either with no other change in the setup of the apparatus. The photodiode and its accompanying circuitry fit onto a 3 inch diameter circuit board at the head of the detector housing. A cable transversing the distance between the circuit card and the back of the PMT where the pre-amplifiers are attached is required and is line balanced to minimize signal degradation.

Photodiodes have been best applied in the near-IR in time resolving primary donor reactions of the reaction centers. As discussed in Chapter One, the primary donor in photosynthesis is contained in the reaction center. The reaction center in green plants, P_{680}^{+}, has a characteristic absorption band at 820 nm. One of the first diode lasers, used with a diode detector, emits a usable line at 820 nm, and Van Best and Mathis (1979) were able to obtain extremely well resolved kinetic decays of P_{680}^{+} in the nanosecond time regime.

Though the use of photodiodes has been limited, recent developments have significantly enhanced the intrinsic signal amplification properties, and have extended the spectral responses of photodiodes further into the blue. The development of 'diode array' spectrometers by Hewlett-Packard and Perkin-Elmer, capable of collecting an entire optical absorption spectra at once, hold promise for the development of instrumentation capable of time-resolving entire spectra of fast changing multi-component systems such as those found in photosynthesis. This would represent a considerable enhancement over the current method of taking such a spectrum, which must now be done point-wise.

2.3.4.1. PMT Divider Chains

The potential drop, discussed in the previous section as responsible for the acceleration of the emitted secondary photoelectrons, is usually established by a resistive divider chain, though individual voltage sources could be used instead. Typical divider chain configurations are shown in Figure 2.5 (Dumont, 1963 and RCA, 1985). Normally the design of the divider chain is not part of the design consideration of the detector system. Standard configurations are commercially available for common applications; however, in our case, the requirements are such that the standard configurations are unsatisfactory as explained below.

In the literature, usage of PMTs and discussions concerning their usage falls into one of two classes: 1) low intensity light levels, relatively low time resolution, continuous illumination as found in a more typical scanning absorption spectrometer, or 2) high intensity, pulsed light levels, applications as found in a Raman spectrometer. In the former case a quick response of the divider chain and PMT to changes in the light intensity is unimportant, and the current requirements at the anode are low. Pulse applications, however, have high

a

r

th

si

us

the

a m

eas

radi

mW

addit

divide

and is

current requirement for brief periods, and the divider chains employ capacitors to act as current sources during heavy loads. Between pulses the capacitors recharge, and the time required for recharge is basically the RC time constant. This recharge problem makes their design untenable in a situation with a continuous high current.

Our experimental conditions require that the PMT and the divider chain have a linear and accurate response to small changes of light in high background levels of monochromatic radiation for periods of time lasting up to several seconds. In addition, the divider chain should have the capacity to recover quickly from sudden pulses of light that are orders of magnitude more intense than background incidence. Standard divider designs that accomodate low intensity or pulsed applications do not suffice.

If the current measured at the anode is greater than 5% of the current available in the divider chain then the divider chain has to be allowed time for recharging. This recharge time is dependent upon the current at the anode and the RC time constant. If the expected current will exceed this 5 % limit the simplest solution is to use resistors with a lower resistance. As an example, if the usual operating voltage is 1000 v, each resistor is valued at 200 Kohms, and there are 10 stages; the total current available would be 0.5 mA. This would allow a maximum current at the anode of 0.025 mA. The maximum current could easily be doubled by using 100 Kohm resistors instead; however, the heat radiated by the resistors, I^2R, would now be 25 mW, up by a factor of 4 from 6 mW. Unless cooled, or forced air ventilation, or both is used in the housing the additional heat production will have a deleterious effect on the PMT, and the divider chain, and an inaccurate and noisy output signal will result.

A reasonable design for the divider chain was reached by trial and error and is as shown in Figure 2.6. Capacitors are wired in parallel instead of in

series as shown in Figure 2.5. Referencing the dynodes to ground localizes any possible, sudden drop in the voltage between any two dynodes as a result of current surges. The first two dynodes use 100 V zener diodes to force a constant voltage drop. Dynodes #9 through #11 are open, and dynode #8 serves as the anode. This reduces the amplification by roughly a factor of 10 per stage for a total reduction of 1000, but the cathode can now be operated at a higher and therefore more sensitive potential.

2.3.4.2. Simple Tests

We were able to get an accurate response model from deep in the UV (250 nm) into the blue-green (350 nm), see Figure 2.10. Further, this demonstrates that fractional changes in relative concentrations, dilutions by 0.95 and 0.90, are shown to be reflected correctly. Figure 2.11 shows the linearity of the photomultiplier at 320 nm at 1/10 of the amplification used in real experiments.

2.3.5. Analog Electronics

The signal processing performed by the analog electronics is shown in Figure 2.12. The reasons for two signal processing channels will be explained in the following sections.

2.3.5.1. Relating Measured Light Intensities to Absorption

Beer's law, as described earlier in Equations 2.1, 2.2, and 2.3, allowed us to linearly relate the changes of observed light intensity to concentration. From Equation 2.3, this defined the absolute absorption of the sample, and required information about 'I_0', the incident radiant intensity. Experimentally, with a single beam spectrometer, the determination of I_0 is awkward. Fortunately, we are only

interested in the absorption relative to the absorption before excitation. We can thus write:

$$dA = A^f - A^i$$

$$= -\log(I^f/I^f_o) - (-\log(I^i/I^i_o)$$

$$= \log(I^i/I^i_o) - \log(I^f/I^f_o) \qquad (2.4)$$

'I^i_o' and 'I^f_o' are the radiant intensities upon the sample before and during excitation and it is reasonable to assume that these do not change; i.e., $I^f_o = I^i_o$. Rearranging cancels out the unabsorbed radiant intensity terms and we have:

$$dA = \log(I^f/I^i) \qquad (2.5)$$

The quantities I^i and I^f can be replaced by their voltage equivalents as the current response of either detector is linear with respect to light intensity. Substituting V_{off} for I^i and rewriting I^f in terms of V_{off} and dV:

$$dA = \log(V_{off}/(V_{off} - dV)) \qquad (2.6)$$

Use of Equation 2.6 indicates that determination of relative absorption changes requires information about the initial amount of transmitted light through the sample, V_{off}, and continuous information regarding the change in intensity relative to the initial value, dV. This is still an awkward equation to deal with experimentally, but only from the aspect of performing the mathematical manipulations, the division and logarithmic operations, not from the aspect of selecting the individual values.

c

a

n

sa

ou

cap

cap

cha

inve

to *gi*

mode

charg

signal

referen

signal

Figure

2.3.5.2. Detector Amplifier Circuitry.

Obviously, the difference, dV, in Equation 2.6 is critical as it is a direct determination of the extent of the changes of the photosynthetic samples. Analogue to digital converters (ADCs) typically span a voltage range, e.g., +5.0 V to -5.0 V. If an ADC has 8 bits, that means that a 10 V span will have 256 divisions, or 39 mV per division. An absorption change of 10^{-4} on a background of 10 V corresponds to a change of 40 mV; i.e., 1 division. If the 10 V background level was removed from the signal a maximum amplification factor of 250 could be applied to fill the digitizing window of the ADCs (see Figure 2.9) with kinetic information as opposed to just the background.

The separation of the analogue signal into separate baseline and differential channels required a complete redesign of the detector pre-amplifier and amplifier circuitry (Figure 2.2) as well as of the storage ADC itself. The signal from the detector and pre-amplifier are simultaneously input into a tracking sample and hold amplifier (SHA) and a normal cascade amplifier chain. The output signal from the tracking SHA is split into two. One side is connected to a capacitor referenced to ground. This has the effect of storing a charge on the capacitor equal to the voltage output from the tracking SHA, and this charge changes as the output changes. The other output from the tracking SHA is inverted and summed (resulting in a subtraction operation) with the original signal to give a final signal that is zeroed. When triggered, the SHA enters into a 'hold' mode, the pre-amplifier input is disconnected from the capacitor, and uses the charge stored on the capacitor to provide its output; this then forms the reference signal. Changes in input levels are summed with respect to the inverted original reference, and the final output signal is one in which the background reference signal has been removed; the effects of this on the signal are also shown in Figure 2.7.

Two difficulties with this design revolve around the use of an analog SHA. A consistent droop is induced into the output signal during the hold phase, and this is because the discharge of the capacitor is exponential. There are also slight phase problems resulting in the introduction of some spurious frequencies, and these are related again to the use of a capacitor. Replacing the analogue capacitor storage system with a digital system that uses a separate analogue to digital and digital to analogue converters would solve both of these problems. When in a hold mode, the reference charge would be maintained digitally and would not droop.

2.3.5.3. Final Filtering.

One of the drawbacks to digital sampling of analogue signals is the possibility for aliasing - the introduction of spurious frequencies into a sampled digital signal due to undersampling of high frequency components (Cooper, 1978) These high frequency components are those that are present in the input signal that are higher than allowed by the Nyquist sampling theorem. (a rather simple explanation of this theorem is given by Swanson *et al.*, 1975) This sampling theorem states that the sampling rate must be greater than twice the highest frequency component in the signal. As an example, if a signal contains a component of of 1 MHz frequency, then the signal must be sampled at a rate no slower than 2 MHz.

To prevent the introduction of these high frequencies as spurious low frequencies, a fourth order filter (see Figure 2.3 for the diagram and Figure 2.4 for rolloff characteristics) was designed and used to process the differential channel signal before digitization to prevent aliasing errors. While not proving to be critical for the information presented in this dissertation because of the relatively low sampling rates reported here, a distinct benefit accrued as the filter

eliminated high frequency ringing components that occasionally triggered the entire system into oscillation.

As an aside, it is not quite true that sampling must be performed at twice the desired signal frequency for accurate digitization. A practice known as interleaving may be performed and, depending upon the degree of interleaving, essentially the frequency of the signal to be sampled will be independent of the frequency at which the signal can be sampled. A discussion on this interleaving may be found by Verdun *et al.* (1988). Basically, assume a signal with a frequency of 1 MHz and a maximum sampling rate of 1 MHz. The first digitization run on the data is stored and then the second digitization run is delayed by one half of thes sampling period. Store this second run with the first run and the two summed together equal one digitization run sampled at 2 MHz. In this fashion high frequency signal frequencies can be sampled with less expensive components with only a tradeoff in terms of the total amount of time required to collect the data.

2.4. CONCLUSION

Frequently, problem occurrences were masked by others. As an example, one baffling problem, though simply solved, was caused by the rotation of a bar magnet in a stir plate near the output light beam from the xenon arc lamp. There was no effect on the low-impedance analog signal lines that were positioned nearby, nor was was there any coupling of a mechanical vibration onto the spectrometer platform. However, a distinct, ~60 Hz oscillation of the probe beam intensity was observed, and this is usually indicative of A.C. line current coupling into the signal lines. It finally turned out that the rotation of a magnetic bar in a nearby stir plate at a frequency of ~60 Hz was inducing the oscillation observed. Only through a coincidental movement of the stir plate and noticing

the removal of the periodic component from the probe beam on an oscillation was this particular problem resolved.

2.4.1. Susceptibility to mechanical vibrations

The spectrometer, light source, monochromator, detector, and all structural supports, were mounted on a heavy rigid platform. This platform was supported by labjacks that were in turn isolation mounted on a regular laboratory bench. Isolation mounting can only be done when the platform is heavy enough to compress the isolation cushion by a significant amount. Otherwise, mechanical vibrations continue to couple into the platform. This particular problem is expected to be rectified when the equipment is remounted on an isolation table designed for this.

2.4.2. Imprecise Optical Feedback Control of Xenon Arc Lamp.

A second problem, though, is much more difficult to solve and rises largely because of the single beam design. The small area design of the electrode tips and current feedback loop of the xenon arc lamp allow the stability of the probe beam to be only tolerable at best. While better stability can be achieved with a tungsten-halogen lamp, the lamp output is decreased considerably, particularly in the UV and near-UV, and the detection problems encountered in the prototype due to too low of a probe beam intensity resurface.

The self-correcting aspect of a dual beam spectrometer can be obtained via an additional feed-back path. A beam-splitter could be inserted into the path of the probe and a fraction diverted to a photodiode. The output from the photodiode, properly amplified, could be used to correct fluctuations in the PMT output due solely to fluctuations in the arc lamp. The only remaining optical problem then remaining would be uncorrected changes in sample absorption due

to probe beam photochemistry, and, as demonstrated, if the exposure before excitation is kept under 15 ms this will not be a problem.

2.4.3. Alternative Approaches

Apparently, the group led by Van Gorkom in Germany (Dekker, 1988) has taken a somewhat different tack in their experimental setup. It was earlier shown that the magnitude of the intensity changes in a probe beam is related to the intensity of the probe. Therefore, the traditional approach has been to use as intense of a probe beam as possible given other constraints such as probe-induced photochemistry (Junge, 1976). According to Dekker, their group uses a defocused probe of low intensity. This allows them to run their optical experiments with the samples continuously exposed to the probe light.

From a technical point of view these differences in experimental technique has two principal advantages: 1) Mechanical vibrations that couple into the platform from the opening and closing of the shutter are no longer a factor as the shutter is left open during the course of an experiment. 2) Steady state and transient response demands of the PMT are not as severe as the constraints imposed by our design. Our design requires that the PMT has recovered and is tracking accurately with a few milliseconds after the shutter has opened and the sample exposed to an intense probe beam.

From an experimental point of view, this methodology raises the question of what is happening with the sample that is being continually exposed to low-level illumination. It is entirely possible that the low-level illumination modifies the short term dark adapted S-state distribution and this in turn would affect the S-state absorbance spectra. Model results bear this out; Lavergne (1986) and Saygin and Witt (1985) have modeled transient absorbance changes of the OEC that clearly show differences of the absorption change patterns merely by altering

the initial S-state distribution. Unfortunately the existing experimental data (Saygin and Witt, 1985) does not select one distribution over another.

FIGURE 2.1

Block Diagram of Flash Absorption Spectrometer

Dashed lines indicate control lines, block arrow lines are data pathways. single lines are signal carrying lines (either analogue or digital). Components in this Diagram are from those discussed in Chapters Two and Three. The PDP-11 computer is shown as being central. Data pathways go out to the Timing Controller and to the Fast/Ultrafast ADC. The Timing Controller provides the direct control over the other components shown. The Fast/Ultrafast ADC digitizes the analogue signal output from the Amplifier, and is transferred.

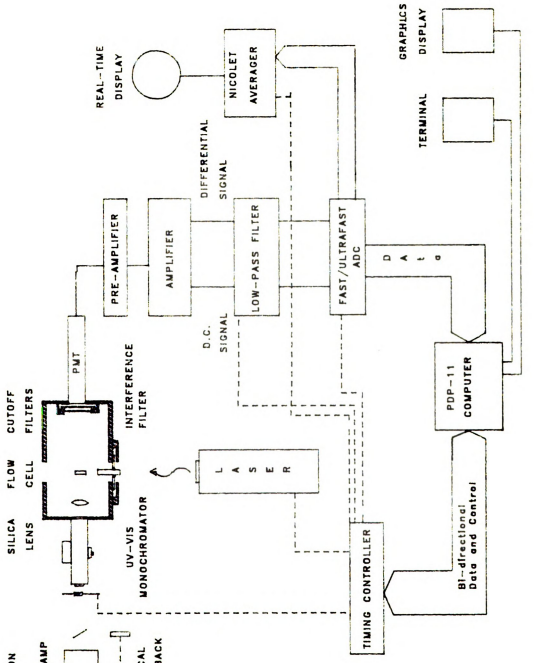
XENON
ARC-LAMP
OPTICAL
FEED-BACK
SILICA
LENS
FLOW
CELL
CUTOFF
FILTERS
UV-VIS
MONOCHROMATOR
PMT
INTERFERENCE
FILTER
L
A
S
E
R
PRE-AMPLIFIER
AMPLIFIER
LOW-PASS FILTER
D.C.
SIGNAL
DIFFERENTIAL
SIGNAL
FAST/ULTRAFAST
ADC
NICOLET
AVERAGER
REAL-TIME
DISPLAY
D
A
t
a
PDP-11
COMPUTER
TIMING CONTROLLER
Bi-directional
Data and Control
TERMINAL
GRAPHICS
DISPLAY

FIGURE 2.2

Amplifier Circuitry for PMT.

This circuitry was designed by Marty Rabb and Dwight Lillie, and provides cascade amplification and active low-pass filtering. It has a maximum frequency response of 2 Mhz. Two output signals are provided; SIGNAL OUTPUT, contains the kinetic signal along with the baseline, and RESTORED SIGNAL OUTPUT, which has had the baseline subtracted.

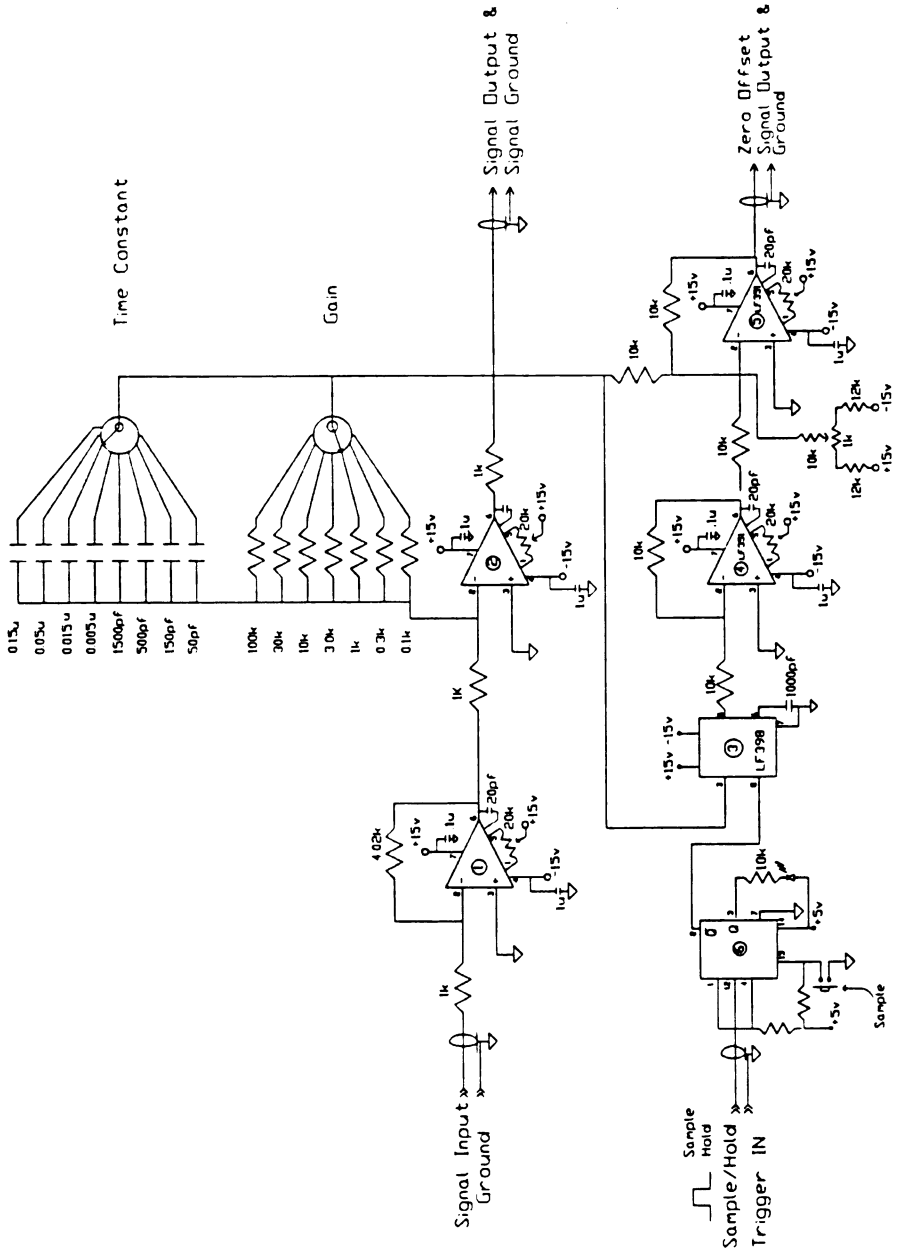
Time Constant
Gain
Signal Output &
Signal Ground
Zero Offset
Signal Output &
Ground
0.15u
0.05u
0.015u
0.005u
1500pf
500pf
150pf
50pf
100k
30k
10k
3.0k
1k
0.3k
0.1k
1K
402k
10k
1000pf
20pf
20k
1u
+15v
-15v
+5v
LF398
Signal Input
Ground
Sample/Hold
Trigger IN
Sample
Hold
Sample

FIGURE 2.3

Fourth order low-pass filter.

This is a series of two cascaded multiple feedback 2nd order low pass filters. The response characteristics of this filter compared to several others is in the next Figure. C_1 = 100pF, C_2 = 22pF, R_1 = 1K, R_2 = 4.7K.

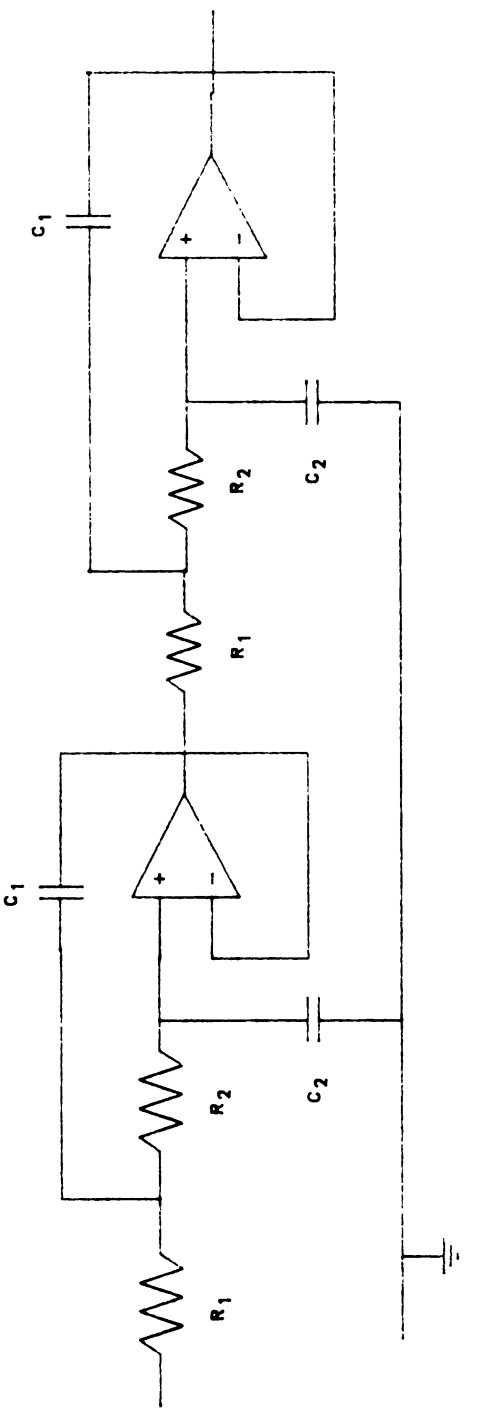
C1
C1
R2
C2
R2
C2
R1
R1

FIGURE 2.4

Roll-off characteristics of Active Low Pass Filters

These characteristics were collected as a result of building and evaluating a series of active low pass filters for final filtering. '.' 4th order filter built from two cascaded 2nd 0.3dB Chebyshev filters. 'x' Modified 2nd order 0.3db Chebyshev. '*' 2nd order 0.3dB Butterworth. 'o' 2nd order 0.3db Chebyshev. '+' Simple passive RC filter. Most advantageous about the filter selected, the 4th order filter, is the steep roll-off characteristics at the $f/f_c = 1.0$ point. Two of the 2nd order filters exhibit significant attenuation before the 0.3dB point, and the other two have significant oscillation before (not shown due to scale of plot) the turnover point.

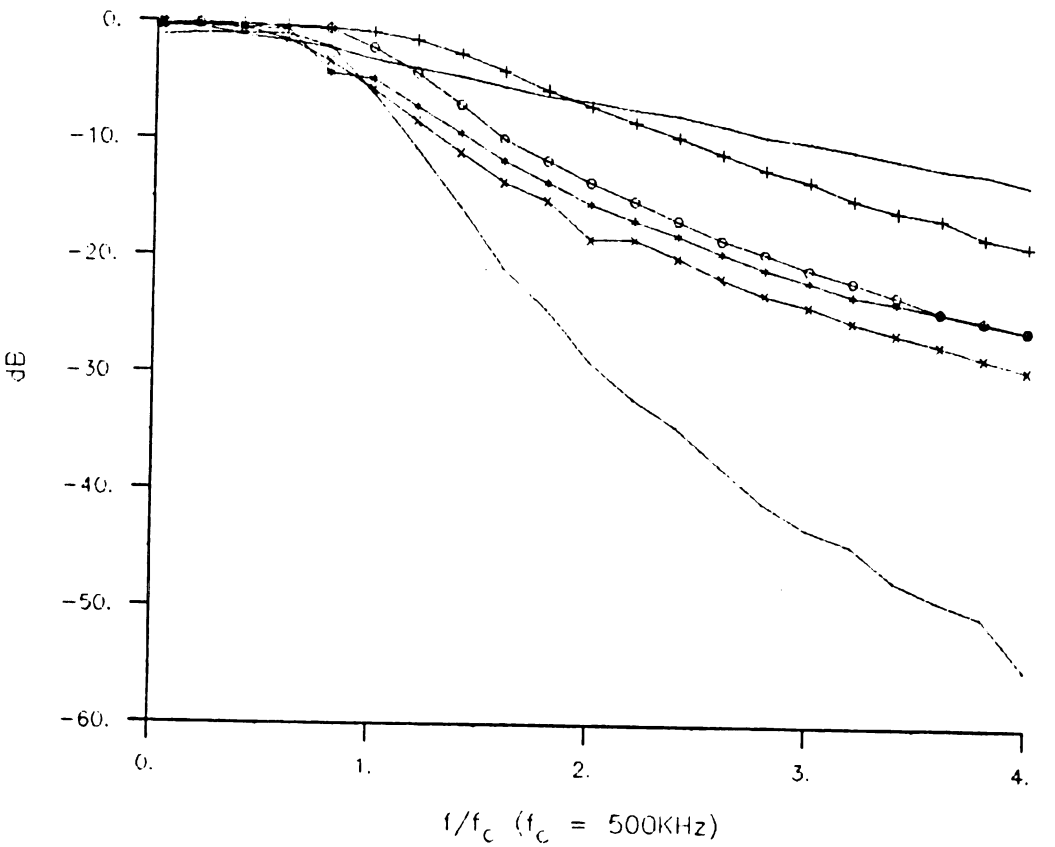
0.
-10.
-20.
-30
-40.
-50.
-60.
dB
0.
1.
2.
3.
4.
f/f_c (f_c = 500KHz)

FIGURE 2.5

Typical Dynode Chains for PMTs

Two designs are shown here. The first design is typical of that used in relatively low intensity, continuously scanning spectrometers. The second design is typical of that found in Raman spectrometers. The series connected capacitors are required only for those dynodes which may be expected to have a peak dynode current of 1/10 of the average current through the entire network. Series connecting the dynodes allows use of lower rated capacitors. R_1 is typically three times the resistance of R_2 R_n. C_1, C_2, and C_3 are on the order of 0.005 *u*F.

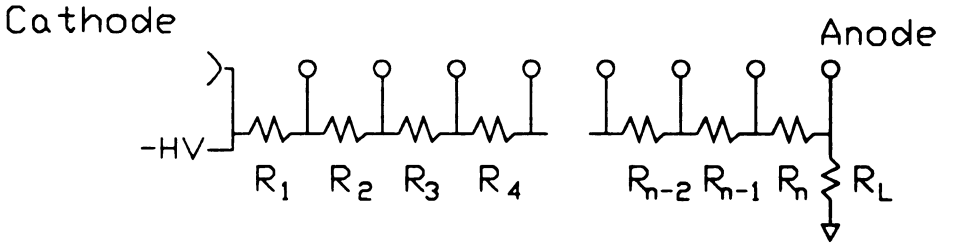
Cathode
Anode
-HV
R1 R2 R3 R4
Rn-2 Rn-1 Rn RL

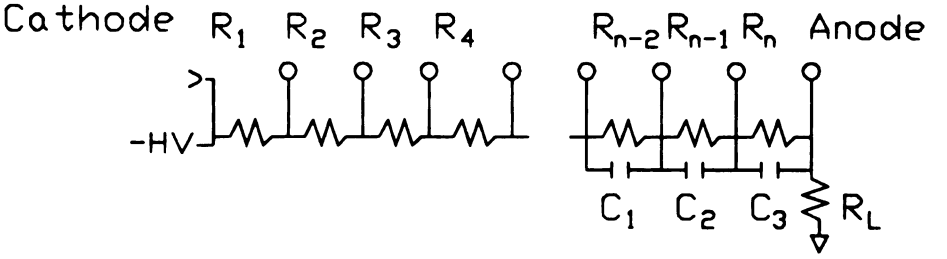
Cathode
R1 R2 R3 R4
Rn-2 Rn-1 Rn Anode
-HV
C1 C2 C3 RL

FIGURE 2.6

Dynode Wiring Design.

This figure shows the divider chain design we adopted. In place of the first two resistors of Figure 2.5, R_1 and R_2, two Zener dynodes are used instead. This insures that the potential drop between the first two dynodes does not change. The rest of the resistors are of the same value. The last four dynodes are left unconnected and dynode 7 is used as the anode. Dynodes 4 through 7 have parallel connected capacitors instead of series connected. This requires capacitors of higher rating, but changes in the potential drop are localized instead of being echoed to neighboring dynodes.

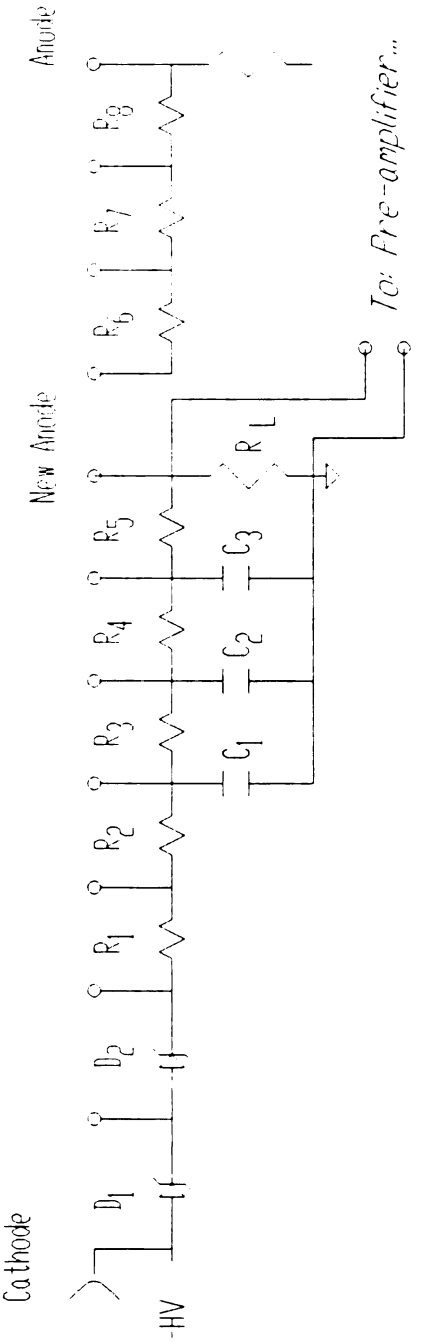
Anode
New Anode
Cathode
-HV
D1
D2
R1
R2
R3
R4
R5
R6
R7
R8
C1
C2
C3
RL
To: Pre-amplifier...

FIGURE 2.7

Events during a Single Flash Sequence

This figure depicts the events that occur during a single sequence. This particular sequence is part of an experiment which is doing repetitive single shot excitation of a sample. Between sequences the sample chamber is continuously flushed from a resovoir of photosynthetic material. Both of the amplifier outputs, which are digitized by the fast and slow Analog to Digital converters, are shown and their relative level(s) with respect to one another. The slow ADC is only concerned with establishment of a baseline level so it handles the Output Signal line. Note that the 'RESTORED' Output Signal only contains useful information after the ADCs are triggered to begin conversion, Pulse 4. The ADCs only convert for a finite period of time and will complete before the shutter is closed, Pulse #6.

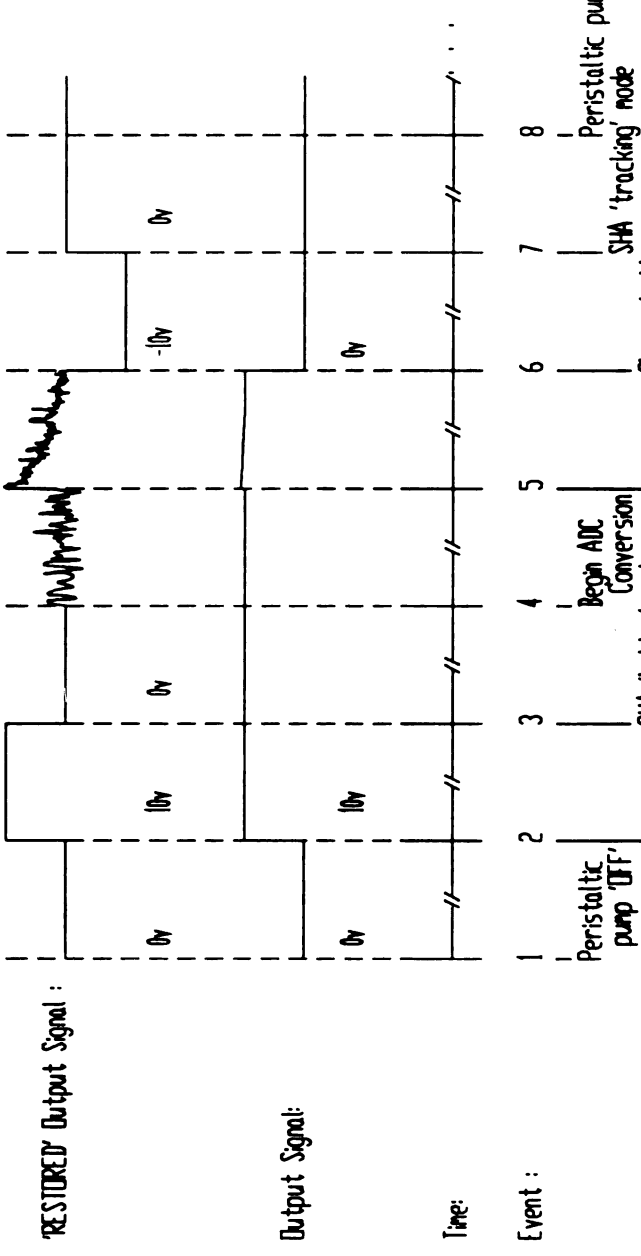
'RESTORED' Output Signal :
0v
10v
0v
-10v
0v
Output Signal:
0v
10v
0v
Time:
Event :
1
Peristaltic pump 'OFF'
2
Open shutter
3
S/H 'holding' mode
4
Begin A/D Conversion
5
Laser Triggered
6
Close shutter
7
S/H 'tracking' mode
8
Peristaltic pump 'OFF'

FIGURE 2.8

Occurrence of Events During Multiple Sequences.

This figure depicts some of the events that must occur during between each flash sequence. The example chosen here is a four flash iteration and each flash sequence is numbered in the order it occurred. The delay times between each flash sequence is constant, except between the fourth and the start of the next iteration. The pump for purging the sample chamber is shut down at the beginning of a cycle and started at the end of the same cycle, the intervening flash sequences do not trigger it. This figure coincidentally displays one of the difficulties we had with multiple flash iterations. Each trace is the average of 16 iterations. The large droop at the the first flash is the result of a door slamming during one flash sequence.

Stop sample chamber flush
load timers
delay fixed time
trigger
(shutter closes)
1024 points uploaded, processed,
summed, and stored in temporary
load timers
delay intra-sequence delay time _#1
trigger
(shutter closes)
1024 points uploaded, processed,
summed, and stored in temporary
load timers
delay intra-sequence delay time _#2
trigger
(shutter closes)
1024 points uploaded, processed,
summed, and stored in temporary
load timers
delay intra-sequence delay time _#3
trigger
(shutter closes)
1024 points uploaded, processed,
summed, and stored in temporary
Begin sample chamber flush
load timers
delay intra-sequence group delay time

FIGURE 2.9

Removal of background level from signal.

This figure contains two plots of simulated data. The top plot shows a kinetic signal with a maximum change of 40 mV plus a background of 10 V. This is typical of a normal signal. Resolution of the kinetics is impossible because the background completely fills the digitizing window. The bottom plot shows the kinetic signal after subtraction of the background and subsequent amplification by 250. This half fills the digitizing window.

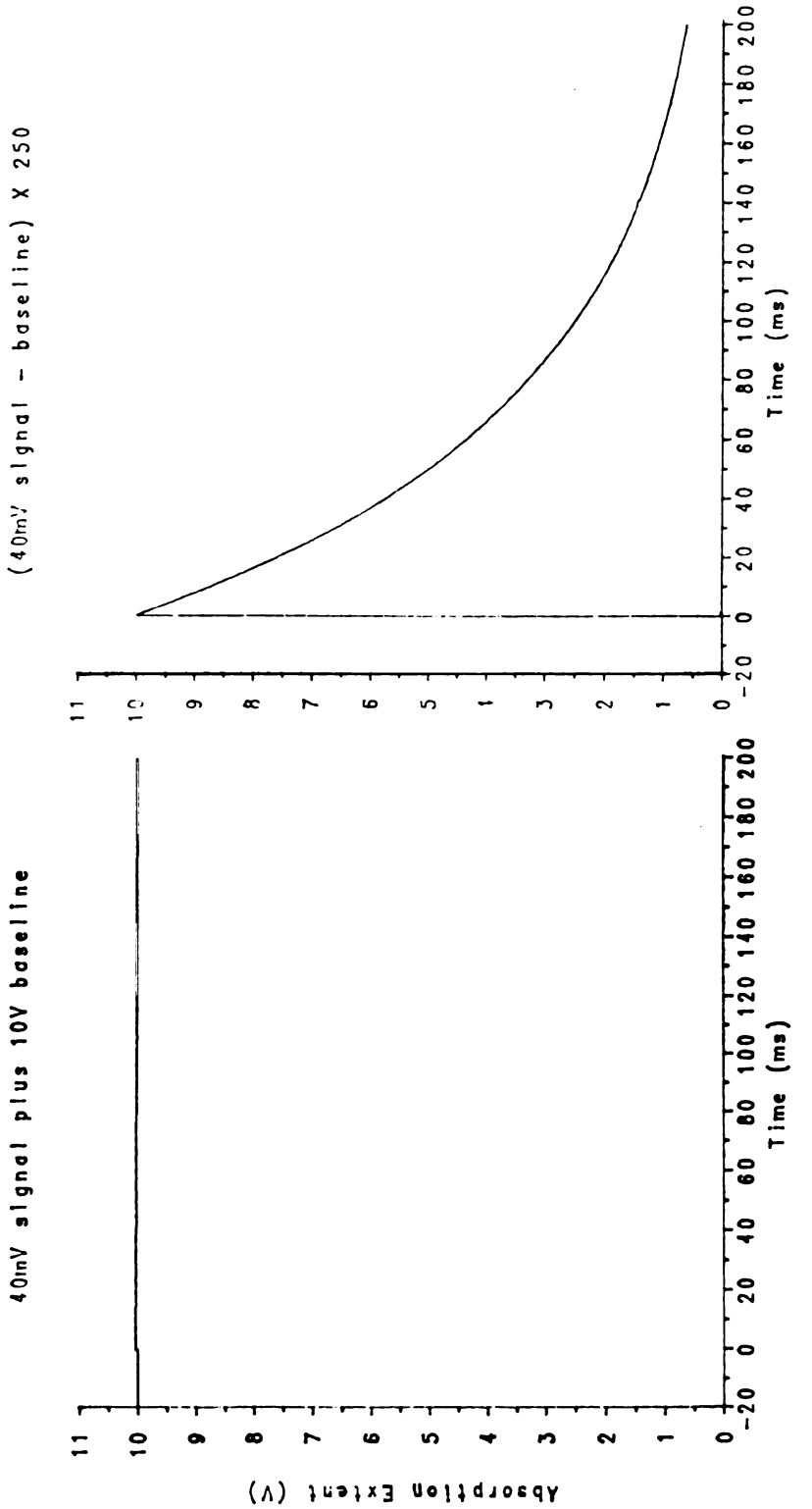
40mV signal plus 10V baseline
(40mV signal - baseline) X 250
Absorption Extent (V)
Time (ms)
Time (ms)

Figure 2.10

PMT accuracy response from 250 nm to 350 nm.

This figure demonstrates the linearity and discrimination of the PMT and the amplification system from 250 to 350 nm. ferricyanide at a stock concentration of 0.625 M in water was diluted to relative concentrations of 0.95 (0.5938 M) and 0.90 (0.5625 M). The absorption spectra of each dilution was taken with the FAS spectrometer. Data was collected by the Nicolet 1074 operating in a slow sweep mode while the grating of the monochromater was driven mechanically from 250 nm to 350 nm. PMT voltage was 600 V, amplification at 1/10. Absolute absorption scale was greater than 2.0, scale shown has been normalized.

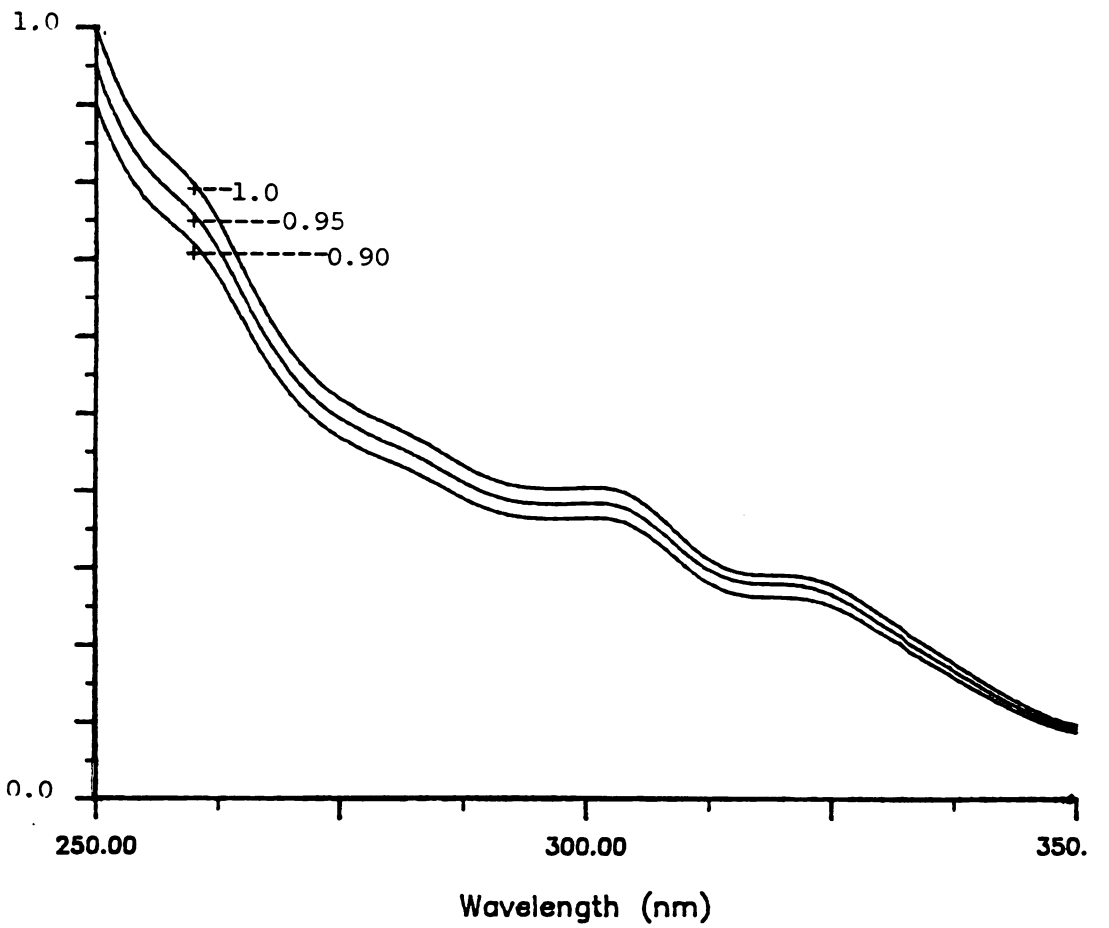
1.0
0.0
1.0
0.95
0.90
250.00
300.00
350.
Wavelength (nm)

FIGURE 2.11

PMT Linearity

This figure demonstrates the linearity of the EMI-9558QB PMT and the amplification system at 300 nm from 0% to 100% transmission. The amplification factor was 0.1 and the voltage range output from the system was 10.4 V at 100% T and 0.0 V at 0% T. PMT voltage was set to 600 V. The transmission was determined through a set of neutral density filters. Three separate sets of experiments were conducted over the course of three weeks. One test occurred immediately after turning on the system, the second test occured just before an experiment, and the third set occured just after a 12 hour experiment (the PMT was not exposed ambient light during the entire 12 hours).

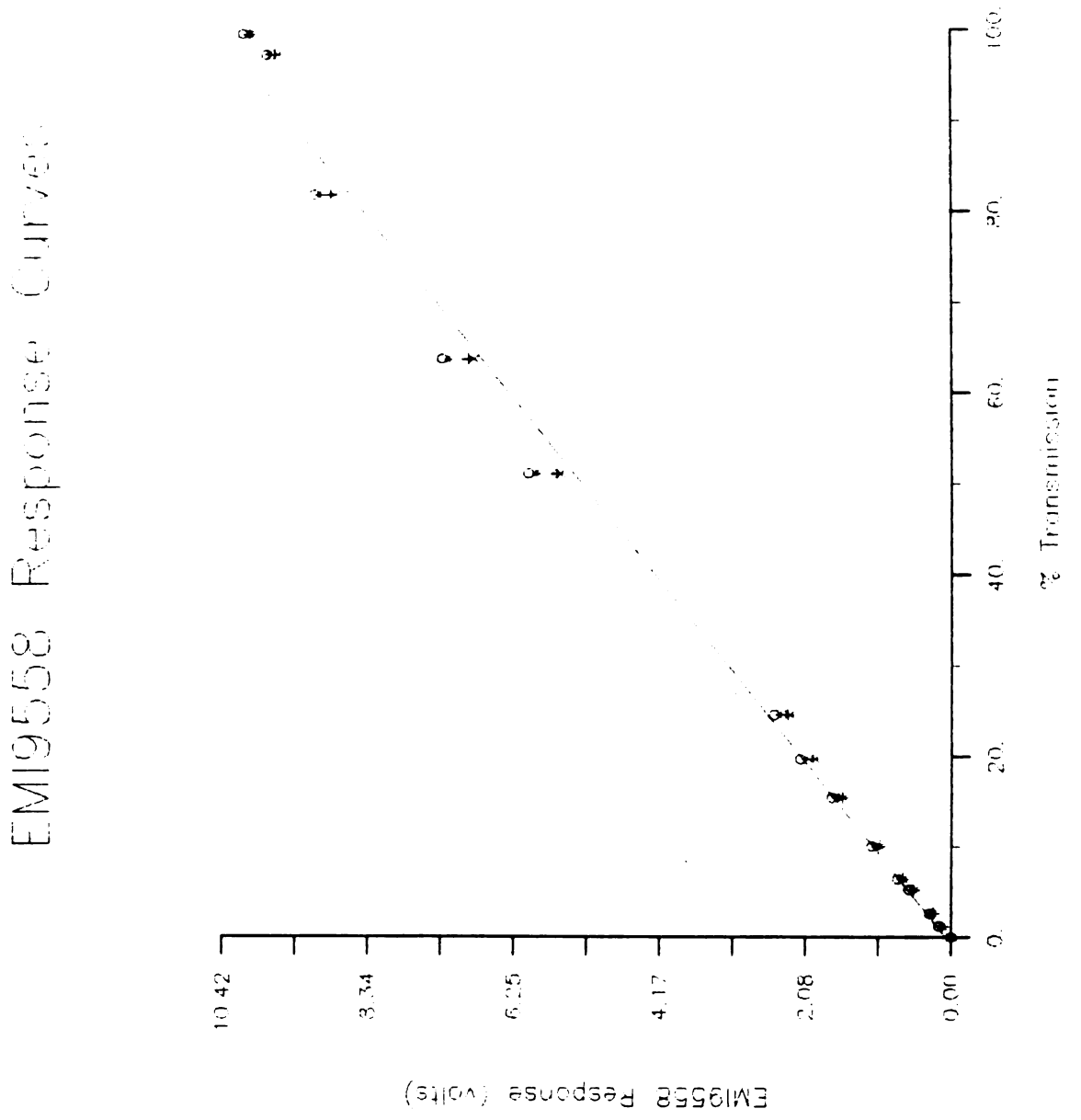
EM9558 Response Curves
EM9558 Response (volts)
10.42
8.34
6.25
4.17
2.08
0.00
0.
20.
40.
60.
80.
100.
% Transmission

FIGURE 2.12

Layout of Analog Signal Processing

The separation of the analog signal from the PMT into two channels for signal processing is demonstrated. The analog signal from the PMT is comprised of both the background and the kinetic signal components. The SHA is used to lock onto the background level, this is then inverted and subtracted from the original analog signal. The result is a separate channel containing only the kinetic components. The kinetic signal is amplified to fill the digitizer window, digitized, and stored in the ADC memory buffers. The background level is digitized and stored in the ADC memory buffers. The digitized data is retrieved at some point under computer control.

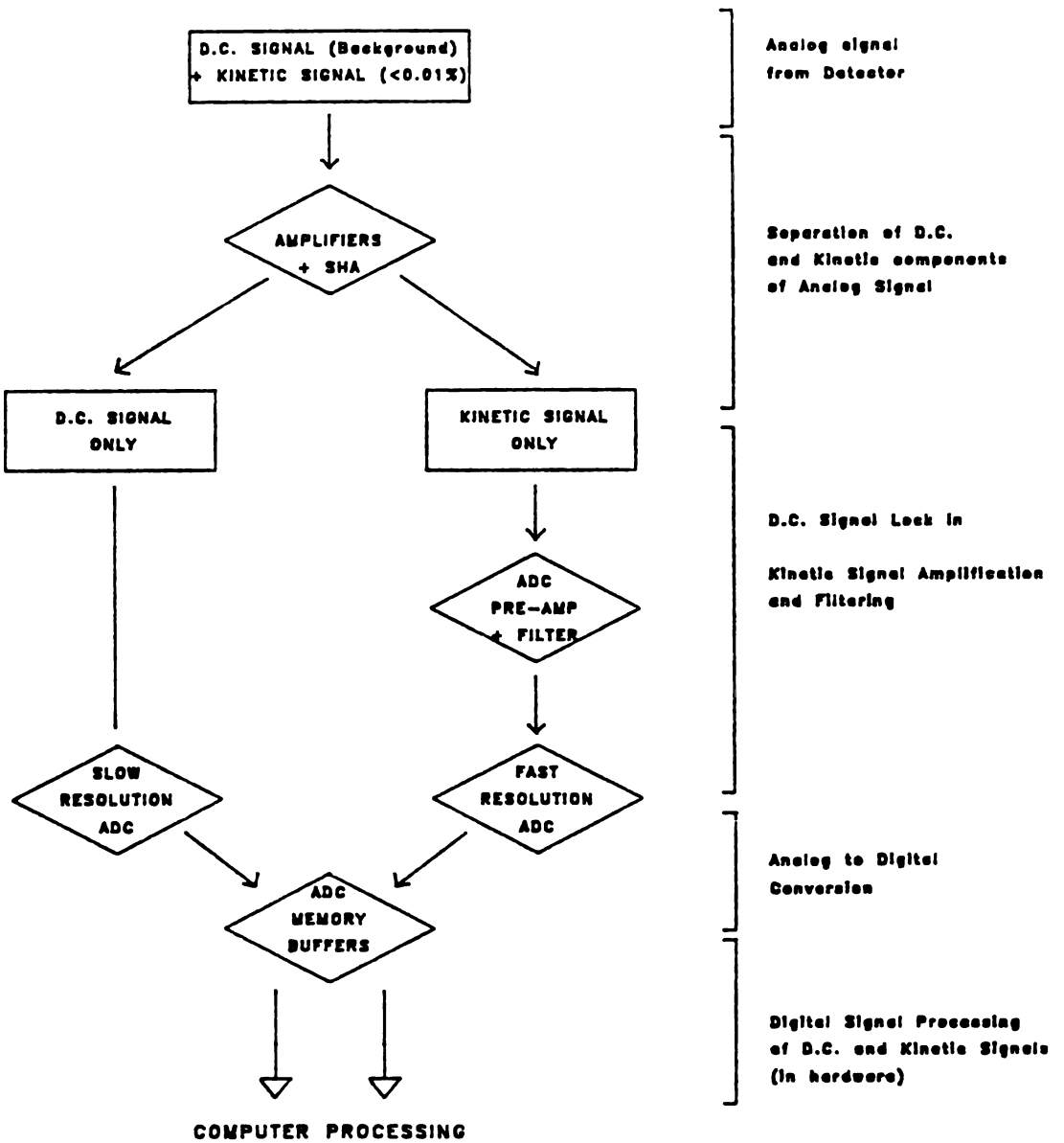
D.C. SIGNAL (Background)
+ KINETIC SIGNAL (<0.01%)
AMPLIFIERS
+ SHA
D.C. SIGNAL
ONLY
KINETIC SIGNAL
ONLY
ADC
PRE-AMP
+ FILTER
SLOW
RESOLUTION
ADC
FAST
RESOLUTION
ADC
ADC
MEMORY
BUFFERS
COMPUTER PROCESSING
Analog signal
from Detector
Separation of D.C.
and Kinetic components
of Analog Signal
D.C. Signal Lock in
Kinetic Signal Amplification
and Filtering
Analog to Digital
Conversion
Digital Signal Processing
of D.C. and Kinetic Signals
(in hardware)

REFERENCES

Buttner, B., (1983) Ph.D. Thesis, "Induced and Natural Delayed Luminescence of Green Plant Photosynthesis", M.S.U.

Cooper, J. W. (1978). "Tranform Techniques in Chemistry," Chapter 4, 72-74, (Griffiths, P. R., ed.), Plenum Press, N.Y.

Dekker, J. P. (1988). Private communication with Dr. Dekker after he accepted a joint Post-Doctoral position with Professors G. T. Babcock (M.S.U) an C. F. Yocum (Univ. of Mich.).

"Du Mont Multiplier Phototubes" (1963). Fairchild Dumont Laboratories, Clifton, NJ.

Junge, W., (1976) "Chemistry and Biochemistry of Plant Pigments," Volume II, Chapter 22, (Goodwin, T. W., ed.), Academic Press, N.Y.

Junge, W. and Jackson, J. B. (1982). "Photosynthesis: Energy Conversion by Plants and Bacteria", Volume I, Chapter 13, (Govindjee, ed.) Academic Press, N.Y.

Lavergne, J. (1986). Photochemistry and Photobiology, **43**, 311-317.

Lillie, D., (1984) M.S. Thesis, "The Development and Characterization of a Flash Kinetic Absorption Spectrometer", M.S.U.

Malmstadt, H. V., Enke, C. G., and Crouch, S. R. (1981). "Electronics and Instrumentation for Scientists", Chapters 3 and 4, The Benjamin/Cummings Publishing Company, Inc., CA

"RCA Photomultiplier Manual" (1985). RCA Corporation.

Sawnson, R., Thoennes, D. J., Williams, R. C., and Wilkins, C. L. (1975). Journal of Chemical Education, **52**, 530-533.

Saygin, O. and Witt, H. T. (1985). Photochemistry and Photobiophysics, **10**, 71-82.

Yerkes, C., (1979) M.S. Thesis, "The Kinetics of Electron Transport in Chloroplast Photosystem II", M.S.U.

Van Best, J., and Mathis, P. (1979). Photochemistry Photobiology, **31**, 89-92.

Verdun, F. R., Ricca, T. L., and Marshall, A. G., (1988). Applied Spectroscopy, **42**, 199-203.

CHAPTER 3

INSTRUMENT DEVELOPMENT - COMPUTER SUPPORT

3.1. Introduction

Complementing the efforts in the spectrometer design have been equal efforts in the areas of computer hardware, software, and interface design to support the instrumental apparatus. The computer used in the prototype was an AIM-65 microcomputer (Rockwell Industries) with 4Kb of RAM memory. The original program development facilities consisted entirely of a BASIC interpreter in ROM, an Assembler in ROM, a primitive line editor, manual cassette tape for mass storage, a 20 character wide single line LED display, and a 20 character wide thermal printer.

The first effort added hardware to support communication with a video or hardcopy terminal. This modification resulted in our ability to examine listings and quickly determine errors in the code. We also connected this communication port to a PDP-11/02, developed communications software, and allowed the PDP-11 to handle the output from the Aim-65. At this point we could then conduct an experiment, and transfer the results from the NICOLET 1074 through the Aim-65 to the PDP-11. The communications software on the PDP-11 would transfer this information to a disk file. A typical experiment would collect 1023 points and the time to transfer these points out of the NICOLET 1074 to the disk file on the PDP-11 exceeded 90 seconds.

The second attempt upgraded the memory of the AIM-65 to 32Kb, re-wrote the Aim-65 control Monitor, wrote a cross-assembler for the 6502 processor to compile the re-written monitor program, added code in the monitor to support true interrupt communications, added additional hardware for the communications, and added the FORTH language. The memory upgrade was to allow a set of successive turnovers of the reaction center to be collected in separate data channels. Rewriting the control monitor and improved communications hardware decreased the time required for data transfer between the AIM-65 and the PDP-11. FORTH is a language has proven to be quite versatile in instrument control systems and it had been hoped we could bypass the difficulties being encountered in mixing BASIC and 6502 assembly.

We were still hampered by mass-storage deficiencies, large timing granularities (discussed later), inadequate memory, and a slow processor. Owing to the access in our laboratory to a Digital Equipment Corporation (DEC) PDP11/23 with the RSX-11M operating system, it was decided to forego any further development with the Aim-65 and base future computer development and support on the PDP-11 rather than continue with the AIM-65 or purchase a IBM-PC type computer. Comparisons of the resources of the Aim-65 and the IBM-PC computer relative to the PDP-11 and IBM-PC are listed in Tables 3.1 and 3.2. Another option available would have been to use a PDP-11 with RT-11, a single-tasking, single user operating system. However, the limitations of the PC based solutions, mainly single task execution, would also have existed.

This chapter will establish the computer resources needed and detail the hardware, software, and instrument interface designed to support the FAS spectrometer. Finally, we discuss whether the path chosen was wise in light of the cost and predominance of PC-type computers and software.

This chapter and the previous one examine at a detailed level the implementation of the FASCI on a component and system level. The user manual for use of the instrument is presented in Appendix A. This should provide a different view of the instrument and its capabilities.

3.1.1. Overview

In the previous chapter we examined in some detail the experimental scenarios and the instrumental requirements. While it is not necessary to go into that detail again, we will return to Figure 2.8 and Equation 2.6.

3.1.1.1. Timing Control for Events.

Figure 2.8 reveals that a number of events occur during the course of an experiment, and that they all occur in controlled time intervals. The timing pattern shown in this particular case is complex and common enough to require that it be easily performed. Time resolution ranging from seconds to microseconds is required for intra-sequence time delays. An intra-sequence time delay is the delay between two consecutive pulses occuring within a sequence. A resolution of seconds to minutes are required for the inter-sequence time delays. An inter-sequence time delay is the delay between two consecutive sequences. Adding to the complexity is the need for inter-sequence delays to be variable to accomodate larger cycles that occur over several sequences, and the need to add or delete individual pulses on a sequence dependent basis.

In the particular case of Figure 2.8, there are four channels of data that must be independently stored, manipulated, and displayed. Individual banks of memory can be built and access protocols devised so that the ADC supports four separate chanels. Simultaneous read of one channel by the computer and write on another channel by the ADC is allowed; however, the maximum number of

separate channels is in the range of 16 to 32 channels, and this then incurs a prohibitive cost.

An easier solution to the channel problem can be arrived at by using the computer to store the channels. The need for more channels than originally designed can be adjusted by modifying the storage space requested by the programs and changing the algorithm limits to accomodate the new upper bound. The difficulty of designing a hardwired timing controller with the ability for conditional pulse generation and alternative delay cycles can also be avoided by using a computer and a series of programmable digital timers with maskable or optionally selectable output signals.

3.1.1.2. Absorption Determination

Equation 2.6 reveals that the information collected by the ADCs, the inital offset voltage and a series of difference voltages, can be used to determine the relative absorption changes. Analogue circuitry can be constructed to perform the division and logarithmic calculations; however, they operate at a rate much slower than the upper data collection rates. Again, the computer can be used to receive the raw binary values output from the ADCs and to perform the necessary calculations.

3.1.2. Implementation Philosophy

The design of computer based instrumentation is challenging because questions continually arise over whether a particular functionality is be implemented in hardware or handled by a software algorithm. In general the implementation of functions in hardware are faster in terms of execution time than if coded in software algorithms, however, a much longer time is required in achieving a working model.

The question takes on special importance in this instance as we have chosen to base the computer support on a multiuser, multitasking computing system in our laboratory . The potential to affect other users as well as to degrade significantly the performance of the FAS spectrometer is large. As an example of the data throughput rates the hardware could provide, the ADC was originally designed to collect and temporarily store 1024 points of 8-bit data, and then to transfer the data immediately into core storage of the NICOLET 1074 at a rate of 200 KHz. Attempting to transfer this quantity of information at this rate can be handled be a dedicated computer; however, a multiuser computer would have such a performance degradation that it would appear to other users to have become inoperable ("crash" is the term coined by computer scientists). It is for this reason that even much more powerful computers than the PDP-11, such as the VAX-11, a 32-bit minicomputer, are generally used singly, or in a 'stand alone' mode, when involved in real-time instrument work.

3.2. HARDWARE ARCHITECTURE IMPLEMENTATION

Figure 2.1 depicts the layout of the hardware supporting the FAS spectrometer. In the last chapter we were only concerned with the analogue components of the spectrometer itself; i.e, optical and signal processing. Now we'll examine some of the other components.

The digital components can be divided into roughly three systems. The first system is responsible for timing pulse generation and distribution of the pulses to the device. The second system is concerned with digitizing the analog data and transfer to the computer itself. The third system, the NICOLET 1074 and display scope, is held over in its entirety from the prototype and serves as a real-time graphics display subsystem.

3.2.1. Timing System

Replacing the simple timer-chip and interupt service routine concept used in the prototype, a timing board (Codar Q-TIMER) with 16 independently programmable channels with a 16-bit count resolution and four independently selectable counting frequencies is used instead. The board is inserted into the Q-BUS (or backplane; an electrical system designed for the systematic distribution of digital signals in a computer system) of the PDP-11 computer. Each timing channel can be programmably enabled to activate a vectored interrupt upon completion of the count as well as triggering one or more channels to begin counting. The logical detail of this is shown in Figure 3.1.

The major advantage of this device in generating timing pulses is the small load on CPU resources while maintaining programmable flexibility. An entire timing pattern handling all devices for a sequence is loaded at once. Each timer had a dynamic range available from 250 ns to 16 s and a granularity as fine as 250 ns. This allowed the computer to continue normal processing completely uninterrupted until the end of a timing sequence. The timing capability of the prototype, however, was limited to one timer and a (pre-load) latch with a dynamic range of 65,535 *us* (2^{16}) with a granularity of only 1 *us* for the chip alone. For each event in a given timing sequence the CPU in the AIM-65 had to be interrupted to load the timer latch with the next delay. Instances where a delay exceeded the dynamic range could only be accomodated by dividing the delay into a multiple of a calculated base count and then a residual. For example, a delay of 136 ms is achievable by two counts of 65535 and one count of 4930 given a 1 MHz counting rate. Multiple base counts and a residual implies that the software must tend the overhead of the loop count and to insure the timer is only enabled on the last residual count.

The net result was that the minimum time between any two pulses was 140 us using the AIM-65, and the minimum time for the PDP-11 was 250 ns. The addition of hardware enable lines on the PDP-11 also gave a conditional pulse capability. This was needed to allow timing patterns as in Figure 2.8. The pulse(s) required for the peristaltic pump were only enabled in the last sequence. Figures 3.8, 3.9, and 3.10 summarize the situations for setup, initializing, and timer completion in pseudo-code.

3.2.2. Data Collection

As already noted, data is collected by a Fast/Ultra-Fast ADC with 1024 points of storage and conversion rates ranging from 33 MHz to 2.5 KHz. The fast ADC was designed and built by Martin Rabb (electronic design engineer, Chemistry Dept., Michigan State University) in support of the delayed luminescence studies in plant chloroplasts by Professor Babcock and W. J. Buttner (Buttner, 1984a and 1984b). As mentioned, this was initially designed to transfer into a Nicolet 1074 for immediate display, and while the display system has been left relatively untouched, the ADC has been modified to support another 8-bit data collection channel and programmed interrupt transfer into a computer.

The original conversion channel is used for the differential signal containing the kinetic information, and the second channel is used to digitize the baseline information. Under interrupt request from the ADC 1024 points of 16 bits of data (8 bits for each digitizer) is transferred into the computer.

3.2.3. Transmission

The data transmission system is the system most susceptible to errors. It is responsible for providing electrical bi-directional transfer pathways between

the computer and the instrument. One of the pathways carries the timing signals, and another pathway carries the data and control signals for the ADC. Since the FAS spectrometer was to be based on our general computer, the computer could not be very well removed from the laboratory if the spectrometer was positioned elsewhere (such as the Laser Facility under construction). To allow for such an eventuality, special attention was paid to insuring reliable data transmission. The potential distances contemplated, ranging from 5 to 100 meters, between the computer system and the apparatus turned this into a significant problem.

After some consideration it was realized that fast data transfer rates could be achieved only through parallel (8 or 16 bits simultaneously) rather than serial (1 bit at a time). The 'fastest' rate for serial transmission used in asynchronous terminal I/O without flow control is 38.4 Kbaud (Kbits/second, or 4.8 Kbytes/second). The hardware capabilities of the parallel port used in the PDP-11 Q-BUS allows rates up to 40 kwords/second, or 80 Kbytes/second.

A dedicated transmission system was designed employing two matched transmitter/receiver pairs (see Figure 3.2) One pair is mounted next to the host computer system. The second pair is mounted on the same equipment rack containing the analog to digital converters. The current medium used to support communication are two (one for each direction) 32 bit data cables.

3.3. SOFTWARE ARCHITECTURE IMPLEMENTATION

The design of the software architecture for the FAS has uniquely applied concepts of distributed processing to the requirements for real-time instrument control, particularly in a multiuser, multitasking operating system environment. The general implication of distributed processing is that tasks can be offloaded or 'distributed' to other processing elements. For the discussion here, a 'processing element' can be defined as a computer system running a task. This definition

allows two tasks running simultaneously on the same processor to be considered as two processing elements.

3.3.1. Distributed Processing: An Introduction

The concepts of distributed processing have become an important area of computer research in both applied and theoretical areas. In some forms, it offers the promise of significantly increasing computing performance at all levels without corresponding order of magnitude increases in the performance of basic computing hardware technology.

Implementation of these concepts have taken shape in many different forms. The vectored array processors by Cray Research Laboratories and Floating Point Systems Inc., are examples of highly specialized implementations designed to solve particular classes of computing problems. The concept of pipes in various implementations of the Unix operating system (Ritchie, 1984) represents a general solution to stream or filter oriented data processing.

A simplistic example of a computationally distributed task can be found in the FORTRAN DO loop:

```
      DO 100 I=1,100
            A(I) = 1.0/B(I)
100         CONTINUE
```

This loop inverts 100 elements in an array B and stores the result in array A. A single processor loops through this 100 times. In the case of a vectored system containing 100 hundred or more computing elements one division would be performed by each computing element reducing the time required by as much as a factor of 100. In practice this is not quite true as there

are loading and pipelining considerations of the data that turn this 100 fold reduction into a lower bound, but this is irrelevant here.

The example given above is representative of one of the simplest classes of parallel processing known as 'Single Instruction, Multiple Data' (SIMD). The same operation, division, is being performed upon multiple instances of data, 100 elements in an array. Other classes of parallel processing machines exist such as those belonging to the class of Multiple Instruction, Multiple Data (MIMD). In MIMD processing, the problem as a whole is considered, broken apart, and discrete processing aspects given to separate, independent processing elements. MIMD type of processing, while normally executing upon a multiple processor architecture, can be simulated on a single processor using a multitasking operating system.

In real-time instrument control several sets of relatively independent events such as data ready notification, user interrupt, timer count down completion, etc., may be occurring simultaneously and each event may require significant attention. Formalization of an algorithm to handle these independent concurrent events can be quite complex and difficult to test. Distribution of the handling of these events to separate processing elements allows development of individual algorithms for each processing element, and these in turn will be simpler as the individual tasks are now far simpler.

In single processor configurations, running multitasking, multiuser operating systems, the Digital PDP-11 or VAX-11 being specific examples, distributed processing can refer to distributing a processing function over two or more active tasks. Within either and across both of the Digital processor families the operating system communication resources or networks are sophisticated enough to allow programs that are designed around distributed processing

algorithms on a single processor to be distributed over multiple processors with little if any change to the software.

3.3.2. Distributed Processing: The Design & Implementation

Processing is distributed over four software systems as listed below and diagrammed in Figure 3.6:

User Command System

Apparatus Control System

Graphics Display System

Operating System Functions

These systems interact with each other directly along communication pathways and indirectly along data pathways (see Figure 3.6). These pathways are provided as a result of the operating system inter-task communications.

3.3.2.1. User Command System

The User Command System (UCS) serves two functions: 1.) Coordination of the activities of all the software components responsible for providing the integrated environment of the FASCI, and 2.) Execution of the user commands. The UCS has multiple display screens depending on the command being executed. A menu portion displays current values for configuration parameters and associated mnemonic commands. Configuration parameters are directly related to the experiment execution and comprise variables such as number of scans to execute, number of timing sequences per scan, type of data conversion (raw, transmission, absorption, summation, averaging), base line duration, conditional pulse generation, etc. These configuration parameters can be directly stored and loaded from files so that common setups can be maintained. Commands directly control program execution such as initiating an

experiment, saving the data, plotting data, etc. Appendix A contains a more detailed discussion of the menu(s), contents, and interaction with user.

The most critical part of the UCS is the Asynchronous Event Handler Subsystem (AEHS) (part of the block for the UCS in Figure 3.6). Asynchronous events are events which occur independent of normal processing. They are handled first by the operating system, and dispatched to appropriate handlers. Each of the systems notify the operating system of the events they want to handle directly; therefore, when an asynchronous event occurs it is given to the appropriate systems' handlers. The AEHS subsystem of the UCS handles asynchronous events in a timely fashion that are of importance to the execution of the UCS. Message arrival notification, successful task initiation, user interrupt, etc. are handled through here.

3.3.2.2. Apparatus Control System

The Apparatus Control System (ACS) is the only system that directly interacts with hardware. Commands are received from the UCS over the communication pathway previously described. It too has an AEHS to handle events. It also has a data pathway it shares with the UCS for the fast transfer of raw data from the ADC for processing.

An Interrupt Control System (ICS) contains the code for the interrupt service routines (ISRs). ISRs, software code entered immediately after hardware notification, are used for fast response. ISRs are generally written to respond to only one interrupt at a time from a device and perform the barest amount of processing because all other forms of processing by the computer, including other tasks and system functions, are locked out. The ICS provides a framework to help prevent potential conflicts arising between multiple interrupts requiring service from one or more ISRs.

Extended periods of time in an ISR degrade system response in a drastic fashion (PDP-11 Processor Handbook, 1981). Opposing this idea of minimal processing while executing at such a high priority, however, is the overhead involved in saving and restoring contexts when ISRs are entered and exited on a rapid basis due to an almost continuous series of hardware interrupts being generated by the same device. The net result is then little useful work being performed by the operating system. 1024 entries into an ISR would not only be wasteful in terms of system resources, but would also result in an unacceptably long period of time to effect the transfer of 1024 points. The ISR, which processes the data from the ADC, when entered, remains until all data has been transferred or an error condition has been established; however, to allow other interrupt processing to occur, the interrupt priority of the ISR is dropped to 0 (lowest).

3.3.2.3. Graphics Display System

Real-time graphics display, the updating of which can be difficult to schedule because of other interrupt and exception sources, is handled via the Graphics Display System (GDS). It too has a communication pathway, and shares a data pathway for access to processed data for plotting.

Upon initiation, the GDS is given the graphics device to use and the number of data sets (maximum of 6) it can display on a subgrid on the device. During the execution of an experiment once a set of data for a particular scan and a particular sequence has been collected, processed, and stored in a memory buffer, a command is issued from the UCS to the the GDS to plot the given set. While the UCS continues on, the GDS accesses the data and plots it.

t

s

p

ei

ac

a lo

This

the

colle

probl

all of t

A batc

subsec

prograr

process

matrix c

pen plott

interventi

T

resulted in

3.3.2.4. Operating System Functions

This is not formally a system in the manner of the previously discussed ones; however, some of the functions of the FASCI rely on services provided by the operating system or other support programs. Two such support programs are a vector to raster conversion job and a data archival job.

At the completion of an experimental run the user may decide to keep the data, plot the data, or both. If the data is to be kept, a 'save' option is selected and a local file is generated containing all of the experimental parameters and the collected data. This file is then queued for archival onto either magnetic tape or other mass storage on another computer system accessible through the DECNET network. Once the file is archived successfully a log is updated describing the file and final location, and the local file deleted. This archival process was handled through the operating system independent of the subsequent execution of FASCI, minimized the storage required for the collected data, and safeguarded it against unintentional deletion or computer problems.

If the 'plot' option was selected then a local file was generated containing all of the experimental parameters and the collected data that was to be plotted. A batch processing job was queued for execution and it ran independently of subsequent execution of FASCI. The batch job used the local file and several programs, BINDMP, MULPLT (Atkinson, 1982), and RASTER (Gregg, 1985), to process and print configurational information and the plots of the data on a dot matrix continuous feed line printer. Use of a continuous feed printer instead of a pen plotter meant that the generation of the plots could be performed without intervention required by either the operator or the FASCI system.

The automation of these processes, archival storage, and plotting, resulted in a significant increase in the number of experiments that be performed

in a given amount of time. This is important when considered within the context of sample lifetime. If samples are reliable for only 6 hours on ice, at the end of the period a new sample must be prepared if the experiments are not completed. Automation of a set of tasks such as plotting simply makes the FASCI available for experiments when it would be otherwise engaged in plotting.

3.3.2.5. Data Communication

As shown in Figure 3.6, the systems have varying access to the Experimental and Runtime Data Bases. These are tables of data created by the UCS for the purpose of storing experimental data. The Runtime Data Base contains digitized data that has been uploaded by the ACS from the transient signal averager(s) but not converted and summed with other data gathered on previous sequences or iterations. The Experimental Data Base contains digitized data that has been converted.

At execution initiation the UCS is started first. It then initializes and establishes the data bases, activates the other programs, and upon their activation are given appropriate access rights to the data bases. For example, the ACS only needs write access to the data base containing just the data which has just been collected. The GDS needs access to the long term converted data for plotting.

Memory resources are conserved by making the Experimental Data Base variably sized. If a given experimental run consists of one sequence, then the size of the region is set to only what is required to hold one set of data. If a run consists of 32 sequences, then the region is resized to hold 32 sets of data.

3.4. SUMMARY

The net result of this effort is a sophisticated instrument interface that allows the experimenter flexible control over the design and execution of an experimental scenario. Designing and developing this type of instrument interface on this powerful of an operating system allowed features to be added, such as the above mentioned archival and plotting programs, that could not be contemplated on other less powerful computing platforms. The type of architecture used for the code design would not have been as modular and independent on a system supporting only single tasking. Some areas of the instrumentation could originally not be considered completely successful, however.

3.4.1. Performance

The performance of the computer as a general purpose multiuser system degraded signficantly during experiments in which the inter-sequence delay time dropped below five seconds, and degraded to the point of being unusable and halting periodically when the GDS was activated. This was particularly bothersome as use of a distributed design was to have lessened the resource usage of the processor.

Replacing the PDP-11/23 with the PDP-11/73 (resulting in roughly a factor of four in terms of a performance increase) removed this problem. This allowed inter-sequence delay times to drop to one second, the smallest value allowed for in the software; however, the GDS still consumed a large share of the available resources because of the extensive I/O and floating point calculations.

Experimentation with a DMA (Direct Memory Access) I/O controller for movement of data related to the graphics display indicated that most of the processor overhead involved in I/O could be eliminated; however, the expense

was determined to be unnecessary as the NICOLET 1074 and its display oscilloscope still functioned adequately for this purpose.

Conversion of the data from two 8 bit words to a real numbers with enough dynamic range to support signal averaging also proved to be a bottleneck because of the logarithmic operations (see Equations 2.4, 2.5, and 2.6). Over 100 ms was required to convert and sum 1024 data point. Linearizing the logarithmic term by using a Taylor series expansion and using only the first three terms of the expansion lowered the required time to less than 10 ms.

3.4.2. Maintenance

As I am the author of this software and hardware system I have an intimate knowledge of it and occurrence of problems can be fixed quickly and in a fashion that is consistent with the design of the system. New features can be added rapidly. Even so a failure in a 7402 integrated logic chip worth about $0.23 required one month to track down and replace. During that time the entire instrument was inoperative.

Those who will use this spectrometer and its computer interface after I have departed will not have this knowledge and experience and, regardless of the documentation and detailed schematics that are prepared, will spend inordinate amounts of time fixing problems that arise because of infamiliarity. This situation will be tolerated only until a product becomes commercially available at reasonable cost.

3.4.3. Evaluation

This implementation has resulted in a methodology aptly suited for the design of computer software and hardware for real time instrument control. A commercial scanning spectrometer has also been interfaced using the same

distributed processing philosophy and many of the same underlying software modules. Both instruments are capable of being operated simulataneously without interference from each other, and other users were able to continue with word-processing, graphics, or data analysis entirely unaffected.

Use of the PDP-11 and in-house developed hardware and software as opposed to PC type machines and off the shelf software appears to be justifiable only if a major focus of the laboratory is the development of computer aided instrumentation or if the needed instrumentation or computer support simply are not commercially available.

In this instance, at the time of conception (1983 - 1984), software was not available and equivalently equipped PC computers were much more costly on a per user basis and on a per task basis than the PDP-11. Today (1988 - 1989), the situation has changed, and data acquisition packages (software and hardware) are available off the shelf. The lower data acquisition ranges of the computer, < 1.0 MHz, are certainly within range of other products. However, the adaptability of the computer to differing experimental senarios, high speed data acquisition, integrated approach to software and data structures (especially if more than one commercial package from different vendors has to be used), and overall utilization of the computer has not yet been matched.

TABLE 3.1

Resource comparison between AIM-65 and PDP-11 computer systems

This table presents a comparison of resources offered by the AIM-65 and PDP-11 computer systems. See text for details.

Equipment	Aim-65	PDP-11
	Original Equipment	
Processor:	6502	PDP-11/23
Address Space:	4Kb	64Kb (per task) 2Mb (total)
Operating Sys.	Monitor	RSX-11M/MPLUS
Number of Users:	1	>12
Number of Tasks:	1	>128
Memory:	4 Kb	256Kb
Editors:	Line Editor	TECO (Line Editor), KED, K52, EDT (key-pad Editors)
Languages:	BASIC Interpreter Assembler Fortran-77 C	BASIC Macro Assember
Mass Storage:	Cassette Tape	492Kb Flexible Diskette 30Mb Winchester
Display	20 Char LED Display Video Terminal Terminals	(3) Tektronix 4010 Emulators (5) VT100
Printer:	20 Character Thermal Printer	132 Column Dotmatrix Printer
Plotter:		HP-7470
	Additional Equipment	
Processor:	upgraded to PDP 11/7	
Added Memory:	32Kb	1280Kb
Languages:	added FORTH	

TABLE 3.2

Resource comparison between IBM-PC and PDP-11 computer systems

Comparison of resources offered by the IBM PC and PDP-11 computer systems. Hardware disparities between the two systems for a single program are not great, but the IBM PC with the MS-DOS operating system is unable to support multitasking. The IBM PC has some advantages over the PDP-11 in the amount of memory available for a single task. The original versions compilers for the IBM limited memory to 64 or 128 Kb, but more recently, the compilers have come to support memory models that easily allow for the entire 640 Kb to be used by a single program. Such an option is not available to the PDP-11.

The processor in the IBM PCs, the 8088, can physically address 1 Mb, but the physical design of the IBM PC limited it to 640 Kb. Other hardware vendors have adopted schemes allowing additional memory, 'expanded' or 'extended' memory to be inserted. This additional memory cannot be used to execute code only data.

Equipment	Aim-65	PDP-11
	Original Equipment	
Processor:	8088	PDP-11/23
Address Space:	64Kb (original)	128Kb (per task)
	128 to 640Kb (vendor dependent)	2Mb (total)
Operating Sys.	MS-DOS	RSX-11M/MPLUS
Number of Users:	1	>12
Number of Tasks:	1	>128
Memory:	640 Kb	256Kb
Editors:	EDLIN (Line	TECO (Line Editor)
	(editor)	KED, K52, EDT (keypad editors)
Languages:	BASIC Interpreter	
		Macro Assember
		Fortran-77
		C
C Mass Storage:	360Kb Flexible Diskette	492Kb Flexible Diskette
	10Mb Winchester	30Mb Winchester
Display:	80 x 25 Video Display:[1] ,	(3) Tektronix 4010 Emulators
		(5) VT100 Terminals
Printer:	132 Column Dot Matrix Printer	
Plotter:	HP-7470 2 pen plotter	
	Additional	
Processor:		upgraded to PDP-11/73
Memory:	'Expanded' or 'extended' memory has become available	increased to 1280Kb

[1]Color Graphics Adapter (CGA), Enhanced Graphics Adapter (EGA), and Hercules (non-IBM, 3rd party standard) adapters. Emulation of Tektronix 401x possible.

FIGURE 3.1

Logical Schematic of Timing Logic

The command control interface unit routes the commands and data to the appropriate timing unit, TUnn, where 'nn' = {1,...,16}. Each timing unit can individually programmed in terms of count, frequency of counting, and execution when its counting is finished. As shown here all but the last timing units have its output connected to the next timing unit. Further details can be found in the text.

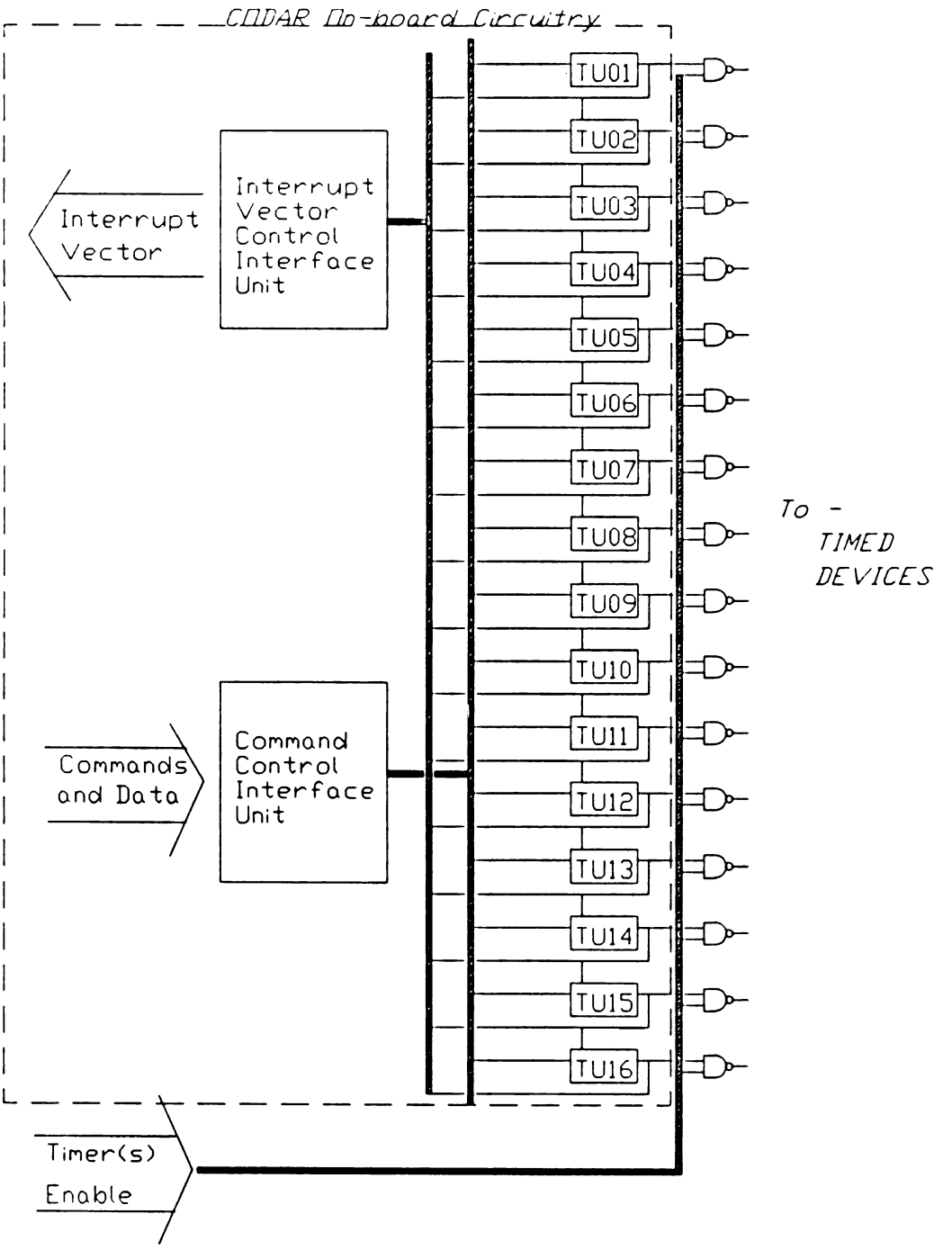
CODAR On-board Circuitry
Interrupt Vector
Interrupt Vector Control Interface Unit
Commands and Data
Command Control Interface Unit
Timer(s) Enable
TU01
TU02
TU03
TU04
TU05
TU06
TU07
TU08
TU09
TU10
TU11
TU12
TU13
TU14
TU15
TU16
To - TIMED DEVICES

FIGURE 3.2

Communications Scheme between Computer and Instrument

Both ends, the computer and the instrument, each have a transmitter and a receiver that manage the parallel data flows. The data in each direction travels through a 32 bit communications pathway. Each end also has a front panel display. The front panel display shows the data activity on each line and while intended for initial debugging, proved to be continually useful for status diagnosis.

The blocks 'Location 1' and 'Location 2' indicate that each group within are located separate from one another. The dashed connecting lines labelled '32 bit communications pathway' simply indicate an indefinite length separating the two locations. In actuality, designing the communications between the computer and the instrument in this fashion remove any dependencies on the actual medium used to support the communication pathway.

Location 1
Host Computer
Transmitter
Receiver
Front Panel Display
32 bit communications pathway
32 bit communications pathway
Location 2
Receiver
Router
Transmitter
ADC #1
ADC #2
Front Panel Display

FIGURE 3.3

Algorithms for Setup of Timing Sequences

These algorithms reflect the pocedures of preparing the AIM-65 and the PDP-11 for performing the hardware and software for timing pulse generation. The timer on the AIM-65, unlike the ones on the PDP-11 CODAR timing board, does not offer a scalable base counting frequency and requires additional counting periods, manipulated by software in the interrupt routine, to extend to some of the timing period intervals needed. The PDP-11, on the other hand, only requires determination of the appropriate base frequency and the number of counts in that base. See text for further discussion.

a) Algorithm to setup, in pseudo code, the single timer for the AIM-65.

```
DO for all pulses (16)
   IF delay count exceed 65535 ticks at 1 MHz
      Calculate and store #  of multiples of counts at 65000 us.
      Calculate and store the leftover residual delay count.
   ELSE
      Store 0 multiples of counts
      Store delay count.
   ENDIF
   Store device enable mask
ENDDO
```

b) Algorithm to setup, in pseudo code, the Codar Q-TIMER for the PDP-11.

```
DO for all pulses (16)
   Calculate and store basic frequency
   Calculate and store counts for basic frequency
   Store device enable mask
   Arm counter
ENDDO
```

FIGURE 3.4

Algorithms for Initialization of Timing Sequences

These algorithms reflect the procedures necessary for initiating a Timing Sequence.

a) Algorithm to initialize, in pseudo code, the single timer for the AIM-65.

```
Load Timer with count Decrement multiple count number
IF multiple count number <> 0
    Load Timer Latch with count
ELSE
    Load Timer Latch with residual count
ENDIF
Trigger Timer to begin
```

b) Algorithm to initialize, in pseudo code, the Codar Q-TIMER for the PDP-11.

```
Trigger first timer to begin
```

FIGURE 3.5

Algorithms to Process Timer Completions (counter finished).

These algorithms reflect event processing that must take place when a timer has completed. Processing occurring in hardware are preceded by '*[...hardware execution...]* and '*==>*.' In the case of the AIM-65 the latch for the timer is loaded by hardware into the counter and the timer is restarted. The software prepares the latch for the following time. If the current time being counted down is to result in a pulse, then the timer is enabled for generating a pulse. Other than the automatic reload all of the operations occur in software and incur a significant overhead in the duty cycle.

Contrast this with the processing required for the PDP-11 and the CODAR timer. Handling of timer completions is performed completely in hardware and only upon the last pulse to be sent out is the processor notified of the event.

a) Algorithm to process timer completion, in pseudo code, for the AIM-65.

```
   [...hardware execution...]
==> Timer counted down
==> Interrupt generated to CPU
==> Count in latch loaded into timer
==> Timer restarted

Decrement mulitple count number
IF multiple count number > 0
    Load residual count into timer latch
ELSE
    Enable Device Pulse
    IF NOT last device
        Load Timer latch with next device count
        Reset multiple count number to new device's
    ELSE
        standby
    ENDIF
ENDIF
```

b) Algorithm to process timer completition, in pseudo code, for the Codar Q-Timer for the PDP-11.

```
   [...hardware execution...]

==> Any Timer but last is counted down
==> Next Timer triggered to begin counting
==> Pulse put out

   [...hardware execution...]

=> Last Timer counted down

standby...
```

FIGURE 3.6

Logical Schematic of Software Control Systems

The User Control System (UCS), Apparatus Control System (ACS), and the Graphics Display System communicate directly via message pathways (dark lines) and indirectly via data access to data bases (broad, light lines).

Access into the data bases for each system is standardized. Each data base was designed so that the first several units of storage are addresses or pointers into the data bases for the information. The location of these offsets are standardized and stored in a file which is used in the compilation of all systems accessing the data bases. In this way, modifications to either the data bases or the programs accessing the data bases is simplified.

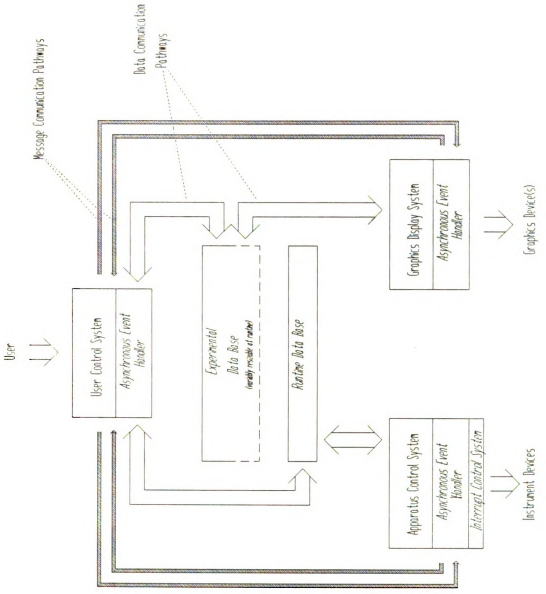
User
Message Communication Pathways
Data Communication Pathways
User Control System
Asynchronous Event Handler
Experimental Data Base
Runtime Data Base
Graphics Display System
Asynchronous Event Handler
Graphics Device(s)
Apparatus Control System
Asynchronous Event Handler
Interrupt Control System
Instrument Devices

REFERENCES

Atkinson, T. V. (1982). Atkinson is author of a program called 'MULPLT' designed to perform vector plotting of multiple data sets. This program was developed at Michigan State University and has been distributed through DECUS, Digital Equipment Corporation User's Society.

Buttner, W. J. and Babcock, G. T. (1984a). Biochimica et Biophysica Acta, 767, 272-287.

Buttner, W. J. (1984b). Ph.D. Thesis, Michigan State University.

Gregg, H. (1985). Gregg is author of a program called 'RASTER' designed to perform generalized vector to raster conversion. This program was developed at Michigan State University and has been distributed through DECUS, Digital Equipment Corporation User's Society.

Ritchie, D. M., 1984. AT&T Bell Laboratories Technical Journal, 63, 8. Reprinted from Lecture Notes on Computer Science, 79, **Language Design and Programming Methodology**, Springer-Verlay, 1980.

PDP-11 Processor Handbook, 1981, Digital Equipment Corporation.

Vax Hardware Handbook, 1982, Digital Equipment Corporation, pp 331-366.

CHAPTER 4

THE PHOTOSYSTEM II ACCEPTOR SIDE

4.1. INTRODUCTION

The chemistry and absorption band locations of the acceptor side quinones that undergo one and two-electron redox reactions were briefly introduced in Chapter One. The uncoupling of their contributions to the transient absorption changes observed in Photosystem II preparations has proven to be key for the interpretation of absorption changes attributed to the oxygen evolving complex as alluded to earlier and detailed in the next chapter. This uncoupling has not proven to be straightforward for reasons related both to the nature of the systems studied and the conditions that researchers use in their studies. This latter fact has only recently become appreciated and will be developed later in this chapter.

At the time we set out to examine optical changes of the OEC (1984) only one group had published a detailed kinetic difference spectrum arising from the reducing side of PS-II as well as a spectrum for the Y_Z^+/Y_Z couple (Dekker *et al.* (1984a). These results were subsequently used for removing reducing side and Y_Z^+/Y_Z contributions from the difference absorption spectra of the S-state transitions of the OEC (Dekker *et al.*, 1984b).

As mentioned in Chapter One and discussed in further detail in the following chapter, the optical results reported by Dekker *et al.* (1984b) relating to the S-state transitions have been controversial because of the methods used to

deconvolvethe S-state spectra and the interpretation of the data. In their procedure it was necessary to remove the contributions arising from Qa^-/Qa and Y_Z^+, and we believed that the experimental protocol used was suspect in regards to the exogenously added electron acceptor and donor systems that supported electron transfer through the tris-washed PS-II systems. In addition, the conditions used for determination of the Qa^- /Qb spectrum differed significantly from the conditions used to determine the S-state spectra. This necessitated repetition of some aspects of their work under conditions we felt were better controlled. This would accomplish two things: 1) Our results would serve then as an independent confirmation of their work. 2) Subsequent experiments we would perform that relied upon detailed knowledge of the spectral contributions arising from the reducing side, such as S-state transitions, would not be incorrectly adjusted if legitimate differences existed between the spectrum we would report for Qa^-/Qa versus that reported by Dekker *et al.* (1984a).

A detailed outline of the reactions undergone by PS-II in response to single flashes of light is shown in Figure 4.1, which reveals a synchronous relationship between the acceptor and the donor sides. The cumulative effects of 'hits' and 'misses' of the OEC do not remain correlated with the reactions undergone by the acceptor side, and thus the two sides dephase with respect to one another and complicate the observed absorption spectral changes.

4.1.1. Separation of Quinone Contributions

Any optical spectroscopic investigation of the acceptor side has to account for absorption changes by both Qa as well as by Qb. In particular, the equilibrium condition between Qa^-Qb <===> $QaQb^-$ must be accounted for. Vermeglio and Clayton (1977) showed that in the near-UV and visible the absorption spectra of $QaQb^-$ and Qa^-Qb in *Rhodopseudomonas sphaeroides*

were nearly indistinguishable; however, in the red and in the near-IR, these two states could be distinguished one from another on the basis of induced absorption band-shifts in the bacteriochlorophyll and bacteriopheophytin. Kleinfeld *et al.* (1985 and 1984) have since demonstrated that the difference of 20 % in the optical extinction coefficients between the states Qa^-/Qa and Qa/Qb^- at 450 nm is large enough to measure reliably and to differentiate between different states of the acceptor side.

4.1.2. Simplification of Reducing Side Chemistry

The chemistry of the acceptor side is the same regardless of the integrity of the oxygen evolving complex, and follows that given in Reactions 1.3, 1.4, and 1.5 assuming that the acceptor used is either plastoquinone or a quinone analogue. Ideally, all modifications to the acceptor side should be reversible. Such a condition demonstrates that the effects measured have not been achieved through irreversible alteration of the composition and states of the Qa and Qb sites.

4.1.2.1. Conventional Inhibition

Figure 4.2a shows known sites of selective inhibition that will affect the yield of Qa^-. Under conditions in which the OEC has been deactivated, such as by tris-washing, which removes the manganese responsible for oxygen evolution, the addition of ferricyanide, $Fe(CN)_6^{3-}$, as an acceptor and a herbicide, such as 3-(3,4 Dichlorophenyl)-1,1 dimethylurea, DCMU, that competes inhibitively with endogenous quinones for access to the Qb binding site, the chemistry will simplify to (Figure 4.2b has more detail):

$$Qa \xrightarrow{h\nu} Qa^- \qquad (4.1)$$

fer

ex

se

80

Qa

kin

un

Pe

Fe

ran

diff

Y_Z

the

Equ

ele

of t

et a

of w

thei

betw

lines

$$Qa^- + Fe^{3+} \text{---> } Qa + Fe^{2+},\ t_{1/2} = 3s \qquad (4.2)$$

There are difficulties with this simplification. The oxidation of Qa^- by ferricyanide can be heterogenous under conditions thought to promote exclusively the slow oxidation of Qa^-. As shown in Equation 4.2, the $t_{1/2}$ is 3 seconds, but the reduction of Y_Z^+ by ferrocyanide, $Fe(CN)_6^{4-}$, has a $t_{1/2}$ of 50 to 80 ms (Dekker *et al.*, 1984a). This allows the backreaction between P_{680} and Qa^-, which has a $t_{1/2}$ of 120 to 200 *us* (Haveman and Mathis, 1976), to become kinetically more competitive. The idea that Qa^- could also undergo fast oxidation under similar reaction conditions as used above was first suggested by Petrouleas and Diner in 1986 (Petrouleas and Diner, 1986). The $t_{1/2}$ for the Fe^{3+} to Fe^{2+} reduction attributed to Qa^- appears to be pH dependent and ranges from 7 to 25 *us* (Diner and Petrouleas, 1987a and 1987b). Another difficulty may be from an interference in the electron flow between the OEC and Y_Z^+.

This difficulty of heterogeneous behaviour can be generalized to include the entire response of the Photosystem II unit. The simple model suggested by Equations 4.1 and 4.2 assume complete reactions for at least this section of the electron transport chain. Melis and Anderson (1983) have questioned the extent of the Qa response in relation to the extent of charge separation and Dennenberg *et al.* (1986) has provided evidence that Photosystem II reaction centers capable of water oxidation consist of two separate populations that are characterized by their differing response to added quinones.

Another apparent difficulty may be an interference in the electron flow between the OEC and Y_Z^+. Hoganson (1988) noted in EPR studies on the lineshape of Y_Z^+ that ferricyanide in concentrations of greater than 1 m<u>M</u>

appear

membr

change

This ox

states.

popula

4.1.2.

reacti

1976)

hydro

remov

3) mir

diges

the bi

prepa

oxidiz

unwe

solub

prepa

the C

The s

manif

be di

appeared to affect the half lives of both Y_Z^+ and of the S-states in Photosystem II membrane preparations.

As a final note, experiments examining multiple, sequential S-state changes can not use ferricyanide because of its slow oxidation of Qa^- to Qa. This oxidation time is long in comparison to the deactivation of the higher S-states. This in turn contributes to the decrease in the homogeneity of the S-state populations.

4.1.2.2. Trypsin Modification of the Qb Binding Site

A different approach to the control of the acceptor side electron transport reaction has been adopted by Renger (Renger, 1976a, 1976b, and Renger *et al.*, 1976). He found that brief incubation periods of chloroplasts with trypsin, a hydrolytic enzyme that attacks lysine and arginine residues, had three effects: 1) removed sensitivity to DCMU, 2) lowered the affinity for acceptor quinones, and 3) minimally altered the affinity for ferricyanide. These effects were attributed to digestion of the intrinsic 32 kDa polypeptide (Renger *et al.*, 1986) thought to hold the binding sites for Qb.

Unfortunately, this technique, when extended to Photosystem II preparations in which the membrane orientation has disappeared and both the oxidizing as well as the reducing sides are exposed to the bulk media, has unwelcome side-effects. Trypsin appears to attack, at a minimum, the water soluble polypeptides of 17, 23, and 33 kDa (Volker *et al.*, 1986). Photosystem II preparations exhibiting the multiline, an EPR signal attributed to the S_2 state of the OEC (see Chapter 1), were subjected to tryptic digestion at pH 7.6 and 6.0. The sample at pH 7.6 lost the multiline completely, but the sample at pH 6.0 manifested no change; however, the water soluble polypeptides all appeared to be digested to some extent. In particular, the 33 kDa polypeptide became a 15

kDa f

its dig

comp

4.1.2.

with c

DCM

Qa^-, a

plasto

as ye

recor

the re

4.1.3

techr

scanr

anoth

perio

base

reflec

beam

excita

kDa fragment. Trypsin appears to be suitable for use in chloroplasts; however, its digestion of polypeptides apparently associated with the oxygen evolving complex make it unsuitable for work with Photosystem II membranes.

4.1.2.3. Cholate Treatment

Bolby and Yocum (1987) investigated the treatment of the reducing side with cholate as it held out fairly strong promise for removal and reconstitution of DCMU sensitivity. They had demonstrated high rates of reduction of Fe^{3+} from Qa^{-}, and these rates were comparable to those achieved by endogenous plastoquinone or exogenously added analog quinones. Unfortunately, they have as yet been unable to prove the reversibility of the cholate treatment and reconstitute DCMU sensitivity. Because of the uncertainty of the modifications to the reducing side, we chose not to take advantage of this treatment.

4.1.3. Spectroscopic Characterization of the Reducing Side

The experiments on the reducing side have reflected increasing technological sophistication. The early experiments were recorded by using scanning spectrometers and conditions designed to pump one state over another. Later experiments relied upon flash methods to generate for brief periods of time the intermediate states, that could then be subtracted from baseline samples. The spectrometer used by Joliot, the 'Joliot spectrometer,' still reflects the state of the art in terms of spectrometer design. This was a dual beam, dual recording spectrometer designed explicitly for differential sample excitation (Joliot *et al.*, 1980, and Joliot and Joliot, 1981).

4.1.3.

reaso

and W

deox

term

had

nm.

spe

pla

sp

ob

ap

(S

4

4.1.3.1. Steady State Absorption Spectra

The so-called steady state spectra due to the Qa^-/Qa couple has been reasonably well known since reported by Van Gorkom (1974) (also, see Stiehl and Witt, 1969, and Pulles *et al.*, 1976). The sample preparation was from deoxycholate enriched Photosystem II membranes ('DOC 2 particles' to use the terminology adopted by Van Gorkom) from spinach thylakoids. These samples had lost the ability to evolve oxygen. Points were collected at a resolution of 5 nm.

Van Gorkom identified the species responsible for the difference spectrum as plastoquinone by comparing it with the difference spectrum of the plastosemiquinone anion obtained by Bensasson and Land (1973). The spectrum collected by Van Gorkom exhibited a 15 nm red shift relative to that obtained by Bensasson and Land; however, Van Gorkom noted that this was apparently similar to a shift seen for ubiquinone in bacterial reaction centers (Slooteen, 1972).

4.1.3.2. Flash Induced Difference Spectra

Flash induced absorption differences have been observed for years in the UV and have generally been associated with acceptor side chemistry. Stiehl and Witt (1968) reported the first definitive correlation; however, the first flash induced spectrum of the Qa^-/Qa couple was not reported until 1984. Dekker *et al.* (1984a) recorded the spectrum at a resolution of 2.5 nm in Photosystem II enriched membranes that were better characterized than those used by Van Gorkom in the steady state experiments. This spectrum was similar to that obtained earlier via steady state techniques in both lineshape and relative peak amplitudes, although, as noted, the steady state and the flash-induced spectrum

are

Ben

tris-

with

blu

to

re

nu

T

tr

(

are red-shifted by 15 nm relative to the *in vitro* semiquinone reported by Bensasson and Land.

Dekker *et al.* (1984a) found, in samples with the OEC deleted through tris-treatment, that the absorption band for Qa^-/Qa is asymmetric around 325 nm with a molar extinction of 13,000 $\underline{M}^{-1}cm^{-1}$ and a half-width of 20 to 30 nm. In the blue, between 410 to 450 nm, the sharp, derivative shaped bands were attributed to blue shifts in the absorption spectrum arising from the pheophytin due to Qa reduction. They related the extent of the flash induced Qa^- absorption to the number of centers undergoing photochemistry by use of the C-550 bandshift. This is a bandshift of the pheophytin intermediate in the Photosystem II electron transport chain (see Figure 1.3) caused by the reduced primary acceptor, Qa^- (Van Gorkom, 1974).

More recently, Velthuys (1988), has likewise performed a spectroscopic characterization of the Qa^- state and is largely in agreement the results of Dekker *et al.* (1984a) in the blue and in the red. He disfavours the blue shift interpretation of the pheophytin, and suggests that a red shift of the pheophytin and a blue shift of the chlorophyll is operative. Unfortunately, his experiments were not carried out deep enough to the blue to also provide independent estimations of the extinction and bandshape of the difference spectrum arising from the Qa^-/Qa couple.

4.2. M

4.2.1.

4.2.1.

(Robir
summ
depeti
a blen
serum
mM Hi
cheese
reache
particu
discar
superr
HEPE
This su
discar
mM su
evolvir
O_2/mg

the ch
final su
of a so

4.2. MATERIALS AND METHODS

4.2.1. Biological Preparations and Handling

4.2.1.1. Chloroplast preparation

Broken thylakoid membranes, referred to as Class II chloroplasts (Robinson *et al.*, 1980), were isolated as described by Robinson *et al.* (1981) as summarized below. Spinach obtained commercially was washed and depetiolated. Approximately 500 to 1000 g were homogenated for ten seconds in a blender in a buffer solution of 0.4 M NaCl, 2 mM $MgCl_2$, 1.0 mg/ml bovine serum albumin (BSA), 1 mM ethylenediamine tetraacetic acid (EDTA), and 20 mM HEPES (pH 7.6). The homogenate was filtered through eight layers of cheese-cloth. The filtrate was then accelerated in a centrifuge until 3500 x g was reached and braked to a stop. This first centrifugation removed any large particulate matter that had passed through the cheesecloth. The pellet was discarded, and the supernatant centrifuged at 7500 x g for 10 minutes. The supernatant from this was discarded, and the pellet resuspended in 20 mM HEPES (pH 7.6), 150 mM NaCl, and 4 mM $MgCl_2$ (first resuspension buffer). This suspension was centrifuged at 7500 x g for 10 minutes and the supernatant discarded. The pellet was resuspended and stored at -40°C in a solution of 400 mM sucrose, 50 mM HEPES (pH 7.6), and 10 mM NaCl (SHN). The oxygen evolving rates of these chloroplasts were typically greater than 300 *u*moles O_2/mg Chl/hr.

Irreversible inhibition of oxygen evolution was accomplished by washing the chloroplasts in a solution of Tris(hydroxymethyl)aminomethane (Tris) before final suspension in SHN. The chloroplast pellet was suspended in 50 to 100 ml of a solution of 0.8 M Tris-HCl and 1 mM EDTA at pH of 8.0. This suspension

was

durin

minu

susp

Phot

follov

4.2.1

refer

(198

Fresh

mate

descr

minut

$MgCl_2$

to the

25% T

and 1

Triton

ice in

solutio

remov

suspe

superr

buffer,

was incubated on ice at 4°C for 20 minutes and exposed to normal room lighting during the incubation. The suspension was then re-pelleted by a 4000 x g, 10 minute centrifugation. If only chloroplasts were to be prepared, the pellet was suspended in SHN and either stored in a -40°C freezer or immediately used. If Photosystem II membranes were to be prepared, the procedures outlined in the following section(s) were followed.

4.2.1.2. Photosystem II membrane preparation

Isolation of the Photosystem II complex in a preparation commonly referred to as 'Photosystem II membranes' was carried out as in Berthold *et al.* (1981), modified as in Ghanotakis *et al.* (1984), and described briefly below. Freshly prepared or frozen stock Class II chloroplasts were used for the starting material. Inhibition of oxygen evolution has already occurred as previously described.

Chloroplasts were dark adapted and incubated on ice for five to ten minutes. An aliquot of a solution containing 50 mM Mes, 15 mM Nacl, 5 mM $MgCl_2$, and 1 mM ascorbate at a pH of 6.0 (Triton Suspension Buffer) was added to the chloroplast suspension such that subsequent dropwise addition of a stock 25% Triton solution (25% by volume of Triton X-100, 50mM Hepes (pH = 7.5), and 15mM $MgCl_2$) yielded a final chlorophyll concentration of 2 mg/ml and 7% Triton. Once the Triton aliquot had been added, the samples were incubated on ice in the dark for 30 minutes. Upon completion of the incubation period the solution was centrifuged at 2000 x g for 1 minute. The supernatant was removed, the pellet discarded, the supernatant suspended in the Triton suspension buffer, and centrifuged at 19,000 x g for 30 minutes. The resulting supernatant was discarded, the pellet resuspended in the Triton suspension buffer, and centrifuged at 19,000 x g for 30 minutes. The resulting supernatant

was discarded and the pellet suspended in a buffer consisting of 0.4 M Sucrose, 50 mM Mes (pH = 6.0), and 10 mM NaCl (SMN buffer). Final concentration was roughly 2 to 4 mg/ml Chl.

This final solution contained less than 1% contamination from Photosystem I as determined by EPR (Berthold *et al.*, 1981). If O_2 evolution was not inhibited then the average preparation was capable of supporting an O_2 evolving rate of 600 to 700 *u*moles O_2 /mg Chl/hr. If the preparations have been washed with Tris then they exhibited no measurable O_2 evolution using a Clark oxygen electrode.

4.2.1.3. Sample Preparation for Flash Absorption Spectroscopy

Tris-washed PS-II membranes obtained from spinach were used in the FAS at concentrations ranging from 75 - 125 *u*M Chl (0.3 - 0.5 *u*M Reaction Centers, assuming 250 Chl/RC). 10 *u*M DCMU was used to block further electron transfer beyond Qa. Problems possibly arising from continual sample excitation were eliminated by recirculating the sample between every laser shot. Samples in the cuvette and tubing represented no more than 10% of the total volume. It was ascertained via steady state oxygen measurements (data not shown), that samples were not damaged from mechanical transport between excitation cuvette and reservoir.

The basic reaction media was prepared by having 100 to 200 ml of buffer consisting of 0.4 M sucrose and 0.05 M Mes at pH 6.0 stirring on ice in a round bottom flask. An aliquot of PS-II membranes at a stock chlorophyll concentration between 2 to 4 mg/ml (2.3 to 4.5 mM) were added slowly in the dark for a final concentration between 75 - 125 *u*M Chl and allowed to stir for five minutes. A second solution containing only buffer (0.4 M Sucrose and 50 mM Mes at a pH of 6.0) at 4^{o}C flowed continuously through the sample chamber and tubing. When

five minutes had passed the sample chamber and tubing were drained of the buffer and the photosynthetic sample in the reaction media was allowed to flow through.

If the reducing side reactions were to be blocked then 1 mM DCMU in EtOH was added to the buffer before the PS-II membrane aliquot for a final concentration of 10 *u*M DCMU. After a five minute dark adaptation an equimolar mixture of ferri- and ferrocyanide was added to achieve a final concentration of 0.25 to 1 mM Fe^{3+} and Fe^{2+}. If the reducing side reactions were not to be blocked 2,5 dichlorobenzene (DCBQ) was added to a final concentration of 400 *u*M.

4.2.

depe

taken

width

optica

The ferrous iron on the reducing side, Q_{400}, (Petrouleas and Diner, 1986), is dependent upon the order of component addition, especially as relating to the use of ferricyanide and DCMU (Ikegami and Katoh, 1973 and Bowes *et al.*, 1979). The participation of Q_{400} is thought to lessen the extent of the absorption change attributable to Qa^- at 325 nm. It was observed that addition of DCMU before ferricyanide slowed down the rate of oxidation of Q_{400} and, therefore its participation in subsequent redox chemistry, by as much as a factor of 25 (Wraight, 1985). Largely based upon the work of Bowes and co-workers (1979), a consistent order of addition of components was followed as discussed above and diagrammed below to avoid any problems arising from inconsistent order of addition. A consideration of the role that Q_{400} might play in these studies is found in the 'Discussion' section.

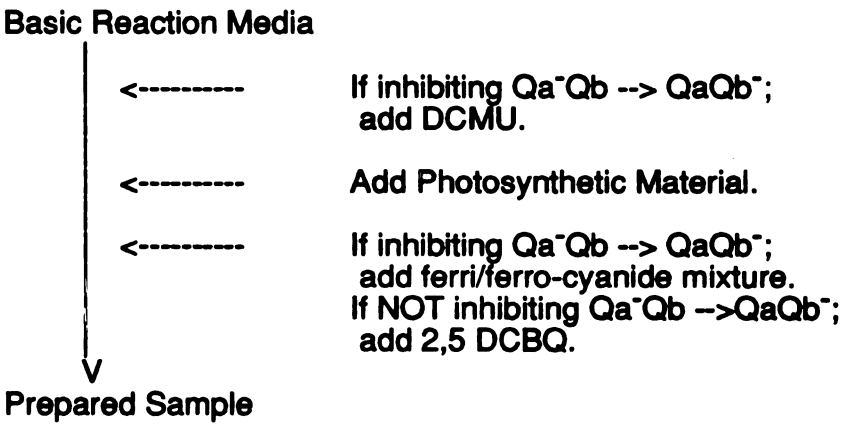

4.2.2. Instrumental Conditions

The instrument time constant and scan rates used were variable and depended on the type of experiment being performed. Kinetic spectra were taken every 2.5 nm (slit width of 0.5 mm, optical bandpass of 3 nm) or 5 nm (slit width of 1.0 mm, optical bandpass of 6 nm) in the range 280 to 450 nm. The optical feedback variance limits for the xenon probe beam were set to 0.95 (i.e., If

the average power output of the probe beam was 100 watts (W), the optical feedback unit kept the power variation of the probe beam on the millisecond time scale between 95 and 105 W.) Data points collected for the purpose of constructing difference absorption spectra were taken randomly along the wavelength range to minimize systematic errors. For each spectra between 4 to 16 flashes were averaged per point.

4.2.3. Data Handling

Absorption difference spectra were produced from a set of kinetic decay traces collected over the selected wavelength range in a fashion analogous to a boxcar integrator (for a brief description, see Malmstadt *et al.*, 1981). Each trace, one for each sampled wavelength, was stored along with its baseline data in a computer readable format. The baseline data were used to correct the decay trace data in the construction of the absorption difference spectra. All points falling within a selected time window were averaged and one point resulted for that window. Multiple windows were often specified for each trace. These points were then plotted versus wavelength. This process is depicted in Figure 4.10. Lines through the points were derived either by using an interpolative cubic spline fit to the data if the point density was high enough, or by applying a Savitsky-Golay (Savitsky and Golay, 1964) 5-point triangularly weighted, smoothing function to the data. Coefficients in the latter case were chosen for minimal distortion. In all cases, manipulation of data involved the actual data points, and not the lines that were generated from the data points. The lines were generated to serve only as an aid to the eye.

Conditions or modifications that are different from those described here are specified in the figure legends.

4.3. RESULTS

These experiments were conducted to provide several pieces of information: 1.) Proof of saturation of the Qa/Qa transition, 2.) Verification that we were observing the Qa^-/Qa transition by observing if the lifetime of the Qa^- species decreases through the use of a quinone acceptor rather than ferricyanide, 3.) Verification of the results obtained by Dekker and co-workers (1984a) regarding the quantitative shape and extent of the Qa^-/Qa spectrum, and 4.) Confirmation of the EPR results obtained by Ghanotakis and Babcock (1983) that showed that the addition of hydroxylamine in low concentrations caused a reversible interruption of electron flow between Y_Z and P_{680}^+. In the original experiments, the decay of P_{680} under hydroxylamine treated conditions was followed. In the experiments reported here the decay of Qa^- was followed.

4.3.1. Saturation of the Qa^-/Qa Transition

Incomplete saturation of photochemistry leads to a situation in which all of the PS-II centers fail to participate in charge separation and Qa reduction; thus, the detected extent of absorption change becomes a function of both the chlorophyll concentration and the excitation energy. This will result in an absorption difference spectrum of Qa^-/Qa that cannot be linearly related to the concentration of the reaction centers. A difference spectrum produced under such conditions cannot be used for the quantitative removal of Qa^-/Qa contributions from other spectra.

A saturation profile was performed for chlorophyll concentrations ranging from 50 to 200 *u*M [Chl] against laser intensity to determine if photochemistry, as measured by Qa^- reduction, was complete. The highest chlorophyll concentration used, 200 *u*M [Chl], is shown in Figure 4.3. Saturation was

reached at 30% of the maximum laser power used for this set of experiments (85 mJ per pulse, 400 ns pulse duration, 213 kilowatts, kW).

4.3.2. The Qa^-/Qa Difference Spectrum

Figure 4.4 is the spectrum we derived from a series of kinetic traces collected point by point in wavelength range of 280 to 550 nm. In the UV and near-UV the points were collected every 1 nm and in the visible the points were collected every 2.5 nm. Slit widths were adjusted so that in the UV the optical bandpass was 6 nm and in the visible the optical bandpass was 3 nm. Figure 4.5 overlays this spectrum on top of that obtained by Dekker *et al.* (1984a). From the comparison in this figure it is clear that there is agreement on most of the major spectral characteristics. However, the 325 nm absorption band we report is broader and its peak is less well defined. Additionally, in our spectrum the derivatively shaped bands between 390 and 450 nm are blue shifted by ~5 nm relative to those reported by Dekker *et al.* (1984a).

Although we were able to reproduce the detailed lineshape reported by Dekker *et al.* (1984a), we were unable to reproduce initially the extinction coefficients, 13 $mM^{-1}cm^{-1}$ at 325 nm, that Dekker *et al.* (1984a) had reported for the Qa^-/Qa couple. The first effort we made to resolve this discrepancy was to use a spectroscopically related feature known as the C-550 bandshift. First reported by Van Gorkom (1974) and used by Dekker *et al.* (1984a), this is a bandshift centered around 545 nm of the absorption spectrum of an intermediate pheophytin induced by the reduced state of Qa^-. This is a region in which our Flash Absorption Spectrometer, the FAS, had already been shown to operate acceptably, Lillie (1984).

Under conditions identical to those used for determining the difference spectrum of the Qa^-/Qa couple, the C-550 spectrum was collected in the same

fashion as described earlier (see Materials and Methods) and compared against that reported by Van Gorkom (1974). As with the Qa^-/Qa spectrum the lineshape and the extinction coefficient, ~2.6 $m\underline{M}^{-1}cm^{-1}$, we measured was similar to that reported in the literature (Van Gorkom, 1974). There have been two other independent measurements of the C-550 bandshape and magnitude. McCauley and Melis (1986) reported the magnitude to be twice that reported by Van Gorkom (1974), 5.2 $m\underline{M}^{-1}cm^{-1}$; however, Jursinic and Dennenberg (1988) support our results and those reported originally by Van Gorkom (1974).

The only reasonable explanation that occurred to us at the time for this linear attenuation of the absorption changes in both the UV and visible regions was that Qa was already partially reduced prior to the laser pulse. This could happen if dark adaptation was incomplete, if other chemical reactions were occurring in the dark, or if the probe light beam was inducing photochemistry. The latter option was examined first by determining the extent of the absorption change versus the sample exposure time after opening the shutter (Figure 4.6). As can be seen in the figure, there is a direct correlation between the extent of the flash induced absorption change and the length of the exposure time of the sample to the probe beam. Our initial experiments used an exposure time of 50 ms and determined the extinction coefficient for 325 nm to range between 9 and 10 $m\underline{M}^{-1}cm^{-1}$, which is confirmed by Figure 4.6. Subsequently, the exposure time to the probe before excitation was shortened to less than 10 ms for all further experiments. The affect of this on the C-550 change can be seen in Figure 4.9 and on the Qa^-/Qa change in Figure 4.4. It proved to be unnecessary to explore the other possibilities. This point is considered further in the following discussion section.

4.3.3. Kinetics

The above experiments showed that we were spectroscopically observing similar phenomological events to those reported by Dekker *et al.* (1984a); however, without further evidence, such as kinetic data, the association cannot be convincingly made. Therefore, the behaviour of the Qa^-/Qa redox couple was studied by using various combinations of the ferri- /ferrocyanide and 2,5-DCBQ acceptor systems.

Figure 4.7 compares two decay curves of Qa^-. The upper trace is from a tris-washed sample treated with DCMU to block electron transport to endogenous quinones and a ferri- /ferrocyanide acceptor system for oxidation of Qa^-. The lower trace is from a similarly prepared sample except that DCMU was omitted and both ferri-/ferro-cyanide and 100 *u*M 2,5-DCBQ were added as the acceptor systems. The lower trace exhibits a faster decay time ($t_{1/2}$ ~ 1 - 1.5 ms) indicating that oxidation of Qa^-, presumably by 2,5-DCBQ, is much faster than with the inorganic oxidant alone. The oxidation of Qa^- can be slowed down in this sample by addition of DCMU and exposure of the sample to the probe light for one minute (data not shown).

Fast reduction of Qa^- in the presence of a quinone acceptor system and slow reduction in the presence of an inorganic oxidant is conclusive for an operational Qb site on the reducing side of the Photosystem II membranes. Quinone acceptor systems bind in the Qb site in order to oxidize Qa^-. Inorganic systems do not use the Qb site, have a longer distance over which electron transfer must occur, and thus exhibit slower decay constants.

4.3.4. Hydroxylamine

Hydroxylamine was observed by Ghanotakis and Babcock (1983) to decrease the EPR signal arising from Y_Z^+. A model was suggested (see Figure

4.2c) in which hydroxylamine interfered reversibly with electron flow between Y_Z and P_{680} and, as a result of this interference, P_{680} is reduced by Qa^-. This model relied upon the EPR data Ghanotakis and Babcock (1983) reported as well as upon fluorescence information obtained from *Chlorella* by Den Hann *et al.* (1976). The evidence implicated Y_Z^+ as being the locus for inhibition as opposed to P_{680}. It was thought that, in repeating the same experiment, but observing the decay of Qa^- directly, we would observe a decay component of $d[Qa^-]/dt$ with a $t_{1/2}$ of ~120 *u*s, the half-time for the backreaction between P_{680}^+ and Qa^-.

Tris-washed PS-II membranes were diluted into a reaction media as described in Section 4.2.1.3. 1 m<u>M</u> DCMU was added to block the reducing side reactions and a 0.5 <u>M</u> ferri-/ferrocyanide mixture was used as the accepter system. At varying times before the experiment was started 0.5 m<u>M</u> NH_2OH was added to the reaction media. We were not able to detect the fast decay components expected, $t_{1/2}$ ~ 120 *u*s, of Qa^- back reacting with P_{680}^+. We did observe, though, that the amplitude of the slow decay components, $t_{1/2}$ ~ 50 ms, decreased. This decrease was largely turnover dependent, and not dependent upon dark incubation time in NH_2OH. We were also able to restore the initially observed amplitude by washing out the NH_2OH. Similar experiments using the same apparatus have been performed with the focus on the fast decay components (Xing, 1989). The amplitude of the fast decay components was shown to increase as a function of the number of turnovers.

The correlation between the slow decay amplitude decrease and the number of turnovers, the inverse correlation to the fast decay amplitude increase, and the restoration of the initial signal by washing out the NH_2OH is conclusive of hydroxylamine having only a reversible inhibition before P_{680}^+ and supports the

original model proposed by Ghanotakis and Babcock (1983). These results are summarized in Table 4.1.

4.4. DISCUSSION

We have ascertained that the optical transient we observe whose lineshape peaks around 325 nm is indeed due to the same species as reported by Dekker *et al.*, (1984a). They had related their observation to the species reported by Van Gorkom under steady state conditions (1974) and ultimately to the plastosemiquinone anion radical reported by Bensasson and Land (1973). Our reported line shape and extinction coefficients are not signficantly different from those reported by Dekker *et al.* (1984a), and the kinetic behaviour with regards to exogenous quinone ($t_{1/2}$ ~ 1.5 ms for the reaction Qa^- + DCBQ --> Qa + $DCBQ^-$., Dekker *et al.*, 1984b) and inorganic oxidants appears to be consistent with expectations. Further confirmation exists in the examination of a separate spectroscopic feature, the C-550 bandshift. As a result we can be confident that our reported absorption difference spectrum, taken at a point density of 1 to 2.5 points/nm, is reasonable.

A significant aspect to our independent confirmation of the work reported by Dekker and co-workers (1984a) is that it has proven unnecessary for us to employ kinetic phase deconvolution procedures for the determination and removal of the individual component contributions. Furthermore, the experimental conditions we used for the Qa^-/Qa spectrum determination are the same we employed for examination of the S_1 --> S_2 transition. This is unlike the situation reported by Dekker *et al.* (1984a). In particular, for the Qa^-/Qa determination, Diphenylcarbazide (DPC) had been employed by them as a reductant of Y_Z^+. While the interaction of DPC and its oxidized form with other redox active species, e.g., ferricyanide or ferrocyanide, is uncertain, Dekker *et al.*

(1984a) did note that the stoichiometry for reaction with Y_Z^+ was unknown because the oxidized form of DPC they generated *in vivo* appeared to be different than the chemically oxidized form generated *in vitro* reported by Vernon and Shaw (1969).

Throughout this chapter the simple model of the reducing side suggested by Equations 4.1 and 4.2 has been assumed to be operative; however, in Section 4.1.2.1, difficulties with the model were raised and they will be considered here. The most difficult set of problems appear to revolve around the general issue of heterogeneous populations of reaction centers. This has occurred because of the observation that the apparent number of active reaction centers separately determined from chlorophyll concentrations, extent of Qa reduction (Melis and Anderson, 1983), and evolution of oxygen (Dennenberg *et al.*, 1986 and Graan and Ort, 1986) are not the same. In relationship to the work reported here, understanding this apparent heterogeneity is crucial because of the reliance upon the extent of the absorption change induced at 325 nm as being directly related to the concentration of reaction centers participating in charge separation and oxygen evolution.

4.4.1. Reaction Center Heterogeneity

Graan and Ort (1986), using chloroplasts, determined that the number of binding sites for terbutryn, an inhibitor of the Qb binding site similar in mode of action to DCMU, was higher than the number of centers reducing endogenous plastoquinone. It was found that two populations of PS-II centers existed. One population was effective at utilizing endogenous plastoquinone and could oxidize water, the second population could also participate in water oxidation provided specific exogenous acceptors were used. The effectiveness of these exogenous acceptors was found to be (in decreasing order of promoting fast electron

transfer from Qa) halogenated quinones > methyl-substituted quinones ~ endogenous quinones >> ferricyanide.

4.4.2. Alternative Secondary Electron Acceptors

It is probable that the two populations of PS-II centers they determined were the PS-II_a and PS-II_b centers that had already been proposed (see Melis and Homann, 1978). These two types of centers have been shown to have differing antenna sizes (Melis and Anderson, 1983) and different locations in the chloroplasts (Melis and Homann, 1978); specifically, PS-II_b is considered to be located in the stroma along with PS-I and has a smaller antenna size by at least a factor of two. In the isolation of Photosystem-II membranes, the PS-II_b centers are partitioned with the PS-I centers and removed from the preparation and their existence is therefore of no consequence to this work as the preparations used were almost wholly free of PS-I contamination. Alternative Secondary Electron Acceptors.

Another concern to be addressed involves the existence of alternative secondary electron acceptors and their effects upon the Qa^-/Qa difference spectrum. This was already alluded to earlier in the 'Materials and Methods Section' in discussing the order of addition of various chemicals; i.e., DCMU, ferricyanide, and DCBQ and their effects upon Q_{400}. The existence of these alternative acceptors has been widely reported and met with controversy as the evidence has largely been indirect. As an example, Jursinic and Dennenberg (1988) have proposed the existence of an ancillary (their terminology) or auxiliary quinone acceptor, Aq. The basis for their proposal was the stimulation of the absorption change at 325 nm they observed upon the addition of ferricyanide. The absorption increase was consistent with the increase in the area over the fluorescence curve in the same experiment. They have found that the midpoint

potential of Aq, 318 mV, is independent of pH and has a 0.38:1.0 Aq:Qa ratio. Unrelated experiments aimed at determining stoichiometric quantities of quinone per reaction center (Takahashi and Katoh, 1986, and de Vitry *et al.*, 1986) were unable to support the plastoquinone radical identity for Y_Z^+ (Ghanotakis *et al.*, 1983) because of the lack of quinone. These same conclusions are applicable here and do not support an ancillary quinone hypothesis.

Itoh (1978) introduced a species, A_H, to explain widely variable rates of Qa^- oxidation under differing conditions as monitored by variable fluorescence. This was refuted by Ghanotakis *et al.* (1983) by use of a simpler model that negated the introduction of another electron transport component. However, the existence has been confirmed in PS-II membranes of an acceptor species designated Q_{400}. Indirect evidence for Q_{400} has been reported since at least 1973 (Ikegami and Katoh, 1973, also see Bowes *et al.*, 1979). Petrouleas and Diner (1986) reported the first direct evidence of Q_{400} by using EPR and Mossbauer spectroscopy to monitor the correlated behaviour of a ferric and ferrous iron and they further demonstrated that this was the non-heme iron on the reducing side of Photosystem-II. This observation was confirmed by Zimmermann and Rutherford (1986).

Under some conditions the ferrous iron becomes oxidized to the ferric state and when Qa^- is reduced, the Fe(III) is reduced back to the Fe(II) state with a $t_{1/2}$ ranging from 7 to 25 *u*s (pH 6.5 and 7.5, Diner and Petrouleas, 1987a, 1987b). This fast reduction, being faster than either the forward or back reactions of Qa^-, can serve to reduce the detected extent of the reduction of Qa. Zimmermann and Rutherford (1986) showed that the iron oxidation could be caused by exogenously added quinones whose solution midpoint potentials are greater than for Fe^{3+}/Fe^{2+}, such as with phenyl-*p*-benzoquinone (PPBQ). The formation of Fe^{3+} was not observed with exogenously added 2,5-DCBQ.

Separately, the iron oxidation was inhibited strongly by the use of DCMU (Wraight, 1985).

Given these constraints on the formation of Fe^{3+} and our consistent use of either 2,5-DCBQ as an exogenously added quinone or of the DCMU and ferri-/ferrocyanide acceptor system, we conclude that our results presented here are not contaminated by Q_{400} oxidation of Qa^- and no conclusive evidence exists for other alternative electron transfer components that may interfere. The experiments described in the following chapter limit themselves solely to the S_1 --> S2 transition and the experimental conditions we use are such that Q_{400} plays no role.

TABLE 4.1

Effect of NH_2OH on the 320 nm Absorbance Change

Effect of Hydroxylamine on the induced absolution change at 320 nm in Tris-washed Photosystem II membranes. The observed extinction at 320 nm before the addition of NH_2OH was 10 $mM^{-1}cm^{-1}$. The granularity of each value reported is 36 turnovers. The final, washed value is a control in which NH_2OH was washed out by two resuspensions in the reaction media. Recovery to with 10% of the original confirms the reversibility of the NH_2OH treatment.

Number of Turnovers in NH_2OH	Total Absorption	Normalized Turnovers Change
0 (no add)	36	1.0
36	72	0.88
36	108	0.56
36	140	<0.25
	[sample washed twice]	
	176	0.9

FIGURE 4.1

Synchronous Relationship between Donor and Reducing Sides

This figure demonstrates 1.) The synchronous relationship between the binary reactions occurring on the reducing side of PS-II and the quaternary relationship on the oxidizing size, 2.) The variability in the order of reactions depending upon the number of oxidizing equivalents that have been accumulated by the OEC.

KINETIC PATHWAYS IN PHOTOSYSTEM II

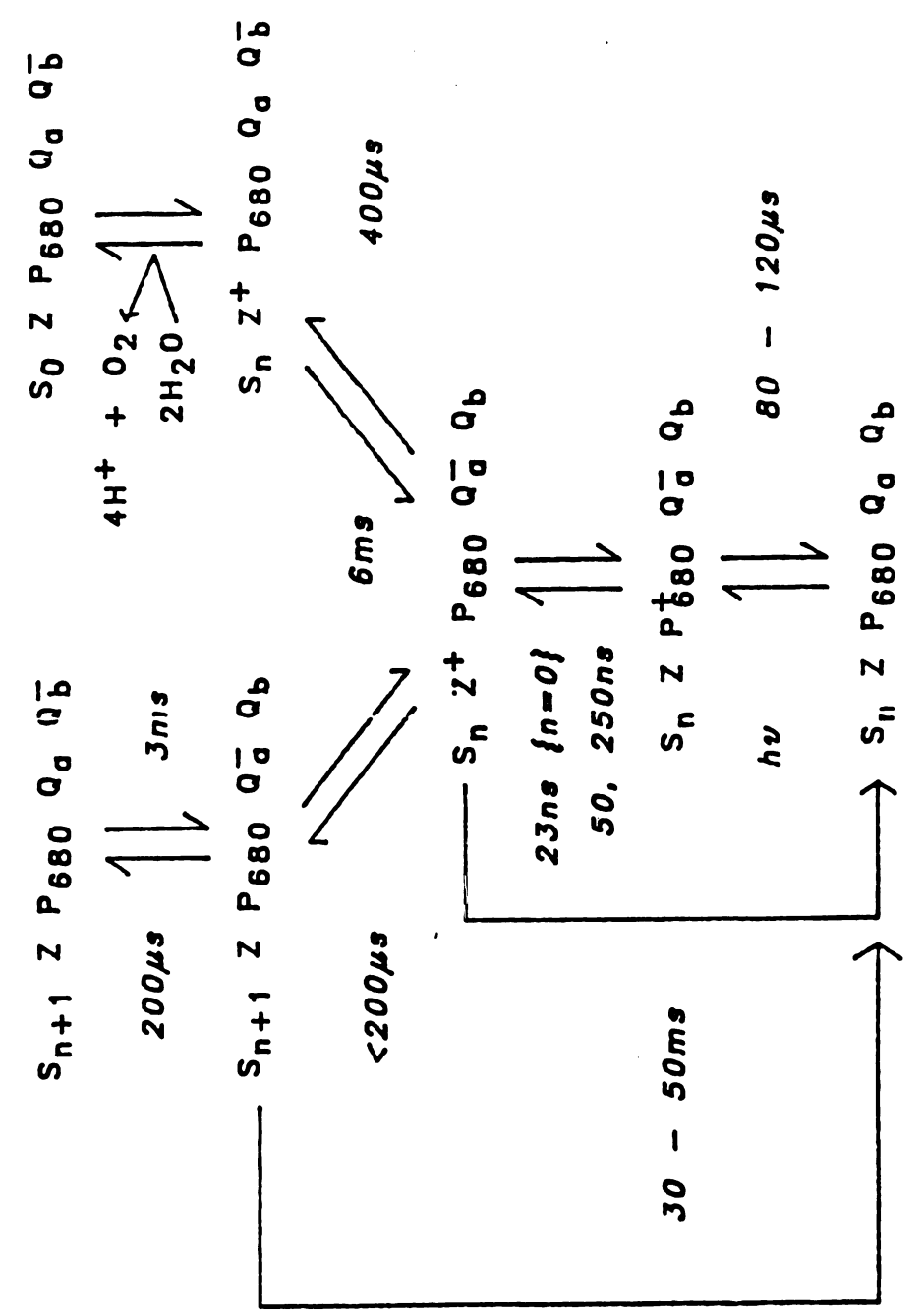

FIGURE 4.2

Inhibitory Sites in the PSII Electron Transport Chain.

a) Sites of selective inhibition in Photosystem II electron transport chain. Back-reaction pathways are not shown. The numbers in parenthesis represent sites of inhibition. See the next chapter for further details on inhibition involving the Oxygen Evolving Complex.

1. Inhibition at the Qb Binding site. Inhibition is either competitive (DCMU), removal of the site altogether (trypsin), or mutation.
2. Inhibition at the Oxygen Evolving Complex. Inhibition classically is heat or TRIS treatment; all of which release manganese, and are irreversible.
3. Inhibition near the Oxygen Evolving Complex. This involves removal of the peripheral polypeptides, the 33 kDa or removal of ionic co-factors. This inhibition is distinctly different from the previous one because the inhibition is reversible.
4. Inhibition interrupting the electron transport between the Oxygen Evolving Complex and Z. Temperature variation allows other endogenous donors such as b_{559} and Signal II_s to become competitive.
5. Inhibition interrupting the electron transport between Z and P_{680}.

b) Electron transfer in Photosystem II after TRIS-washing, inhibition with DCMU, and addition of ferri- and ferro- cyanide.

c) Possible loci of inhibition for NH_2OH. It was thought to either interrupt electron transfer between Z and P_{680} or to act directly upon P_{680}. It is now known that its mode of action is the former.

a)

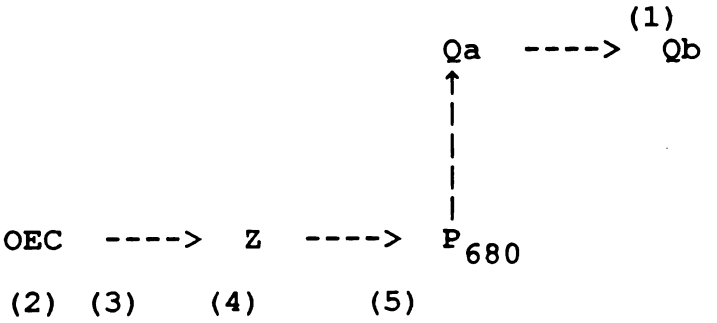
(1)
Qa ----> Qb
OEC ----> Z ----> P680
(2) (3) (4) (5)

b)

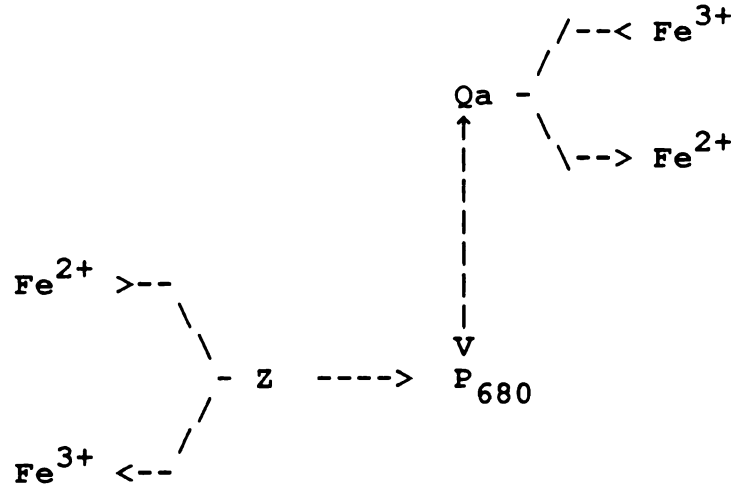
Fe3+
Qa
Fe2+
Fe2+
Z
V
P680
Fe3+

c)

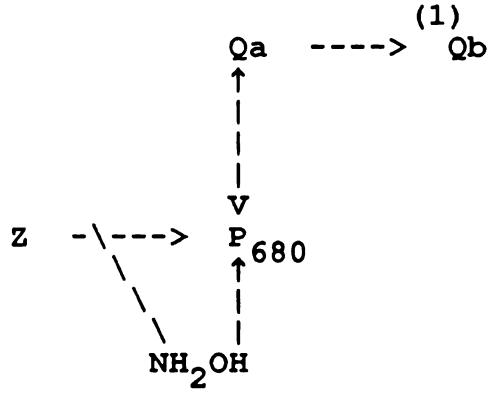
(1)
Qa ----> Qb
V
Z
P680
NH2OH

FIGURE 4.3

Saturation Profile of Qa-/Qa versus excitation intensity

This figure demonstrates that even with the variability in laser power photosynthesis, as measured by the reduction of Qa at 320 nm, is complete at even 1/3 of the original power. 100% laser power = 85 mJ, [Chl] = 200*u*M, tris-washed Photosystem II membranes. Donation to Qb blocked by 1 mM DCMU, and Ferri-/Ferro-cyanide used as acceptor system, 1 mM. The points represented by '+' are the average of 16 turnovers and the points represented by '*' are the average of 8 turnovers. No significant differences related to the onset of saturation was observed. Further discussion can be found in the text.

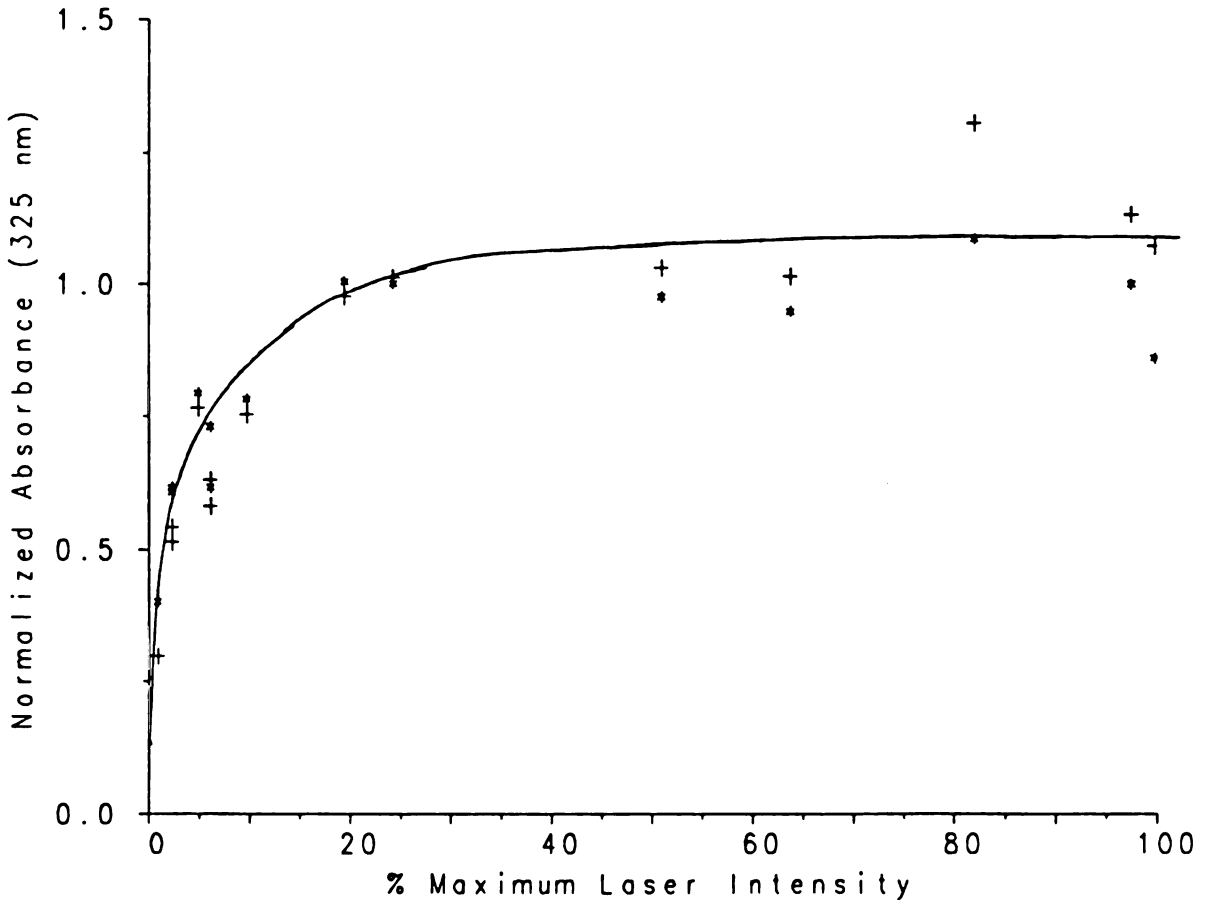
1.5
1.0
0.5
0.0
Normalized Absorbance (325 nm)
0
20
40
60
80
100
% Maximum Laser Intensity

FIGURE 4.4

The Absorption Spectra of Qa-/Qa

This is a point by point absorption difference spectrum of the QaQa transition in freshly prepared tris-washed Photosystem II membranes. The oxygen evolution rates of the Photosystem II membranes before Tris-washing were greater than 600 *u*moles/mg Chl/hr. Sample conditions were as follows: [Chl] = 124 *u*M, 1 mM DCMU, 1 mM ferricyanide, 1 mM ferrocyanide, pH adjusted to 6.0. Each point represents the average of 16 to 49 shots. Shortly before each shot the sample chamber was loaded from the sample reservoir and flushed afterwards. Further discussion can be found in the text.

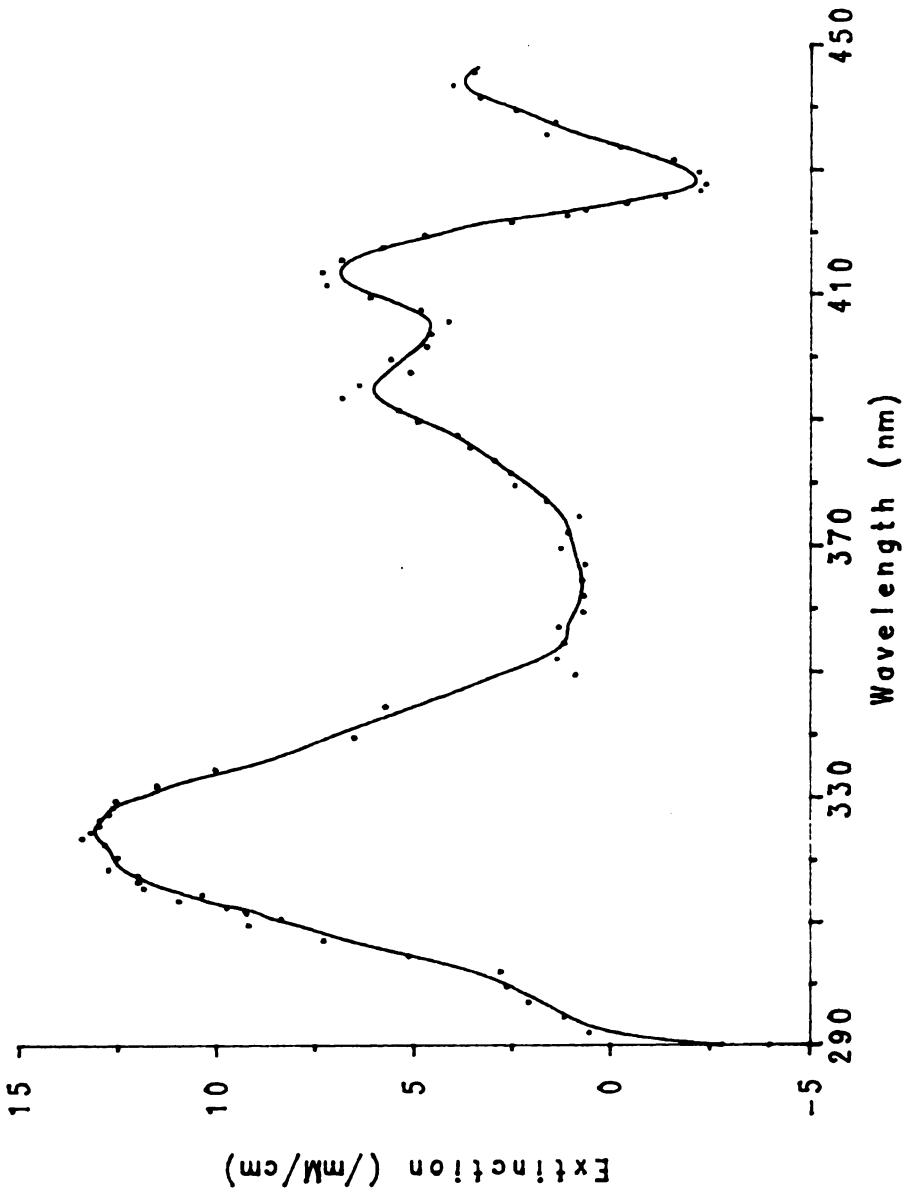
Extinction (/mM/cm)
15
10
5
0
-5
290
330
370
410
450
Wavelength (nm)

FIGURE 4.5

Comparison of Two Qa-/Qa Spectra

This figure compares the Qa^{-}/Qa spectrum we determined and the Qa^{-}/Qa spectrum reported by Dekker and co-workers (1984a). The points and the solid lines drawn through them represent are our results and the dashed line is is the line shape ultimately return This consists of the same spectra as in the previous figure and also plotted over the same wavelength range is the same spectra as shown in previous Figure except for an overlay of the spectra reported by Dekker under similar conditions. As can be seen, the two spectra are quite similar. Sample conditions were as described for Figure 4.4. Further discussion can be found in the text.

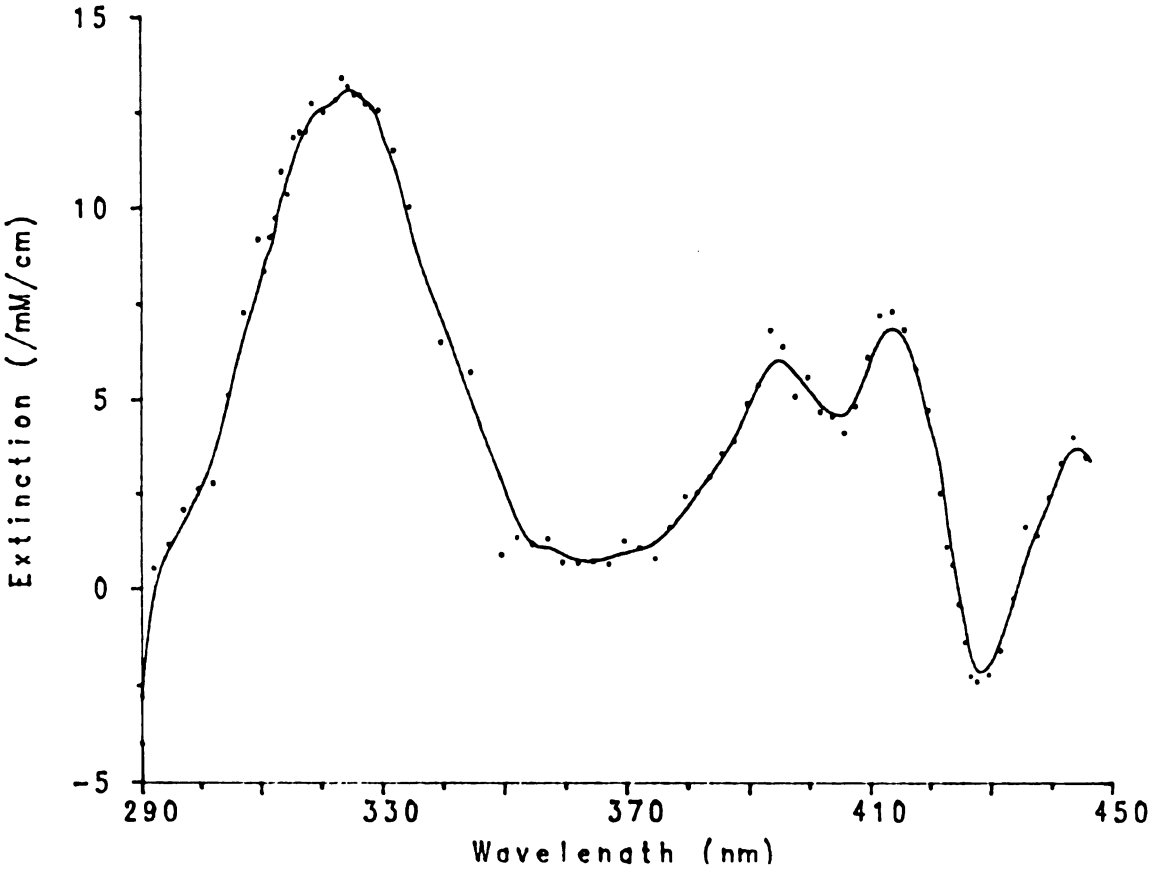
15
10
5
0
-5
Extinction (/mM/cm)
290
330
370
410
450
Wavelength (nm)

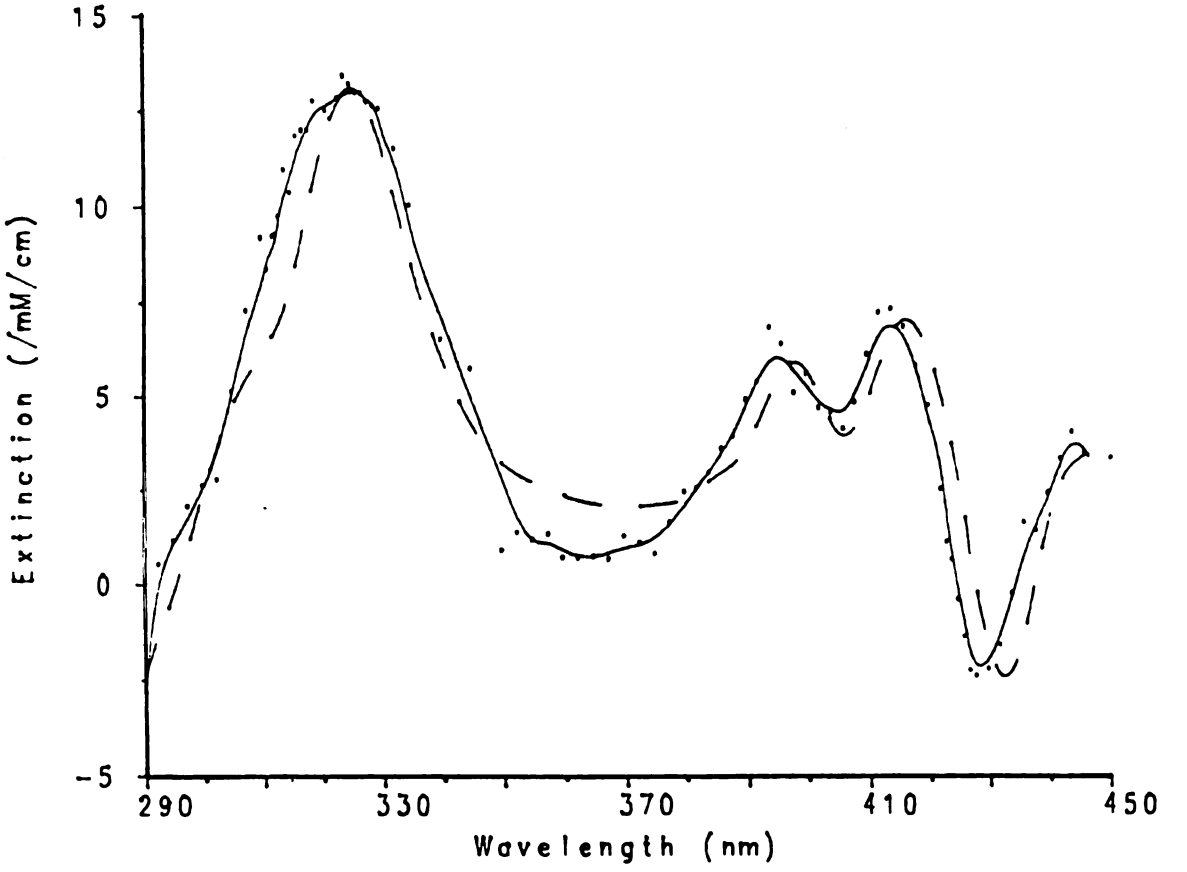
15
10
5
0
-5
Extinction (/mM/cm)
290
330
370
410
450
Wavelength (nm)

FIGURE 4.6

Exposure Time Effects on the Qa-/Qa change.

This figure demonstrates the effect of exposure time to the probe beam on the extent of the Qa/Qa change observed at 320 nm. The absorption extent has been normalized to 1. tris-washed Photosystem II membranes were used for this experiment, [Chl] = 100 *u*M, [DCMU] = 1.0 mM, $[Fe^{3+}] = [Fe^{2+}]$ = 1.0 mM. Each point is the average of 16 turnovers. Further discussion can be found in the text.

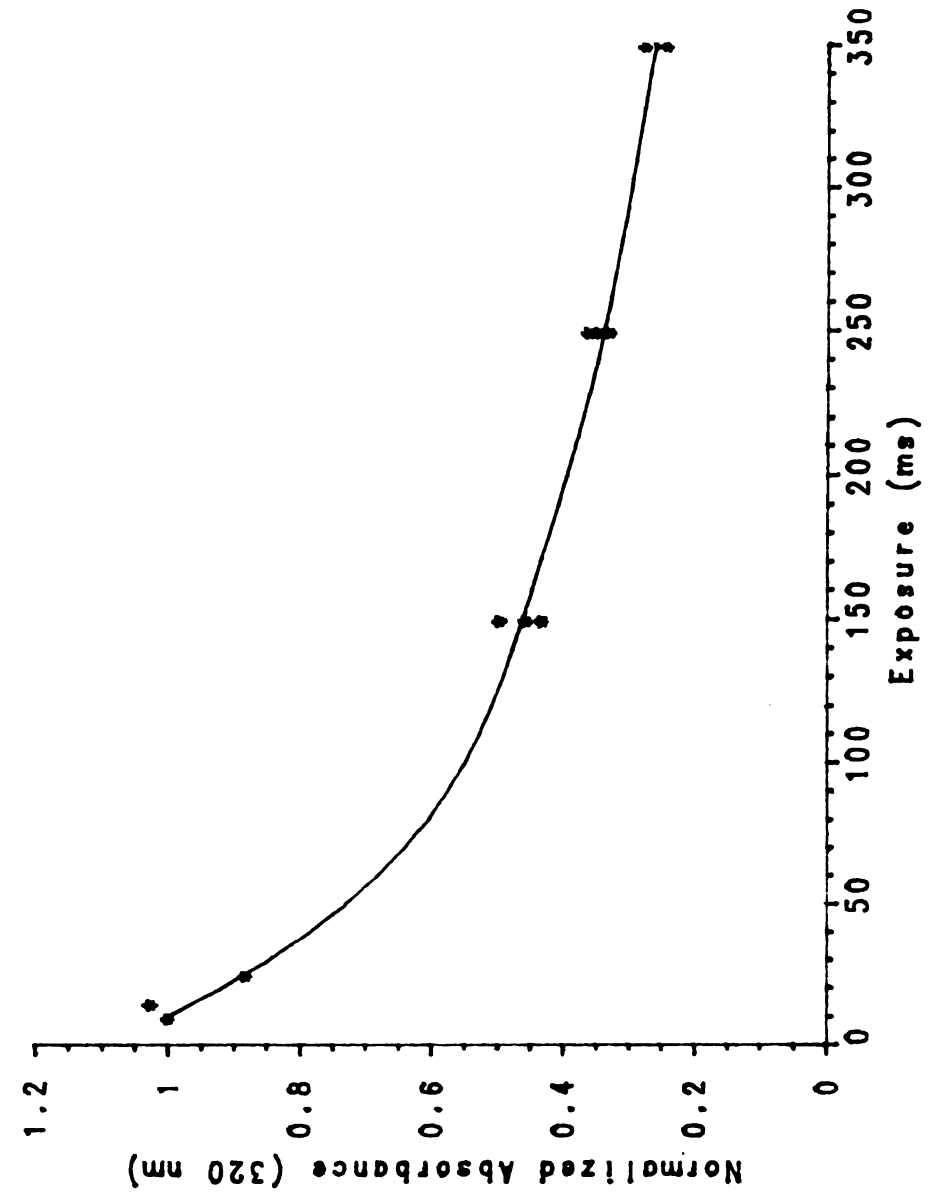
Normalized Absorbance (320 nm)
1.2
1
0.8
0.6
0.4
0.2
0
0
50
100
150
200
250
300
350
Exposure (ms)

FIGURE 4.7

Effects of External Acceptors on d[Qa-]/dt

This figure compares the effects of two different acceptor systems with Photosystem II membranes. Each trace represents the average of 16 turnovers at 320 nm. The top trace was collected using only a ferri-/ferrocyanide acceptor system and DCMU to prevent reduction of Qb. The bottom trace was collected using 2,5-DCBQ in addition to ferri-/ferrocyanide, DCMU was not added. Each trace represents the average of 16 flashes and they were normalized before plotting. Sample conditions were as follows: [Chl] = 120 uM, [DCBQ] = 100 uM, $[Fe^{3+}] = [Fe^{2+}]$ = 0.5 mM, [DCMU] = 1 mM (top trace only), and pH adjusted to 6.0. Discussion in text.

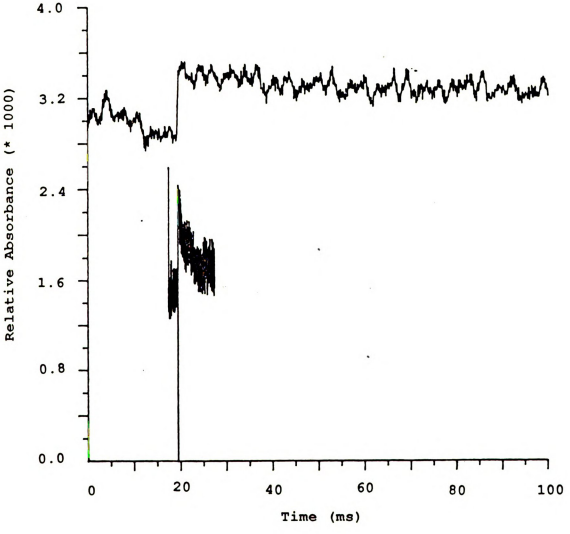
4.0
3.2
2.4
1.6
0.8
0.0
Relative Absorbance (* 1000)
0
20
40
60
80
100
Time (ms)

FIGURE 4.8

Absorption Spectrum of Tris-Washed PS-II membranes

This is an absorption spectrum of tris-washed PS-II membranes shortly after preparation. This is illustrative of the optical thickness of the samples we handle. The difficulty of collecting data below 300 nm can be appreciated by observing the steady increase in background absorption as one goes further into the UV. The sample has a higher background absorption in the green, around 450 nm, but this is compensated for as the sensitivity of the PMT in this region is increasing as well as the output power from the Xenon lamp (data not shown). Another complication, however, is that the background changes very rapidly and so short exposure time to a probe beam is essential to get an accurate baseline.

For this experiment, the [Chl] = 37 mM and the data was collected by a Perkin-Elmer scanning spectrometer.

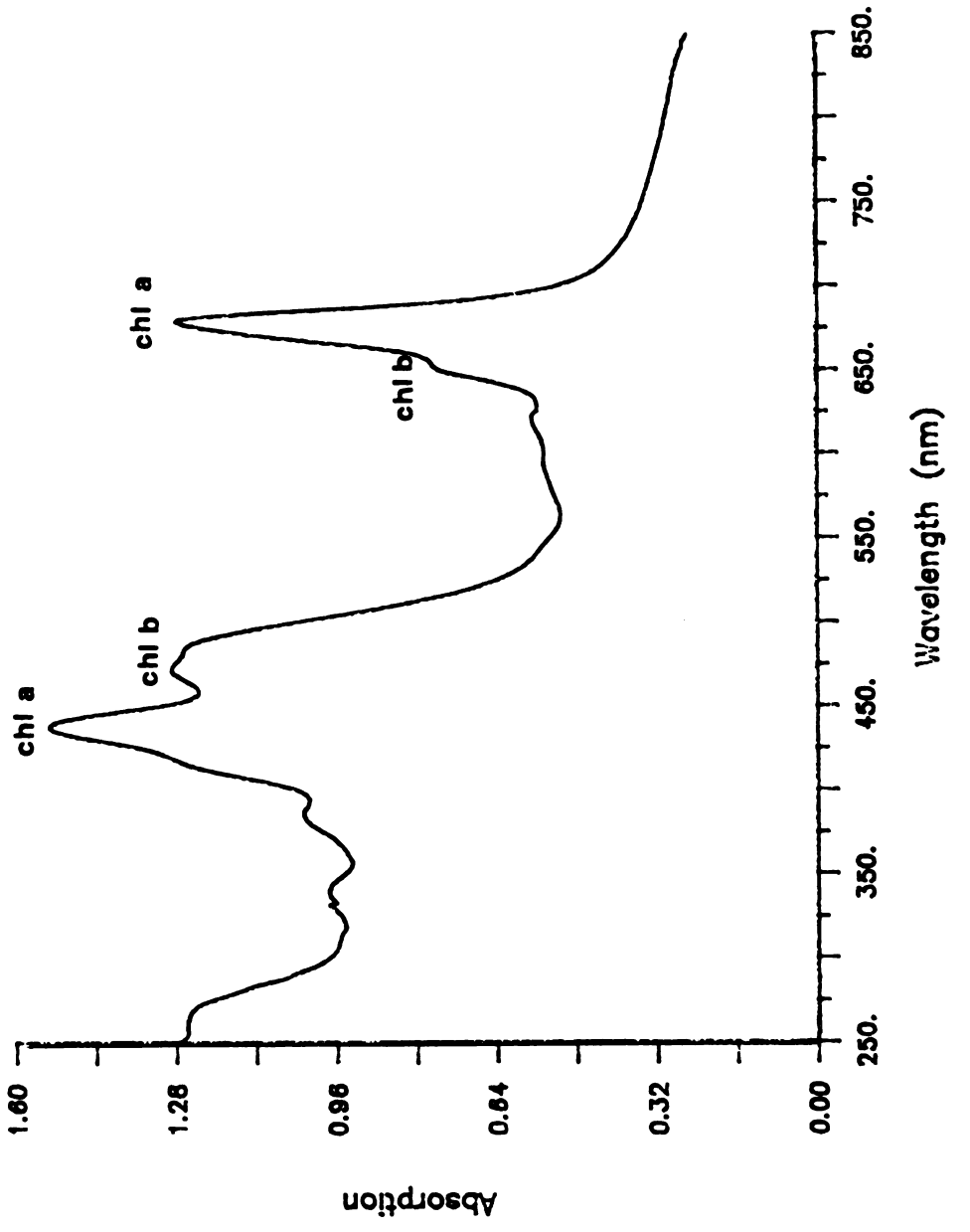
chl a
chl b
chl a
chl b
1.60
1.28
0.96
0.64
0.32
0.00
250.
350.
450.
550.
650.
750.
850.
Absorption
Wavelength (nm)

FIGURE 4.9

C-550 Bandshift

C-550 bandshift in tris-washed Photosystem II membranes. This bandshift is symmetrically centered around 545 nm and is due to the shift of the intermediate pheophytin's absorption spectrum induced by the reduced Qa^-.

Points were collected every 5 nm, slit width = 0.5 mm, wavelength bandpass = 6 nm. [Chl] = 85 *u*M, [DCMU] = 10 *u*M, $[Fe(CN)_6^{3-}] = [Fe(CN)_6^{4-}]$ = 0.5 mM, pH 6.0. Sample exposure time was 3 ms. It was necessary to use another grating optimized for the visible wavelength region in the monochromatoer for these experiments.

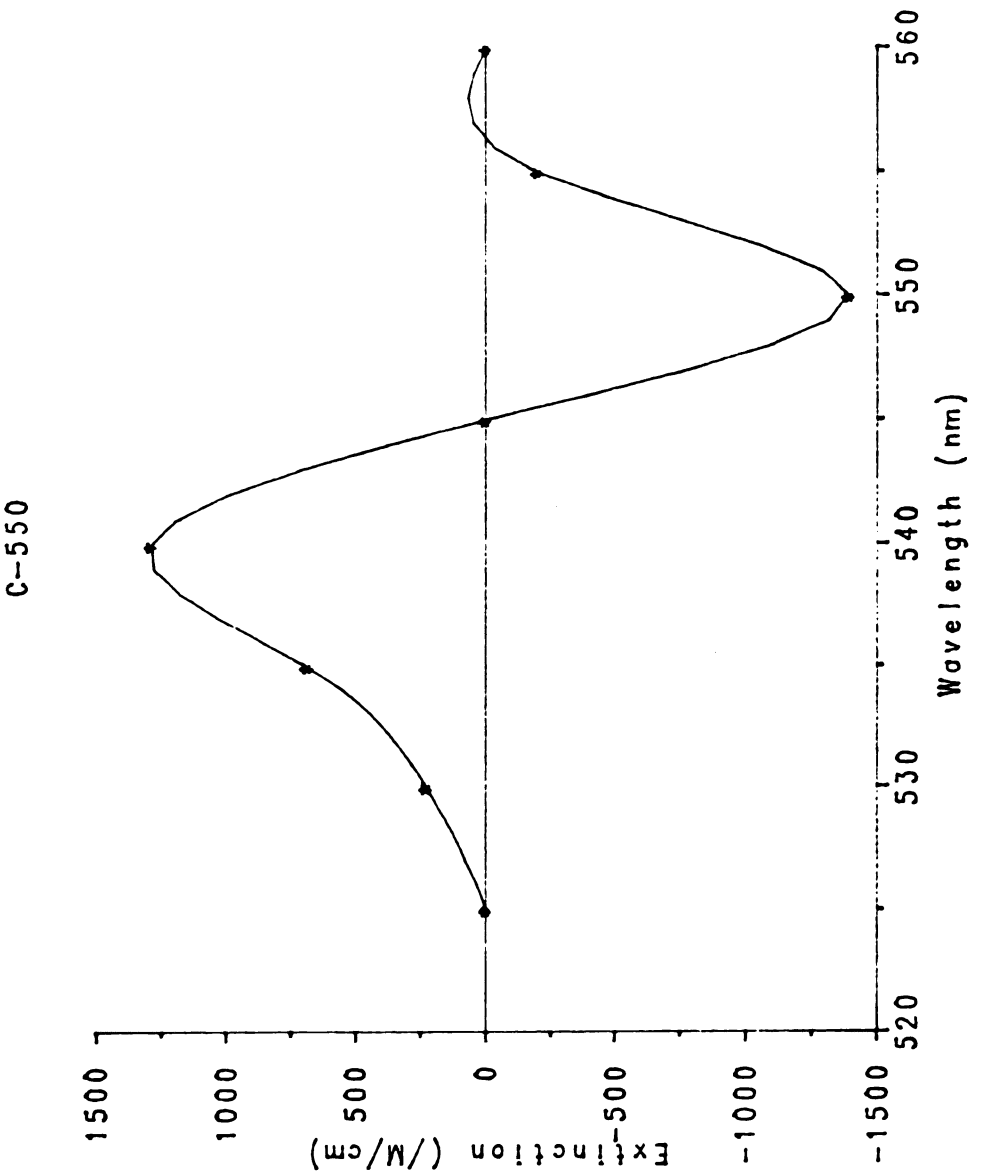
C-550
1500
1000
500
0
-500
-1000
-1500
Extinction (/M/cm)
520
530
540
550
560
Wavelength (nm)

FIGURE 4.10

Kinetic Data Processing

This figure depicts a simplified view of the processing of kinetic data once it has been transferred from the transient signal averager into the host computer. The 'Single Collection' is the actual collection by the transient signal averager of 1024 points in real-time and transmission to the host computer. The 'N Collection' is the summation of the set of data collected and, while not done real-time, is completed for each single collection cycle. The storage to a computer readable file is done when this full set of data has been collected. Further data transformations, such as the construction of the absorption difference spectrum, is performed by other software once all the sets have been collected.

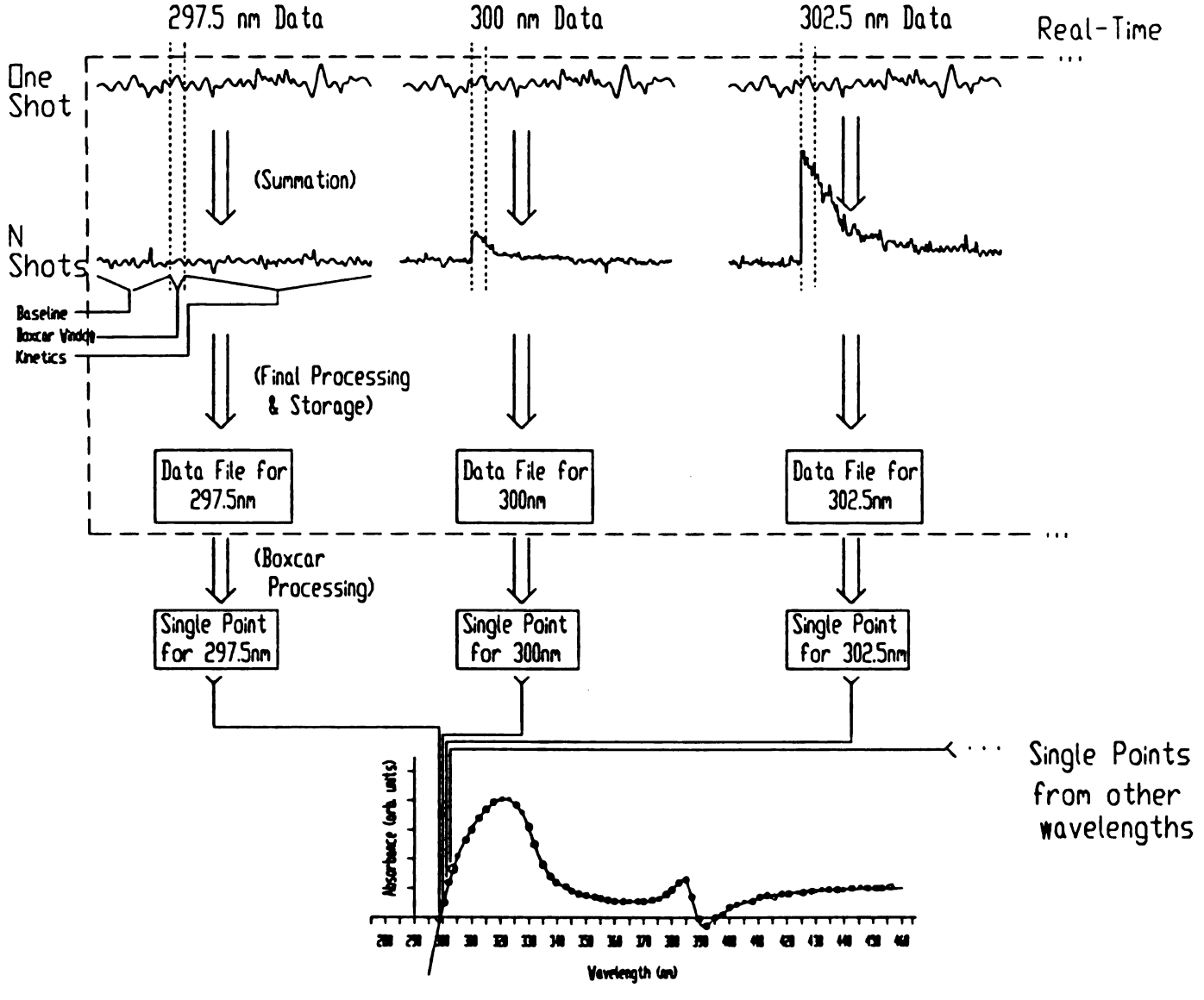
297.5 nm Data
300 nm Data
302.5 nm Data
Real-Time
One Shot
(Summation)
N Shots
Baseline
Boxcar Width
Kinetics
(Final Processing & Storage)
Data File for 297.5nm
Data File for 300nm
Data File for 302.5nm
(Boxcar Processing)
Single Point for 297.5nm
Single Point for 300nm
Single Point for 302.5nm
Single Points from other wavelengths
Absorbance (arb. units)
Wavelength (nm)

References

Berthold, D. .A., Babcock, G. .T., and Yocum, C. F. (1981). FEBS Letters, 134,231-234.

Bensasson, R., and Land, E.J., (1973), Biochimica et Biophysica Acta, 325*, 345-348.

Bolby, N. and Yocum, C. F. (1987). Private Discussions.

Bowes, J. M., Crofts, A. R., and Itoh, S. (1979). Biochimica et Biophysica Acta, 547, 320-335.

De Vitry, C., Carles, C., and Diner, B. A., (1986). FEBS Letters, 196, 203-206.

Den Hann, G. A., Gorter de Vries, H., and Duysens, L. N. M. (1976). Biochimica et Biophysica Acta, 430, 265-281.

Dekker, J. P., Van Gorkom, H. J., Brok, M., and Ouwehand, L., (1984a). Biochimica et Biophysica Acta, 764, 301-309.

Dekker, J. P., Van Gorkom, H. J., Wensink, J., and Ouwehand, L. (1984b). Biochimica et Biophysica Acta, 767, 1-9.

Dennenberg, R. J., Jursinic, P. A., and McCarthy, S. A. (1986). Biochimica et Biophysica Acta, 852, 222-233.

Diner, B. A. and Petrouleas, V. (1987a). Biochimica et Biophysica Acta, 895, 107-125.

Diner, B. A. and Petrouleas, V. (1987b). Biochimica et Biophysica Acta, 893, 138-148.

Ghanotakis, D. F., Topper, J. N., Babcock, G. T., and Yocum, C. F. (1984). FEBS Letters, 170, 169-173.

Ghanotakis, D. F. and Babcock, G. T. (1983). FEBS Letters, 153, 231-234.

Ghanotakis, D. F., O'Malley, P. J., and Babcock, G.T. (1983). "The Oxygen Evolving System of Photosynthesis", 91-101, (Inoue, Y., Crofts, A. R., Govindgee, Murata, N., Renger, G., and Satoh, K., eds), Academic Press, Tokyo.

Graan, T. and Ort, D. R. (1986). Biochimica et Biophysica Acta, 852, 320-330.

Haveman, J. and Mathis, P. (1976). Biochimica et Biophysica Acta, 440, 346-355.

Hoganson, C., (1988) Private Discussions.

Ikegami, I. and Katoh, S. (1973). Plant Cellular Physiology, **14**, 829-836.

Itoh, S. (1978). Biochimica et Biophysica Acta, **504**, 324-340.

Joliot, P. and Joliot, A. (1981). FEBS Letters, **134**, 155159.

Joliot, P. Beal, D., and Frilley, B. (1980). Journal de chimie physique, **77**, 209-216.

Jursinic, P. and Dennenberg, R. (1988). Biochimica et Biophysica Acta, **935**, 225-235.

Kleinfeld, D., Okamura, M. Y., and Fehr, G., (1985). Biochimica et Biophysica Acta, **809**, 291-310.

Kleinfeld, D., Okamura, M. Y., and Fehr, G., (1984). Biochmica et Biophysica Acta, **766**, 126-140.

Ikegami, I. and Katoh, S. (1973). Plant Cell Physiology, **14**, 829-836.

Lillie, D., (1984) M.S. Thesis, "The Development and Characterization of a Flash Kinetic Absorption Spectrometer", M.S.U.

Malmstadt, H. V., Enke, C. G., and Crouch, S. R. (1981). "Electronics and Instrumentation of Scientists," 422-426,The Benjamin/Cummings Publishing Company, Inc., California.

McCauley, S. W. and Melis, A. (1986). Biochimica et Biophysica Acta, **849**, 175-182.

Melis, A. and Anderson, J. M. (1983). Biochimica et Biophysica Acta, **724**, 473-484.

Melis, A. and Homann, P. (1978). Archives of Biochemistry and Biophysics, **190**, 523-530.

Petrouleas, V. and Diner, B. A. (1986). Biochimica et Biophysica Acta, **849**, 264-275.

Pulles, M. P., Van Gorkom, H. J., and Verschoor, G. A. M. (1976). Biochimica et Biophysica Acta, **440**, 98-106.

Renger, G., Hagemann, R., and Fromme, R. (1986). FEBS Letters, **203**, 210-214.

Renger, G. (1976a). FEBS Letters, **69**, 225-230.

Renger, G. (1976b). Biochimica et Biophysica Acta, **440**, 287-300.

Renger, G., Erixon, K., Doring, G., and Wolff, Ch. (1976). Biochimica et Biophysica Acta, **440**, 278-286.

Robinson, H. H., Sharp, R. R., and Yocum, C. F. (1981). Archives of Biochemistry and Biophysics, **207**, 1-8.

Robinson, H. H., Sharp, R. R., and Yocum, C. F. (1980). Biochemical Biophysical Research Communications, **93**, 755-761.

Savitsky, A. and Golay, M. J. E. (1964). Analytical Chemistry, **36**, 1627-1639.

Slooteen, L. (1972). Biochimica et Biophysica Acta, **275**, 208-218.

Stiehl, H. H. and Witt, H. T. (1969). Z. Naturforsch., B. Inorganic Chemistry, Organic Chemistry, Biochemistry, Biophysics, and Biology, **24B**, 1588-1598.

Takahashi, Y. and Katoh, S. (1986). Biochimica et Biophysica Acta, **848**, 183-192.

Van Gorkom, H. J. (1974). Biochimica et Biophysica Acta, **347**, 439-442.

Velthuys, B. R. (1988). Biochimica et Biophysica Acta, **933**, 249-257.

Vermeglio, A. and Clayton, R. K. (1977). Biochimica et Biophysica Acta, **461**, 159-165.

Volker, M., Renger, G., Rutherford, A. W. (1986). Biochimica et Biophysica Acta, **851**, 424-430.

Wraight, C. A. (1985). Biochimica et Biophysica Acta, **809**, 320-330.

Xing, M. X. (1989). Private communication.

Zimmermann, J.-L. and Rutherford, A. W. (1986). Biochimica et Biophysica Acta, **851**, 416-423.

CHAPTER 5

Optical Studies of the S_1 --> S_2 Transition

5.1. INTRODUCTION

The oxygen evolving complex (OEC) was introduced in Chapter One. Its distinct, spectroscopically observable, five redox state cycle and associated nomenclature in terms of S_0, S_1, ... , S_n terminology was discussed in some detail. In preparations of chloroplasts, Photosystem II membranes, and PS-II 'cores' (Ghanotakis and Yocum, 1986) that are active in evolving dioxygen, the OEC will have associated with it three extrinsic water soluble polypeptides of 17, 23, and 33 kDa (these are referred to in the literature by some researchers as 18, 24, and 33 kDa), four manganese, and supporting Ca^{2+} and Cl^- ions. The exact number of supporting ions is uncertain, Cammarata and Cheniae (1987) have reported one Ca^{2+} per PS-II; however, Ono and Inoue (1987) have reported that there are two Ca^{2+} per PS-II reaction center. A recent report by Shen *et al.* (1988) has placed the number back at one again. There is evidence for involvement of the intrinsic 33 kDa polypeptide, the intrinsic 34 kDa polypeptide, or both in manganese binding but the available data is inconclusive and does not pertain to the work here (see Metz *et al.*, 1980, 1984, and 1986). The requirements for the presence of most of these co-factor were listed in Table 1.1. In this Chapter we present flash induced optical absorption spectra corresponding to the S_1 --> S_2 transition in green plant PS-II systems under conditions in which we have systematically depleted the endogenous Cl^- cofactor and reconstituted with a series of monovalent anions known to restore O_2

evolution to some extent. These results are currently being prepared for publication elsewhere (Lillie and Babcock, 1989).

5.1.1. Polypeptide Depletion

5.1.1.1. The 23 kDa Polypeptide

Discriminating between the roles played by the 17 and 23 kDa polypeptides in the OEC has been complex because of the degree of their association. The three extrinsic polypeptides are normally not removed during isolation of O_2 evolving Photosystem II membranes. Incubation in concentrated NaCl will specifically release the 17 and 23 kDa polypeptides and will leave the 33 kDa and the manganese functionally associated with the OEC (Åkerlund *et al.*, 1982, Ghanotakis *et al.*, 1984a and 1984b, and Miyao and Murata, 1984b). This depletion inhibits O_2 evolution. Oxygen evolution can be reconstituted almost wholly in these polypeptide depleted membranes (hereafter referred to as NaCl washed or salt washed) by rebinding the 23 kDa and, optionally, the 17 kDa (Miyao and Murata, 1983). Reconstitution can also be achieved by use of non-physiological concentrations of $CaCl_2$ (Ghanotakis *et al.*, 1984b, Miyao and Murata, 1984a). In fact, Ghanotakis and co-workers showed that the reconstitution is due to the divalent cation instead of the anion by showing 26% and 42% reconstitution by using $MgCl_2$ and $SrCl_2$ respectively and no reconstitution with NaCl. An alternative viewpoint has been expressed, though, by Blough and Sauer (1984) as they claimed it was the relative solubilities of the polypeptides in the salt solutions that was crucial as opposed to the valency of the salts. The NaCl washed PS-II membranes were shown to have lost 40% of their Ca^{2+} and the remaining Ca^{2+} apparently occupied loose binding sites on the membranes (Ghanotakis *et al.*, 1984b). Dialysis of these membranes against

EGTA, a chelating agent, removed the rest of the Ca^{2+}. O_2 evolution was not stimulated in these NaCl, EGTA washed membranes by polypeptide reassociation even though the polypeptides were shown to definitely rebind. O_2 evolution could be stimulated, though, by the addition of Ca^{2+}. Ghanotakis and co-workers also showed that the degree of stimulation was dependent upon the order of addition. If the Ca^{2+} was added before the polypeptides then O_2 evolution was stimulated as soon as the rebinding of the polypeptides occurred. If the Ca^{2+} was added after the polypeptides were rebound then an hour or more of incubation was required to achieve 90% reconstitution. From this it can be concluded that an absolute requirement for Ca^{2+} exists for high rates of oxygen evolution. The ability of Ca^{2+} to reconstitute oxygen activity in NaCl washed and NaCl, EGTA washed membranes and the dependency of the rate of reconstitution upon the order of addition between Ca^{2+} and the 23 kDa polypeptide has led to the conclusion that Ca^{2+} serves in a structural and possibly catalytic role in the OEC (Ghanotakis *et al.*, 1984a). The 23 kDa seems to play only a structural role by providing an environment that lessens but does not eliminate the absolute requirement for Ca^{2+}.

5.1.1.2. The 17 kDa Polypeptide.

A well defined role for the 17 kDa has not yet emerged. It is not essential for O_2 evolution as evidenced by the previous section. Miyao and Murata (1985) and Akabori *et al.* (1984) have suggested that it reduces the requirement for Cl^-. The Cl^- requirement is 5 to 10 m<u>M</u> upon rebinding of only the 23 kDa. Akabori *et al.* (1984) observed that the Cl^- requirement dropped to below 1 m<u>M</u> (also see Imaoka *et al.*, 1986). However, Waggoner and Yocum (1987) have shown that they can deplete the 17 kDa by washing with 60 m<u>M</u> $MgCl_2$ (or $CaCl_2$). Under these conditions, they retain the 23 kDa largely on the membrane in an apparent

functional role. They did not observe a Cl^- effect ascribed by others to the 17 kDa.

5.1.1.3. The 33 kDa Polypeptide.

The NaCl and EGTA treatments do not remove either the 33 kD polypeptide or the four managanese atoms from the PS II membranes. An additional incubation in either 1.0 M $CaCl_2$ or 2.6 M urea is required to remove the 33 kDa (Ono and Inoue, 1984, and Miyao and Murata, 1984b). Either treatment leaves the four manganese atoms functionally associated with the OEC; however, they appear to have become more sensitive to the bulk constituents and their concentrations. Miyao and Murata (1984b) incubated membranes depleted of the 17, 23, and 33 kDa polypeptides for four hours in a series of salt buffers at differing salt concentrations. Those with the highest concentrations of Cl^- (200 mM) retained the highest O_2 evolving activity, and also showed that the cation, in the form of Na^+, K^+, Mg^{2+}, or Ca^{2+}, did not appear to be responsible for retaining O_2 rates, and, with regards to Mg^{2+}, may even have been inhibitory. The 33 kDa polypeptide and Cl^- both appear to function in structural/protectant roles. The evidence is as yet incomplete and does not allow for discrimination between the two.

5.1.2. Spectroscopic Probes of the Internal S-states

5.1.2.1. EPR Signals Arising from the Oxygen Evolving Complex.

All of the S-states of the model proposed by Kok (Kok *et al.*, 1970) are EPR silent except for the S_2 state. In 1980 (Dismukes and Siderer, 1980 and 1981) determined that an EPR signal consisting of 16 or more peaks, the 'multi-line,' was directly correlated with the S_2 state. Another EPR signal that was

found in samples treated with DCMU and exposed to continuous illumination at low temperatures and is centered around g = 4.1 (hereafter referred to as the g4.1) had also been observed. de Paula and Brudvig (1985) definitively associated the g4.1 signal with a configuration of the S_2 state different than that which gives rise to the S_2 multiline EPR signal. The formation of the S_2 state in NaCl washed and Cl^- depleted PS-II membranes has been controversial. Blough and Sauer (1984) reported that the amplitude of the multiline they observed paralleled the percentage inhibition of oxygen evolution in NaCl washed and reconstituted PS-II membrane samples. Franzén *et al.* (1985) are in agreement concerning the NaCl washed membranes. However they have also observed that Cl^- depleted, but not polypeptide depleted samples, while not exhibiting steady state oxygen evolution, do exhibit a strong multiline signal, indicating that an S_2-like state can been formed. Ono *et al.* (1987) did not observe a multi-line on a single flash. They did note however, that if Cl^- were added the multi-line would form after a single flash had been given. Beck (1988) has repeated the experiments described by Franzén and Ono and found that the g4.1 signal is formed and is converted to the multiline upon addition of NaCl. It was further realized that the nature of the cryoprotectant, 0.4 M sucrose or 30% ethylene glycol, strongly affected the conformation adapted by the S_2 state. The g4.1 state appears to be the stable state when sucrose is used.

5.1.2.2. Optical Signals Arising from the Oxygen Evolving Complex.

The first report for the S_1 --> S_2 optical transition was a difference spectrum recorded by Velthuys (1981) in choloroplasts. The difference spectrum he reported was characterized by a broad, symmetrical band that peaked at 320 nm. He used NH_2OH treated PS-II membranes to obtain an optical spectrum for which the contributions arising from the S_1 --> S_2 transition had been eliminated

(Joliot, 1966). This spectrum was then subtracted from a spectrum obtained from untreated PS-II membrane, and the resulting difference spectrum was due, it was presumed, solely to the OEC. Velthuys suggested that the magnitude of the absorbance changes observed with successive excitations followed the pattern {0,1,0,-1}. This is a short hand method of describing the changes: the first '0' is the magnitude of the change for the S_0 --> S_1 change, the '1' is for the S_1 --> S_2 change, the next '0' and '-1' are for the S_2 --> S_3 --> S_4 changes respectively. Dekker *et al.* (1984a) reported an absorption difference spectrum for the S_1 --> S_2 transition in DCMU inhibited Photosystem II membranes by subtracting out spectral contributions from Qa^-/Qa and Z^+/Z. The spectra for these were determined separately in tris-washed PS-II membranes. They extended the work (Dekker *et al.*, 1984b) by determining the absorption difference spectrum for all of the S-state transitions. Unlike the results reported by Velthuys, the S_1 --> S_2 spectrum reported by Dekker *et al.* (1984a) was asymmetric, peaked at 305 nm, and the absorbance pattern for the set of S-state changes was {1,1,1,-3}. On the basis of the S_n --> S_{n+1} bandshape similarity to the difference spectrum between Mn(III) and Mn(IV) gluconate complexes they assigned the S_1 --> S_2 transition to a Mn(III) --> Mn(IV) transition. The interpretation of Dekker and co-workers of the optical changes attributed to the OEC has been the subject of considerable controversy in the literature in terms of the assignment of the Mn(III) --> Mn(IV) transitions and the similarity of the absorption spectra throughout the S-state cycle. Lavergne (1986) favors the model proposed by Velthuys (1981) in which the absorption changes follow the pattern {0,1,0,-1}. His analysis of the data reported by Dekker *et al.* (1984a and 1984b) indicates that the experimental results could not distinguish definitively between either model. He presented additional data from a mutant strain of *IC. sorokiniana* in which the initial S_0/S_1 ratios had been varied. This data further supported the {0,1,0,-1} model.

Lavergne (1987) presented optical difference spectra for the S-state changes and showed that the S_1 --> S_2 and S_2 --> S_3 spectra were similar in shape though differing in magnitude, and both differed considerably from the S_0 --> S_1 spectrum. The S_1 --> S_2 spectrum reported by Lavergne is of similar shape to that reported by Dekker *et al.* (1984b). Vincent and Christou (1986) challenged the identification of the manganese oxidation states on the basis of their manganese model compound results. They have reported that the UV and visible difference absorption spectra of Mn(II,III) and Mn(III,III) oxo-bridged carboxylate complexes are as similar to the transitions reported by Dekker *et al.* (1984a) as are the manganese gluconate complexes. Renger and Weiss (1986) obtained spectra for the S_0 --> S_1 and S_2 --> S_3 transitions that were similar to each other and peaked at 320 nm. The S_1 --> S_2 was shown to be different. They used trypsin treated PS-II membranes in conjunction with ferricyanide to remove acceptor side contributions; however, trypsin has been shown to digest the OEC in part (see Chapter 4, Section 4.1.2.2) and the spectra they show in the presence of an exogenous quinone acceptor appear to have binary oscillation components. This is suggestive that the trypsin treatment has not been successful at removing all of the acceptor side contributions. Saygin and Witt (1985) initially differed with Dekker and co-workers as well. They showed that differences between various models rely in effect upon variations in S_0/S_1 distributions and could not be resolved from experimental data. They went on to use NH_2OH to set the S-state population to one S-state specifically and used silicomolybdate as an electron acceptor to bypass Qa to Qb donation (however, see Grann, 1986, regarding this misconception). Their results were similar to those reported by Renger and Weiss (1986) in that the changes for S_0 --> S_1 and the S_2 --> S_3 were similar and those for the S_1 --> S_2 were different. Recently, a joint paper was published (Kretschmann *et al.*, 1987) in which the two

groups agreed that the S_1 --> S_2 and S_2 --> S_3 transitions have similar spectra and are due to Mn(III) --> Mn(IV) transitions. The S_0 --> S_1 spectrum is different and they concluded that it is most likely due to a Mn(II) --> Mn(III) transition.

5.1.3. Goals of this Chapter

It is clear, given the above discourse, that resolution of the optical difference spectra of the S-states is complex and lacking in external controls that can be applied unambiguously to remove spectral contaminants such as Qa^-/Qa, Qb^-/Qb, and Q_{400}. Another approach, however, could be to examine relative changes of the absorption bands as a result of Cl^- depletion and X^- reconstitution, where X^- = {OH^-, Cl^-, Br^-, and NO_3^-}; note: throughout this chapter, X^-, will be used and without qualifying terms it will be meant to include the set of anions listed here. In principle, since the only factor changing in these experiments is the anion co-factor, the other component contributions cancel out. This Chapter, therefore, analyzes these relative changes for the S_1 --> S_2 transition.

5.2. MATERIALS AND METHODS

5.2.1. Biological Preparations and Handling

Chloroplasts and Photosystem II membranes were prepared as described in the previous Chapter. The following procedures presume the availability of such materials, either from frozen stock (stored at -40^{o}C) or freshly prepared. The viability of the samples was determined strictly from their capacity to support sustained oxygen evolution under continuous illumination. See the 'Oxygen Evolution Assays' section for details.

5.2.1.1. Polypeptide Depletion

Polypeptide depletion procedures are as described in Ghanotakis *et al.* (1984b) and outlined here. The Photosystem II membrane sample is adjusted to a concentration of 2 mg Chl/ml in a buffer of 400 mM sucrose, 50 mM Mes (pH 6.0), 5 mM $MgCl_2$, 15 mM NaCl (resuspension buffer). After stirring in the dark for 5 minutes, an equal volume of 4 M NaCl and 50 mM Mes (pH 6.0) was added dropwise, stirred for an additional 5 minutes in the dark, and allowed to incubate on ice for 1 hour. The mixture was then centrifuged at 40,000 x g for 30 minutes. The supernatant was discarded and the pellet suspended in the resuspension buffer. This was then centrifuged at 40,000 x g for 30 minutes. The supernatant was discarded and the pellet was suspended in the resuspension buffer at a concentration of approximately 2.0 mg Chl/ml. If this were not to be used within 6 hours the sample was stored at -40^{o}C; otherwise, it was kept on ice in the dark. The resulting Photosystem II membranes were free of the 17 and 23 kDa polypetides as determined by Ghanotakis *et al.* (1984a).

5.2.1.2. Chloride Depletion.

The same procedure as that described above was followed; however, the last suspension took place in a salt-free media, 400 mM sucrose and 50 mM Mes (pH 6.0). The suspension was stirred in the dark on ice for 30 minutes and then centrifuged at 40,000 x g for 30 minutes. The supernatant was discarded, the pellet resuspended in the salt free media, stirred in the dark on ice, and again centrifuged for 30 minutes at 40,000 x g. These samples were used within 6 hours of their preparation. We experimented with using SO_4^{2-} as a replacement for Cl by adding 5 mM Na_2SO_4 to the salt free buffer solution. No significant differences were observed between the behaviour noted with chloride depleted and reconstituted samples in either the salt free or SO_4^{2-} buffers if the samples

were used within 18 hours of preparation. Samples stored in salt free media for longer periods of time exhibited less of a percentage of reconstitution upon $CaCl_2$ addition compared to their respective controls than did the samples stored in the SO_4^{2-} buffers. The decrease in the percentage of reconstitution over time in the salt free media was most likely due to a leaching out of functional manganese from the membranes.

5.2.1.3. Oxygen Evolution Assays

The intactness of the Oxygen Evolving Complex in control and treated Photosystem II membranes was measured by the rate of oxygen evolution in continuous illumination by using a Clark-type polarographic electrode as described by Berthold *et al.* (1981). Control O_2 evolving PS-II membranes are defined for our purposes as the PS-II enriched membranes that are derived as a result of the preparative procedures described in the previous chapter. Determination of control rates was carried out as follows: 3.5 ml of a reaction media consisting of 50 mM Mes (pH 6.0) and 250 *u*M 2,5-DCBQ was added to a temperature controlled, water jacketed reaction cell and allowed to equilibrate (the reaction media was suspended in the same resovoir that supplied the water for the reaction cell and so equilibration required no more than two or three minutes). An aliquot of the photosynthetic sample, quantity adjusted for a final chlorophyll concentration of ~7.5 *u*M, was added and followed by an addition of ferricyanide, final $[Fe^{3+}]$ = 2.5 mM. One minute of further equilibration was allowed and then a white light source (General Electric, EJL, intensity ~8 kJ m^{-2} s^{-1}) was turned on and the evolution of oxygen with respect to time was measured by a YSI model 53 Oxygen Probe Monitor connected to a strip chart recorder. Freshly prepared Photosystem II membrane preparations that exhibited an oxygen evolution rate of less than 550 *u*moles O_2/mg Chl/hr were discarded.

Photosystem II membranes from frozen stock not exhibiting a rate within 10% of their rates before freezing were also discarded. Polypeptide depleted membranes not capable of at least a 65% restoration of control oxygen rates with the additional infusion of 15 mM $CaCl_2$ into the reaction media were discarded. All untreated Photosystem II membranes preparations were discarded within two weeks of the date of their preparation. These criteria regarding the viability of the samples for these experiments have arisen out of a concern for the quality of the preparations. The oxygen evolving reaction centers that have been polypeptide and chloride depleted become inhibited more quickly with respect to oxygen evolution under continuous illumination than control samples that had not undergone these treatments. The preparations that exhibited lower initial O_2 evolution rates deactivate even more quickly than companion preparations that have high (> 550 *u*moles O_2/mg Chl/hr) rates (data not shown). This is suggestive, though not conclusive, that while damaged preparations may be able to support O_2 evolution for a short time, they do deactivate and may continue to have unwanted spectral contributions. This does not necessarily reflect a direct causal effect; rather, it is probably indicative of the disintegration of OECs that were already damaged during the depletion phases.

5.3. RESULTS

5.3.1. Steady State O_2 Evolution Measurements

5.3.1.1. Anion Effects in Control and Cl^- Depleted PSII Membranes

The effects of various anions substituting for Cl^- on oxygen evolution rates in both control and NaCl washed, Cl^- depleted Photosystem II membranes were examined. We were principally interested in observing if the effects of the

differing anions varied between the control and treated samples. The divalent cation and the sum total of the monovalent anion concentrations were kept constant and the oxygen evolution rate was monitored as a function of the mole fraction of the substituting anion relative to chloride. Figure 5.1 shows the effect upon the oxygen evolution rate when NO_3^- is the substituting anion. As can be seen, little difference is exhibited regarding the required anion stoichiometries as the slopes of the lines are nearly equal. The absolute magnitude of the response differs, but this is to be expected because the exogenous polypeptides are in place in the control samples, which is likely to limit access of the substituting anion to the Cl^- binding sites. Similar experiments were conducted for Br as well with nearly identical results (data not shown); i.e., stoichiometry for anion effect upon addition does not change between control and treated samples. In addition, the reconstitution of oxygen evolution by the four anions separately, Cl^-, Br^-, $CH_3O_2^-$, and NO_3^-, was examined and the results summarized in Table 5.2. This confirms that our inhibition of O_2 evolution is relatively complete and reversible. Further, given the rates of reconstitution for Br^-, Cl^-, and NO_3^-, the behaviour of the OEC for successive turnovers should be consistent with the expectation of the OEC not being integrally damaged and able to participate in 'normal' S-state transitions. These results are also consistent with those obtained by Damoder *et al.* (1986). They examined oxygen evolution and the multiline formation with different anions in Cl^- depleted PS-II membranes, and observed the order of reactivation to be $Cl^- > Br^- \sim NO_3^- >> OH^-$ for steady state O_2 evolution. However, they also found that for multiline reconstitution Br^- was as effective as Cl^-.

5.3.2. Absorption Difference Spectra

5.3.2.1. The S_1 --> S_2 Transition in Untreated Samples

The optical absorption difference spectrum of the S_1 --> S_2 transition in untreated Photosystem II membranes was acquired at a resolution of 5 nm and is displayed in Figure 5.2. The conditions were identical to those used to acquire the Qa^-/Qa difference spectrum (Figure 4.4). This figure displays the spectrum with no attempt to remove possible contaminating species. This spectrum was normalized at 325 nm, and the curve drawn is a best fit to the data (the point at 320 nm is considered an anomaly and discarded) without trying to induce spectral features that are not warranted by the density of the data. Figure 5.3 displays the same S state transition and overlays the Qa/Qa spectrum (normalized at 325 nm) from Figure 4.4. The peak of the absorption band for the oxygen evolving sample is clearly shifted to 320 nm even though the data point for 320 nm is rejected because of its extremity. As a comparison, consider the first flash spectrum in oxygen evolving Photosystem II particles under conditions similar to ours that was published by Dekker (1985). When his spectrum is normalized at 325 nm and compared to the spectrum in Figure 5.2 (see Figure 5.9), the bandshapes are largely similar; however, the spectrum reported by Dekker peaks at 325 nm while the one we collected peaks at 320 nm.

5.3.2.2. The S_1 --> S_2 Transition in NaCl Treated Samples.

Oxygen evolving Photosystem II membranes were treated with high salt to remove the 17 and 23 kDa polypeptides and incubated in Cl^- free media to Cl^- deplete the membranes. The first flash normalized (325 nm) absorption difference spectra for the cases, Cl^- depleted and no further addition (a condition that corresponds to OH^- repletion), Cl^- depletion and Cl^- repletion, Cl^- depleted

and Br^- repletion, and Cl^- depleted and NO_3^- repletion, were collected and are displayed successively in Figures 5.4, 5.5, 5.6, and 5.7. A reproduction of these for comparison in one figure is given in Figure 5.8. The OH^- and Br^- substituted were collected point by point every 2 to 2.5 nm, and the Cl^- and NO_3^- were collected every 5 nm. The experimental conditions were identical to those used for the acquisition of the S_1 --> S_2 transition in untreated Photosystem II membranes. The lines drawn are a smoothed fit without trying to induce spectral features not warranted by the data. The OH^- and the Br^- substituted spectra have shifted the peak of their absorption bands to 325 nm and the Cl^- and NO_3^- spectra remain relatively centered around 320 nm. All of these spectra decrease in intensity towards 290 nm. Only the OH^- substituted spectra reaches the zero-crossing point in the range 290-295 nm as also shown by the Qa^-/Qa spectrum, a feature indicative of only quinone contribution in that wavelength region. A comparison of these first flash difference spectra corresponding to the S_1 --> S_2 transition with varying anionic co-factors, possibly serving as ligands to the manganese in the OEC, show that there are differences apparently related to the differing anions; however, the underlying cause for the differences is not immediately clear. In an effort to distinguish the relative changes, the normalized spectrum arising from the untreated Photosystem II membranes was subtracted from the others and the results of each such subtraction are displayed in Figure 5.10. For each spectra that has been subtracted, the bottom curve depicts the differences. A quantitative measure of the correlation between the untreated PS-II spectrum and the spectra arising from X^- substitution can be determined by summing the square of the differences. The results of this operation on each of the difference spectra are given in Table 5.1. Throughout the range of available data, 300 to 380 nm, the degree of spectral similarity, as determined by the summed square differences, in descending order is, $Br^- > NO_3^- > Cl^- >> OH^-$.

Focusing upon the broad absorbance band centered roughly at 320 - 325 nm, through the range, 300 to 350 nm, the similarity of the spectra, in descending order are NO_3^- > Br^- ~ Cl^- >> OH^-. Qualitatively, the leading slope of the 325 nm absorption band in the OH^-, Br^-, and Cl^- substituted spectra, from 305 to 325 nm, is identical to the slope in the untreated spectrum except for differing amplitudes. The following slope for the same band differs except for the the Cl^- substituted case.

5.4. DISCUSSION

5.4.1. Justification for Spectral Manipulation(s).

It is certainly possible to adjust the first flash absorption difference spectrum obtained in untreated Photosystem II membranes for the contributions arising from Qa/Qa, Z^+/Z, and Q_{400}. Since there is quite a similarity between our spectrum and the one presented by Dekker (1985), we have, in fact, been able to obtain a spectrum remarkably similar to that presented as the S_1 --> S_2 transition through just such manipulations (data not shown). However, as discussed earlier, without a technique independently separating the spectral contributions of the active reaction centers from those partially and completely inactivated, this would be a futile exercise and could not be further applied to unknown situations. Our method of examining the S_1 --> S_2 transition under conditions of varying anionic co-factors provides us with the means to compare the relative differences in the spectra as they presumably arise because of the varying anionic co-factors. The assumptions we are forced to make regarding reaction center and OEC integrity can be largely supported by steady state oxygen evolution measurements. The spectra have all been normalized on the point(s) obtained at 325 nm as this is the putative peak for the Qa^-/Qa transition. One of the critical

assumptions we make is that centers inactive with respect to oxygen evolution do not undergo Qa --> Qa^- transitions that will be detected during the timescale of our experiments. This assumption is supported by the extinction coefficient at 325 nm obtained for the first flash for the anion repletion cases of OH^-, Cl^-, Br^-, and NO_3^-, as shown in Table 5.3. The absolute peak height appears to be linearly related to the degree of reconstitution of oxygen evolution, data for these conclusions are given in Table 5.2. Therefore, normalizing the spectra at 325 nm allows us to standardize the Qa^-/Qa contribution(s).

5.4.2. Role(s) Played by the Anion Co-Factors

Distinct spectral changes are observed that are dependent upon the anion cofactor, and the O_2 evolution data (Figure 5.1) indicates that the anions probably operate in mechanistically similar fashions. The optical data we present here would indicate that the large absorption band centered asymmetrically at 320 - 325 nm is shifted relative to the absorption band recorded for native O_2 evolving PS-II membranes upon depletion of Cl^- and X^- repletion for the S_1 --> S_2 transition. Additionally, the steady state O_2 evolution data reveals a nearly identical stimulation of evolution of O_2 between Cl^- and NO_3^-. This is suggestive of a structural role in the OEC being played by the anion. The alteration of the band shape with reconstitution by Cl would also indicate that the structural change of the OEC upon Cl depletion is irreversible though not inhibitory. In apparent contradiction, however, are the results from Yachandra *et al.* (1986a and 1987). For conditions forming the multiline or the g4.1 they report that no structural changes occur between the S_1 and the S_2 states and that, while the EXAFS data is unable discriminate between the presence or absence of a Cl^- ligand, high resolution studies of the multiline (Yachandra *et al.*, 1986b) do not show any differences between Cl^- and Br^- reconstituted samples. There are two

factors that may weigh heavily here regarding the role of halides in the OEC. Yachandra and co-workers (1987 and 1986a) have reported Mn-Mn distances of 2.7 Å, 1.75 Å, and 1.98 Å, and a composite Mn association number of 0.5 to 2.0 Mn atoms at an average distance of 2.7 Å. A binuclear or trinuclear configuration of the Mn could be responsible for the multiline and the g4.1 signals and the remaining Mn could be at a distance greater than 3.0 Å; Cl^- ligated to these non-participatory centers would not necessarily be detected. The second factor to consider is the structure giving rise to the multiline. It has been shown that various model systems of bi- and tri- nuclear centers can exhibit multiline-type of signals (for example, Mabad *et al.*, 1985, and Kessissoglou *et al.*, 1989) in the g ~ 2 region. The detection of a multiline signal in PS-II membranes does not necessarily imply that the configuration is identical for all cases in which the OEC has been perturbed.

5.4.3. Identification of the First Flash Absorption Differences

As discussed above Yachandra *et al.* (1987) have concluded that the S_1 --> S_2 transition reflects an oxidative state change of the manganese, probably Mn(III) --> Mn(IV), not requiring the participation of a halide as a ligand to the manganese (Yachandra, 1986a). Beck (1988) has shown that in the absence of Cl^- the g4.1 is formed and converts to a multiline upon the readdition of Cl^-, and there is some evidence suggesting that a multiline will form in presence of at least Br^- (de Paula, 1988). In light of the work from Yachandra and co-workers (1987), the formation of the g4.1 must also correspond to a manganese oxidation. From this it can be presumed that, given our experimental conditions, the multiline is formed on the first flash for Cl^-, Br^-, and NO_3^- reconstituted PS-II membranes and the g4.1 formed for the case where only OH^- was present.

5.4.4. Conclusions

EXAFS, EPR, and the results we have shown here with UV optical difference spectra clearly indicate that substitution of endogenous Cl^- for exogenous anions do not affect the spectroscopically observable S_1 --> S_2 transition. This could be interpreted as showing that Cl^- is not involved as a ligand to the Mn of the OEC; however, this is in direct contradiction to the O_2 evolution data, obtained from both continuous and pulsed illumination turnovers of the OEC, that anions are required for advancement beyond a functional S_1 state[1] and is unlikely to be the case.

A more reasonable explanation is that the asymmetric absorption band, centered at 320 to 325 nm, simply does not arise from a charge transfer from the Cl^- ligand. This is supported by the fact that we were able to effectively exchange the endogenous ligand for a series of exogenous ligands, OH^-, Br^-, and $NO3^-$, and not observe major changes in the absorption band. The only other likely ligand candidate responsible for this absorption band is oxygen. Unfortunately, this hypothesis is difficult to test directly; however, this does provide some insight into model complexes that need to be constructed.

The adamantane models of Brudvig and Crabtree (1986) served as useful starting points and somewhat more realistic models from a synthetic point of view have been employed by Vincent and Christou (1986 and 1987). Using these models as starting points, modifying terminal and bridging oxygen ligands in a systematic fashion should result in determining the spectroscopic phenomena that are sensitive to these changes. Alternatively, one could find models that are dependent upon liganding anions such as Cl^- and by

---

[1] As discussed in an earlier section, a modified S_2 state that is of the same oxidation state as the normal S_2 can be obtained in the absence of an anion but further advancement does not appear to be possible without addition of an anion; therefore, it is a non-functional S_2 state.

systematically varying the anion determine the observable property sensitive to anion substitution.

TABLE 5.1

Correlation between S1 --> S2 spectra taken in untreated O2 evolving PS-II membranes and in Cl- depleted, X- reconstituted PS-II membranes

This table presents a correlation between the spectrum of the S_1 --> S_2 transition in untreated PS-II membranes and a spectrum of the same transition in Cl^- depleted, X^- reconstituted, where X^- = {Cl^-, Br^-, NO_3^-, OH^-}. The correlation is measured by the sum of the square of the individual differences between each set of two spectra. The first table makes use of the full range of data, and the second table is restricted to data that contributes to the 325 nm absorbance band.

Range: 300 - 390 nm

Substituting Anion	$(dA(O_2) - dA(X^-))^2$
Cl^-	0.009
Br^-	0.007
NO_3^-	0.008
OH^-	0.012

Range: 300 - 350 nm

Substituting Anion	$(dA(O_2) - dA(X^-))^2$
Cl^-	0.009
Br^-	0.009
NO_3^-	0.007
OH^-	0.012

TABLE 5.2

Effect of CaX2 salts upon O2 evolution in untreated and in Cl- depleted, X-reconstituted PS-II membranes.

Effect of $CaCl_2$, $CaBr_2$, $Ca(NO_3)_2$ and $Ca(OAc)_2$ upon oxygen evolution in untreated and salt washed, Cl^- depleted PS-II membranes. Conditions were as outline in Materials and Methods. See text for discussion.

Rates before Salt-Washing : 750 *u*moles O_2/mg Chl/hr

Rates after Salt-Washing and Cl^- depletion : 70

Addition		% Reconstitution
Untreated		
None		100
$CaCl_2$	5.7 mM	95
$CaCl_2$	14.3 mM	97
$CaBr_2$	5.7 mM	95
$CaBr_2$	14.3 mM	81
$Ca(NO_3)_2$	5.7 mM	98
$Ca(NO_3)_2$	14.3 mM	90
$Ca(OAc)_2$	5.7 mM	45
$Ca(OAc)_2$	14.3 mM	37
Treated		
None		<10
$CaCl_2$	5.7 mM	50
$CaCl_2$	14.3 mM	92
$CaBr_2$	5.7 mM	41
$CaBr_2$	14.3 mM	84
$Ca(NO_3)_2$	5.7 mM	30
$Ca(NO_3)_2$	14.3 mM	65
$Ca(OAc)_2$	5.7 mM	16
$Ca(OAc)_2$	14.3 mM	<10

TABLE 5.3

Relative absorption peak heights for Cl- depleted, X- reconstituted PS-II membranes.

Relative peak heights of the first flash absorption difference spectra under Cl^- depleted and OH^-, Cl^-, Br^-, and NO_3^- repleted conditions, adjusted for differences in Chlorophyll concentrations.

Addition	Relative Peak Height
Cl^-	1.0
Br^-	0.8
NO_3^-	0.4
OH^-	0.3

FIGURE 5.1

Effect of Replacement of Cl- with NO3-.

The normalized rate of O_2 evolution versus the mole fraction of Cl^- in non-Cl^- depleted (control) and Cl^- depleted Photosystem II membranes is plotted. The maximum O_2 evolving rate in the control PS-II membranes was used for normalizing both sets of data. The same data in somewhat different form are also presented in tabular form below. The reaction media consisted of [Chl] = 7.5 *u*M, 250 *u*M 2,5-DCBQ, and 2.5 mM ferricyanide. See text for discussion.

Rates before Salt-Washing : 695 *u*moles O_2 /mg Chl/hr
Rates after Salt-Washing : 150

$[Ca^{2+}]$ mM	$[Cl^-]$ mM	$[NO_3^-]$ mM	Control *u*moles O_2/mg Chl/hr	normalized[2]
14	29	0	695	1.0
14	23	6	569	0.82
14	14.5	14.5	598	0.86
14	6	23	511	0.74
14	0	29	473	0.68

$[Ca^{2+}]$ mM	$[Cl^-]$ mM	$[NO_3^-]$ mM	Cl^- depleted *u*moles O_2/mg Chl/hr	norm[3]	norm[4]
14	29	0	498	1.0	0.72
14	23	6	526	1.06	0.76
14	14.5	14.5	404	0.81	0.58
14	6	23	394	0.79	0.57
14	0	29	356	0.72	0.51

[2]Normalized with respect to maximum rate in Control PS-II membranes.

[3]Normalized with respect to maximum rate in Cl^- depleted PS-II membranes.

[4]Normalized with respect to maximum rate in Control PS-II membranes.

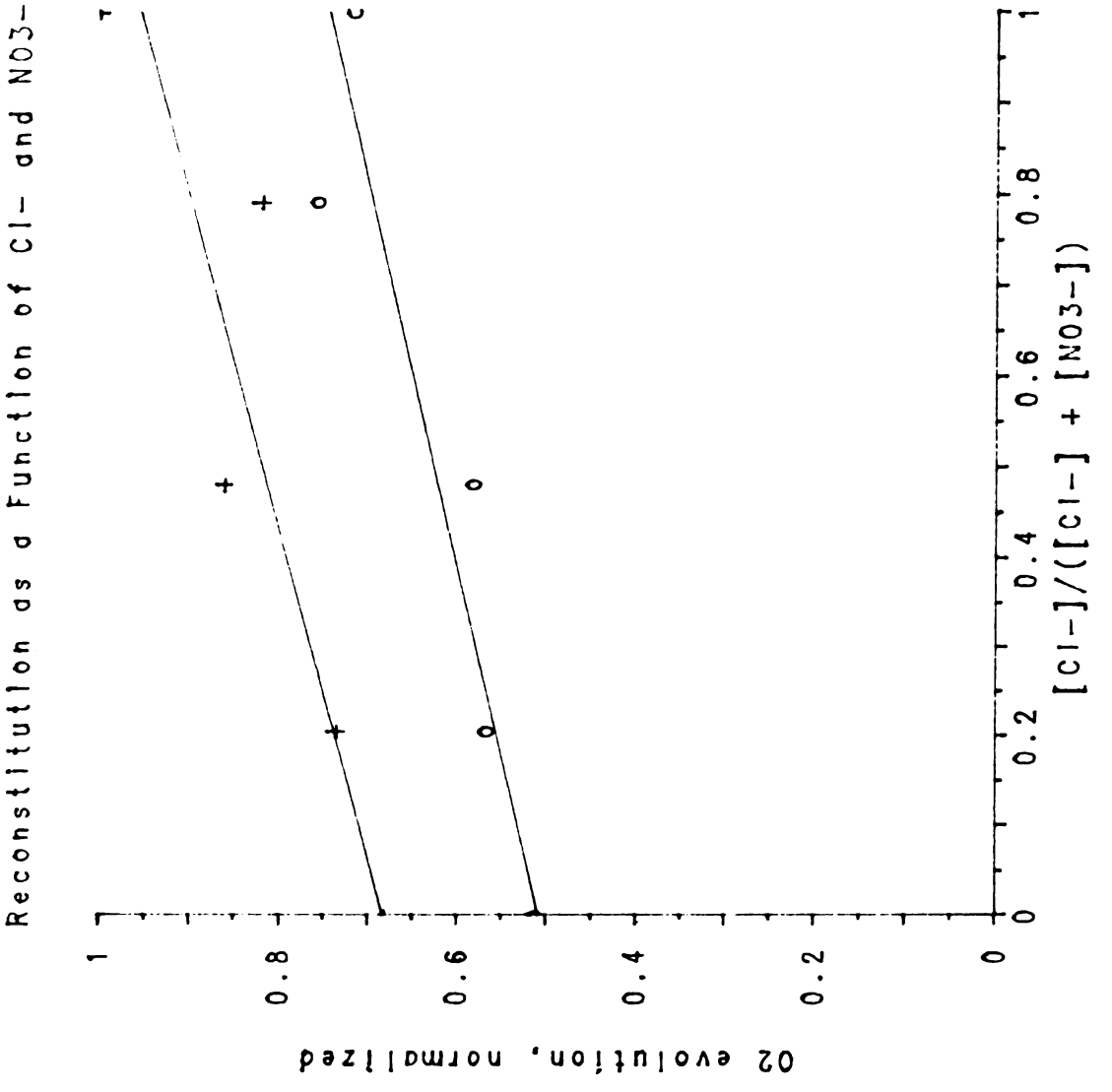
Reconstitution as a Function of Cl- and NO3-
O2 evolution, normalized
[Cl-]/([Cl-] + [NO3-])
0
0.2
0.4
0.6
0.8
1

FIGURE 5.2

S2/S1 Absorption Difference Spectrum in O2 Evolving, Uninhibited Samples.

This figure is a point by point difference spectrum of the S_1/S_2 transition in freshly prepared Photosystem II membranes, 700 *u*moles O_2/mg Chl/hr. The spectrum was normalized at 325 nm, [Chl] = 80.2 *u*M ([RC] ~ 0.32 *u*M), 1 mM DCMU, 20 mM $CaCl_2$, 1 mM Fe^{3+}, 1 mM Fe^{2+}. Each point is the average of between 8 to 16 shots. Other conditions are as described in the Materials and Methods, see text for discussion.

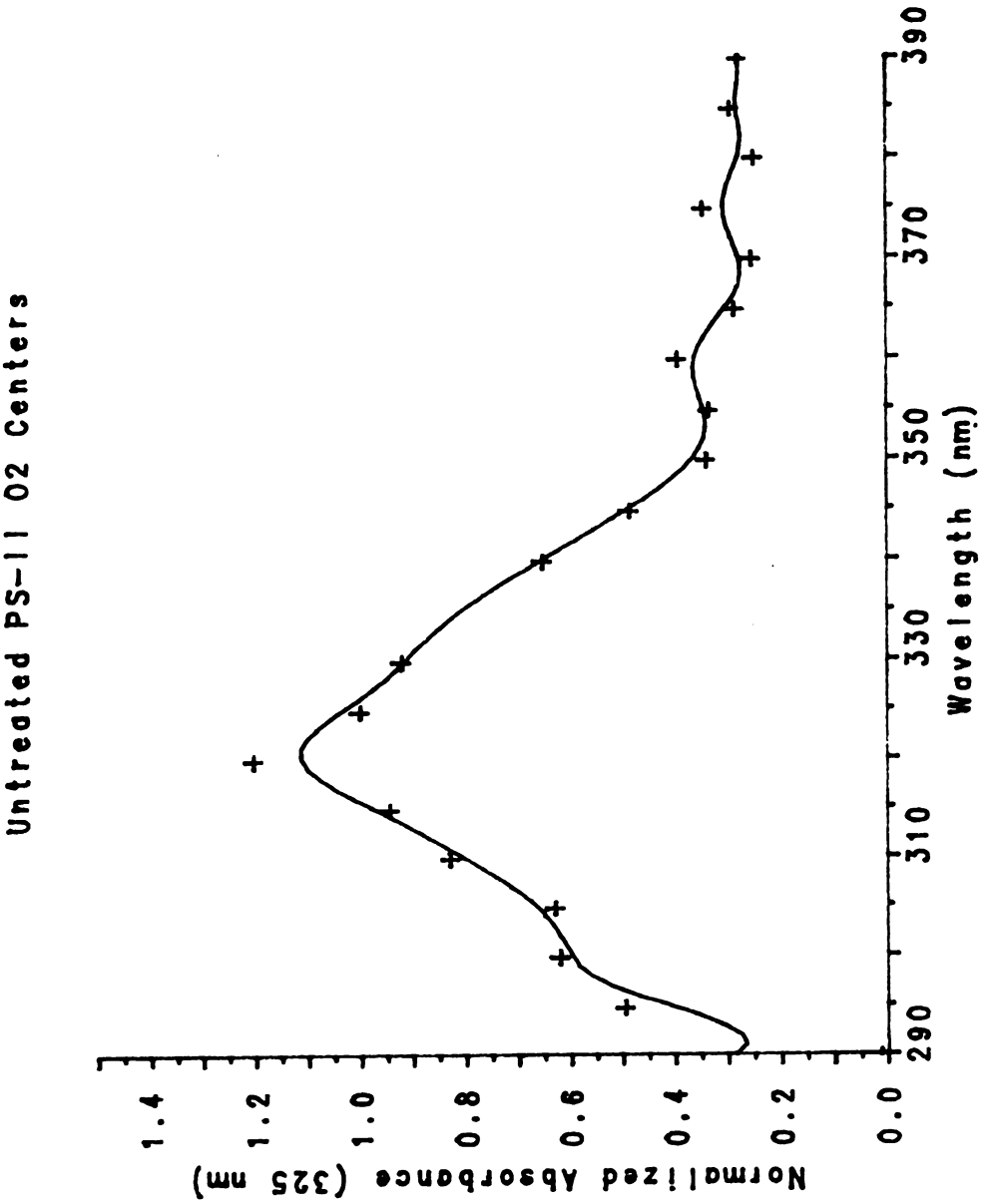
Untreated PS-II O2 Centers
Normalized Absorbance (325 nm)
0.0
0.2
0.4
0.6
0.8
1.0
1.2
1.4
290
310
330
350
370
390
Wavelength (nm)

FIGURE 5.3

A Comparison Between the S2/S1 and the Qa-/Qa Spectra.

This figure presents a comparison between two point by point spectra for the S_1 --> S_2, '+', and Qa --> Qa^-, '.', transitions. Both spectra have been normalized at 325 nm. The inset spectrum is the same data except shown over the full wavelength range for which we have collected the Qa^-/Qa spectrum. Conditions for the S_1 --> S_2 spectrum are as described for Figure 5.2. Conditions for the Qa --> Qa^- spectrum are as described in Figure 4.4. See text for discussion.

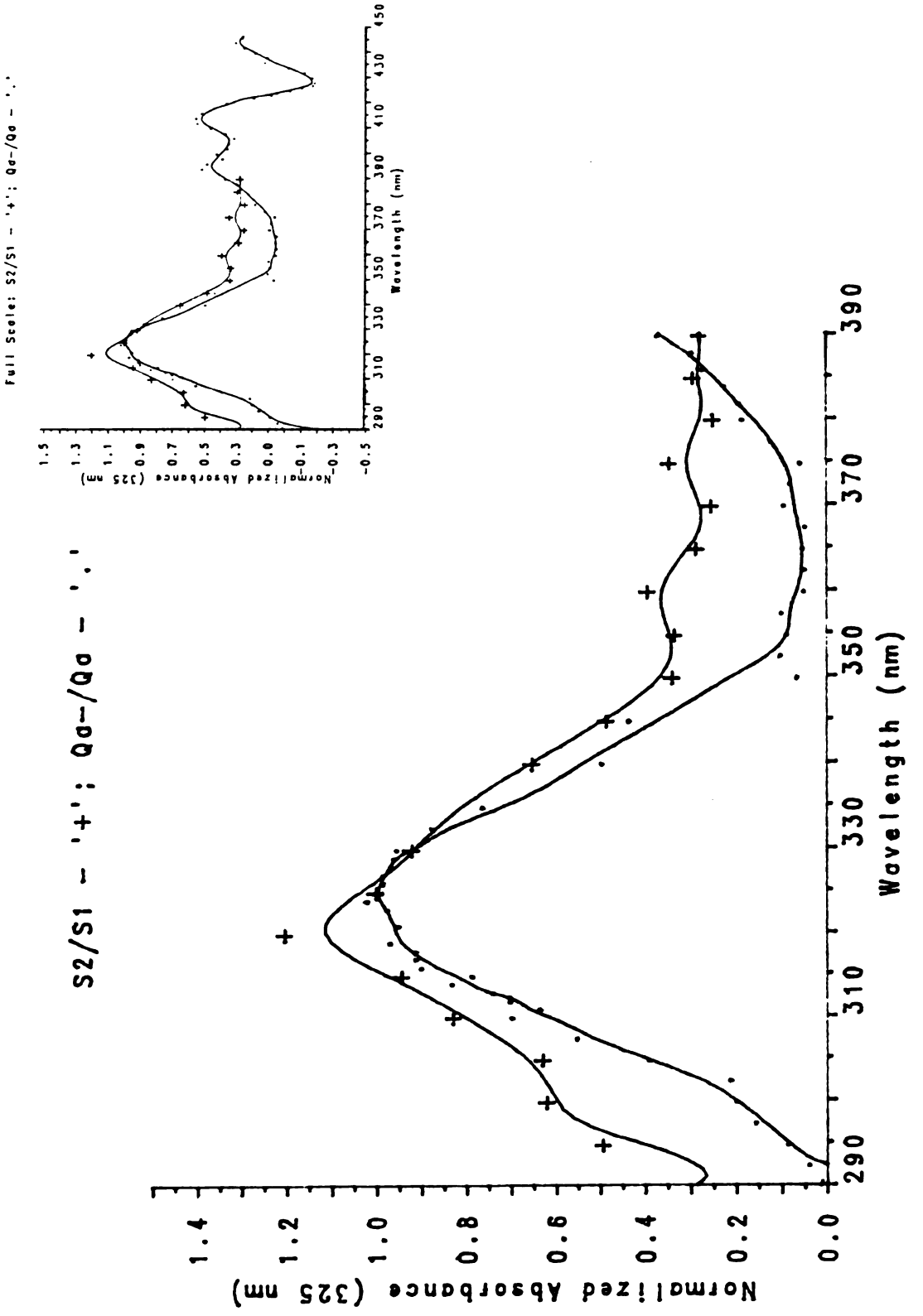
S2/S1 - '+'; Qa-/Qa - '.'
Normalized Absorbance (325 nm)
Wavelength (nm)
0.0
0.2
0.4
0.6
0.8
1.0
1.2
1.4
290
310
330
350
370
390
Full Scale: S2/S1 - '+'; Qa-/Qa - '.'
Normalized Absorbance (325 nm)
Wavelength (nm)
-0.5
-0.3
-0.1
0.0
0.3
0.5
0.7
0.9
1.1
1.3
1.5
290
310
330
350
370
390
410
430
450

FIGURE 5.4

Cl- Depleted, No Addition (OH-), 1st Flash Difference Spectrum.

Point by point difference spectrum of the S_1/S_2 transition in salt washed, Cl^- depleted and no added anion, corresponds to OH^- substitution instead. Spectrum was normalized at 325 nm. [Chl] = 80.2 *u*M ([RC] ~ 0.32 *u*M), 1 mM DCMU, 20 mM $CaCl_2$, 1 mM Fe^{3+}, 1 mM Fe^{2+}. Each point is the average of between 8 to 16 shots. Other conditions are as described in the Materials and Methods, see text for discussion.

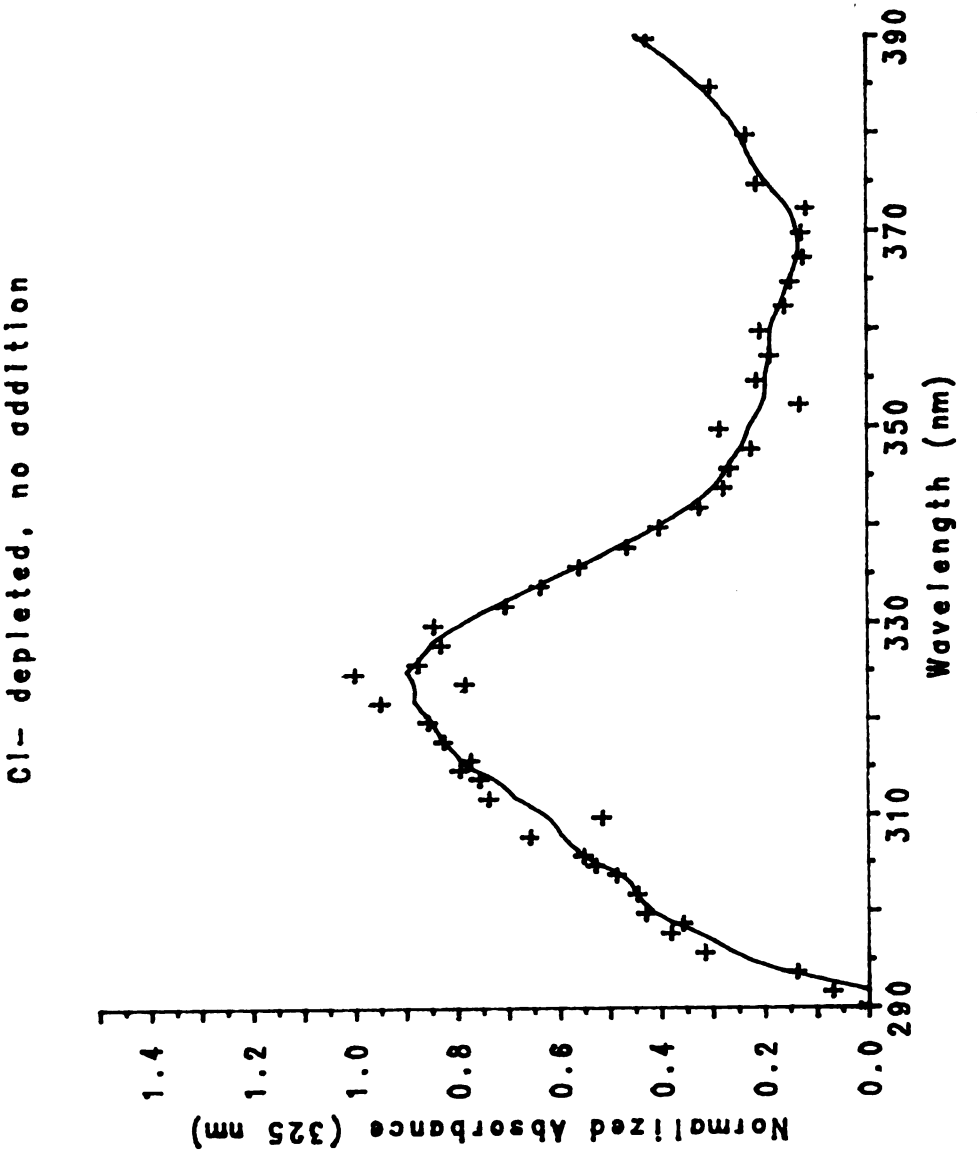
Cl- depleted, no addition
Normalized Absorbance (325 nm)
0.0
0.2
0.4
0.6
0.8
1.0
1.2
1.4
290
310
330
350
370
390
Wavelength (nm)

FIGURE 5.5

Cl- Depleted, Cl- Repleted, 1st Flash Difference Spectrum.

Point by point difference spectrum of the S_1/S_2 transition in salt washed, Cl^- depleted, Cl^- repleted Photosystem II membranes. Spectrum was normalized at 325 nm. [Chl] = 100 uM ([RC] ~ 0.4 uM), 1 mM DCMU, 20 mM $CaCl_2$, 1 mM Fe^{3+}, 1 mM Fe^{2+}. Each point is the average of between 8 to 16 shots. Other conditions are as described in the Materials and Methods, see text for discussion.

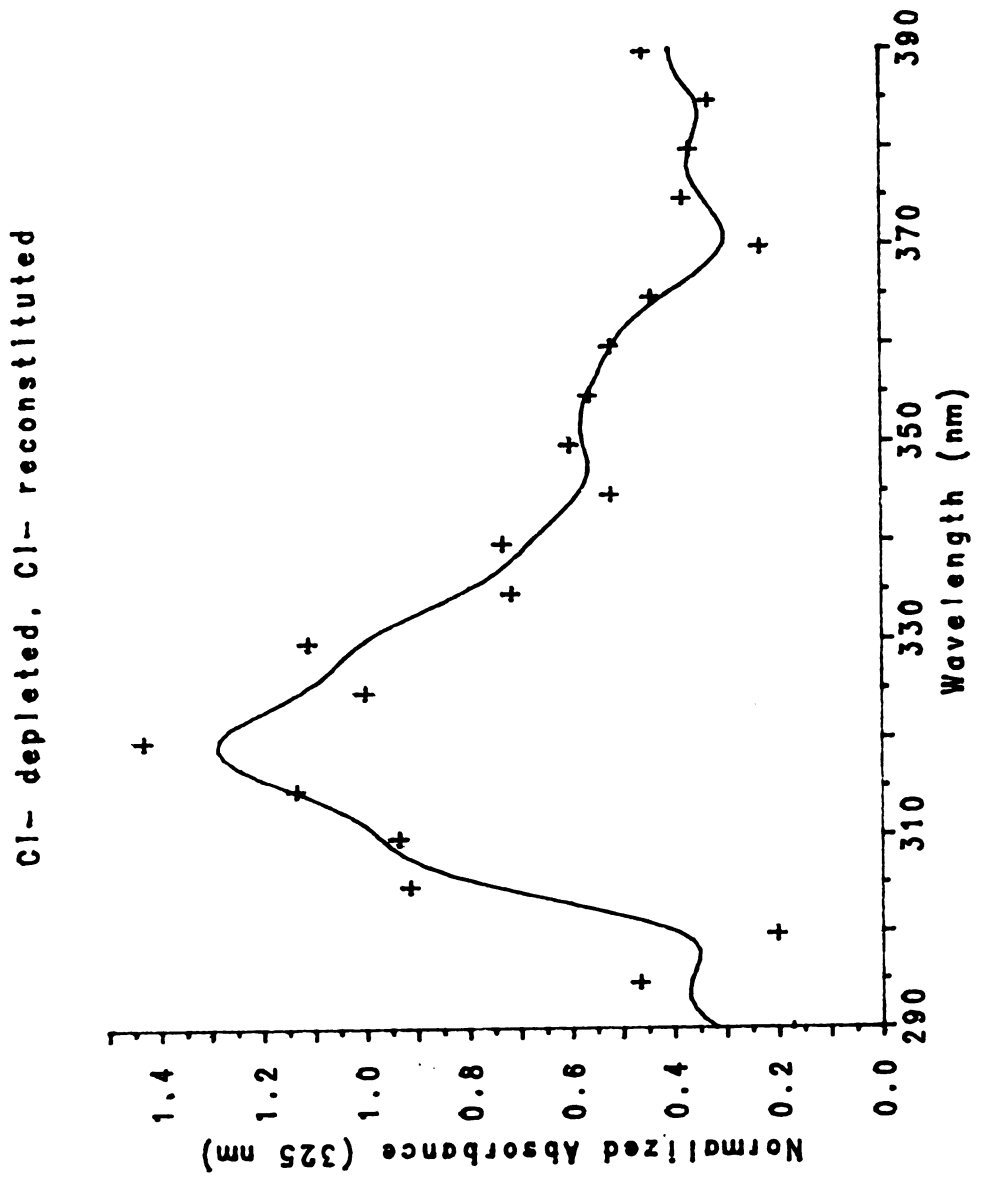
Cl- depleted, Cl- reconstituted
Normalized Absorbance (325 nm)
0.0
0.2
0.4
0.6
0.8
1.0
1.2
1.4
290
310
330
350
370
390
Wavelength (nm)

FIGURE 5.6

Cl- Depleted, Br- Repleted, 1st Flash Difference Spectrum.

Point by point difference spectrum of the S_1/S_2 transition in salt washed, Cl^- depleted, Br^- repleted Photosystem II membranes. Spectrum was normalized at 325 nm. [Chl] = 100 uM ([RC] ~ 0.4 uM), 1 mM DCMU, 20 mM $CaCl_2$, 1 mM Fe^{3+}, 1 mM Fe^{2+}. Each point is the average of between 8 to 16 shots. Other conditions are as described in the Materials and Methods, see text for discussion.

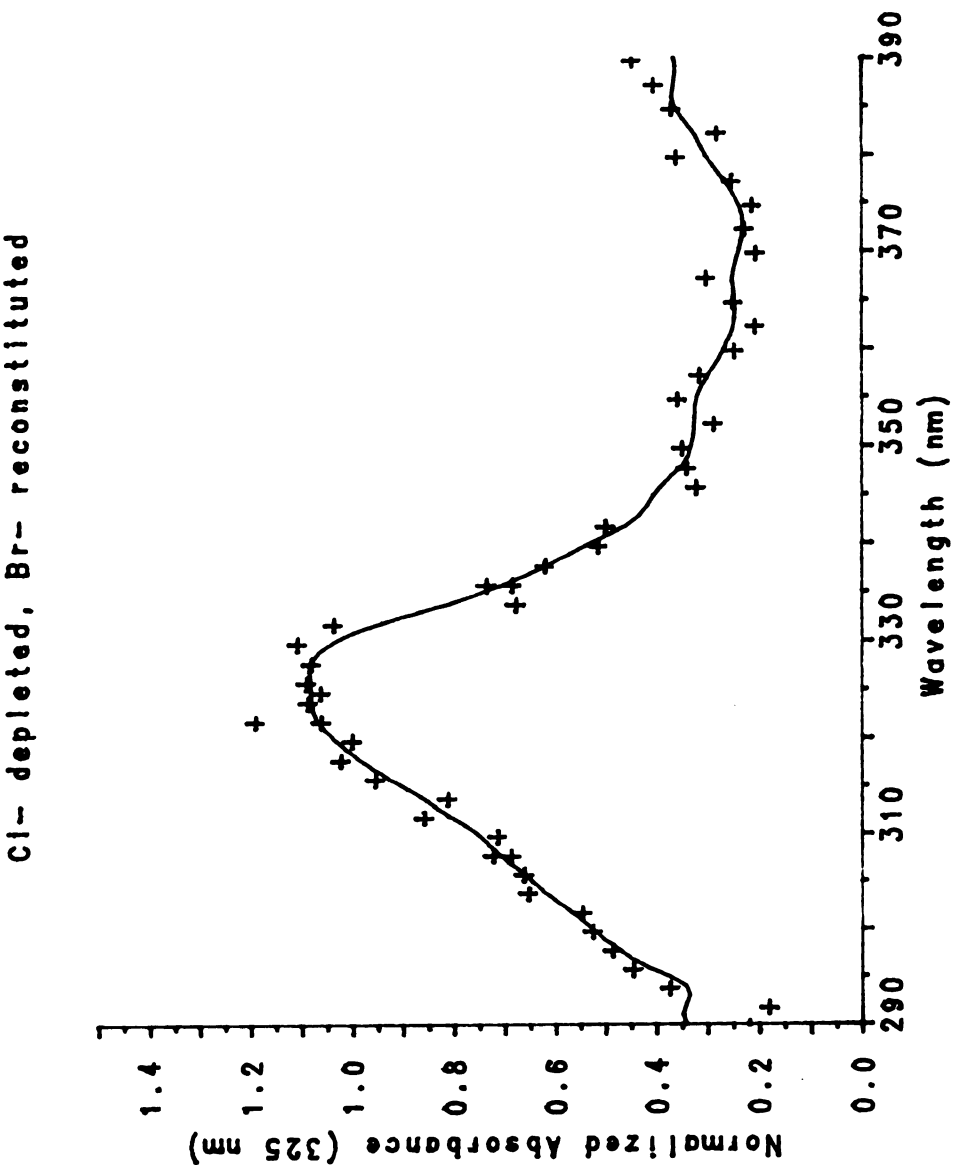
Cl- depleted, Br- reconstituted
Normalized Absorbance (325 nm)
0.0
0.2
0.4
0.6
0.8
1.0
1.2
1.4
290
310
330
350
370
390
Wavelength (nm)

FIGURE 5.7

Cl- Depleted, NO3- Repleted, 1st Flash Difference Spectrum.

Point by point difference spectrum of the S_1/S_2 transition in salt washed, Cl^- depleted, NO_3^- repleted Photosystem II membranes. Spectrum was normalized at 325 nm, [Chl] = 100 *u*M ([RC] ~ 0.4 *u*M), 1 mM DCMU, 20 mM Ca^{2+}, 1 mM Fe^{3+}, 1 mM Fe^{2+}. Each point is the average of between 8 to 16 shots. Other conditions are as described in the Materials and Methods, see text for discussion.

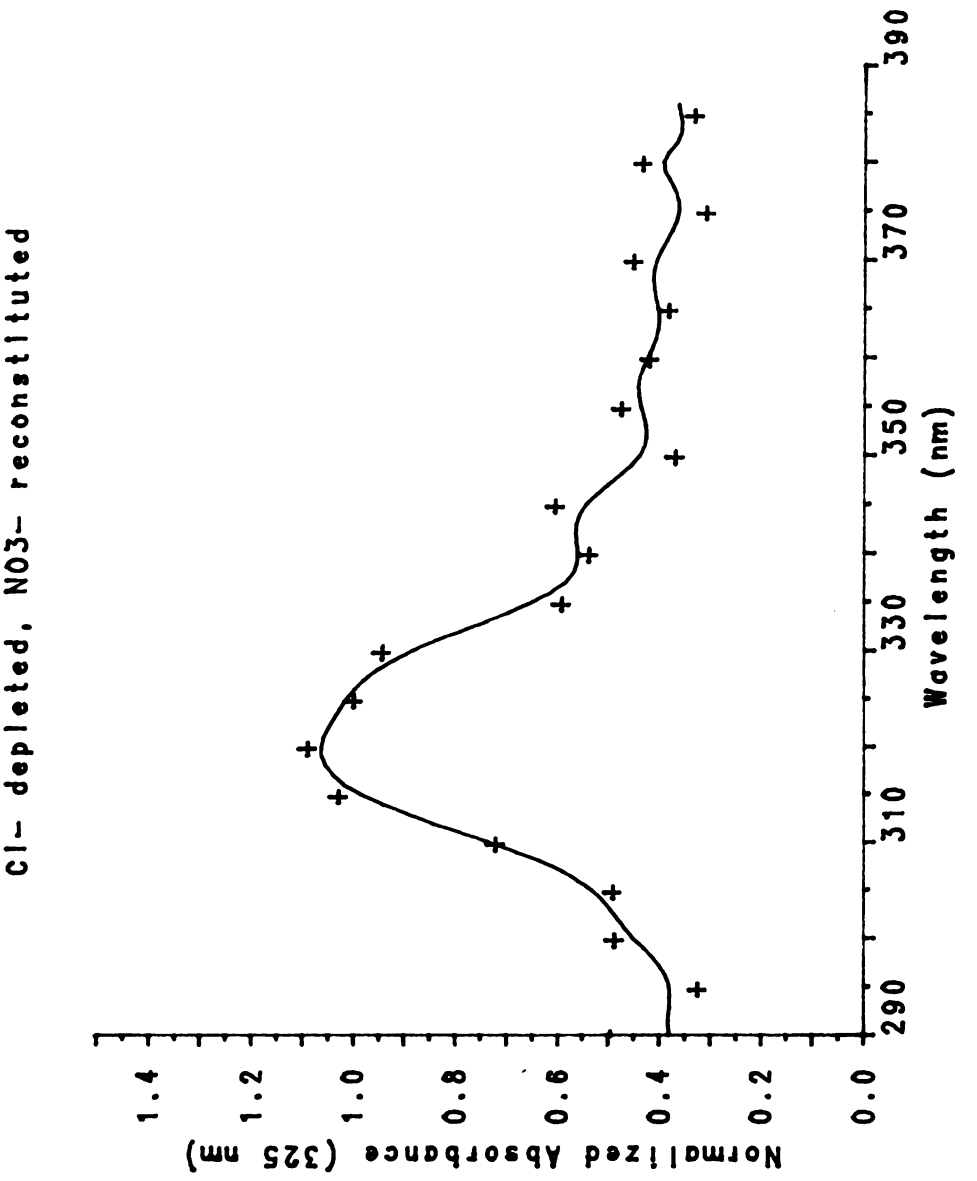
Cl- depleted, NO3- reconstituted
Normalized Absorbance (325 nm)
0.0
0.2
0.4
0.6
0.8
1.0
1.2
1.4
290
310
330
350
370
390
Wavelength (nm)

FIGURE 5.8

Cl- Depleted, X- Repleted, 1st Flash Difference Spectra.

Reproduction of the data in Figures 5.4, 5.5, 5.6, and 5.7 onto one page for easier comparison. Each plot is labelled, conditions for each can be found in the corresponding figure legend.

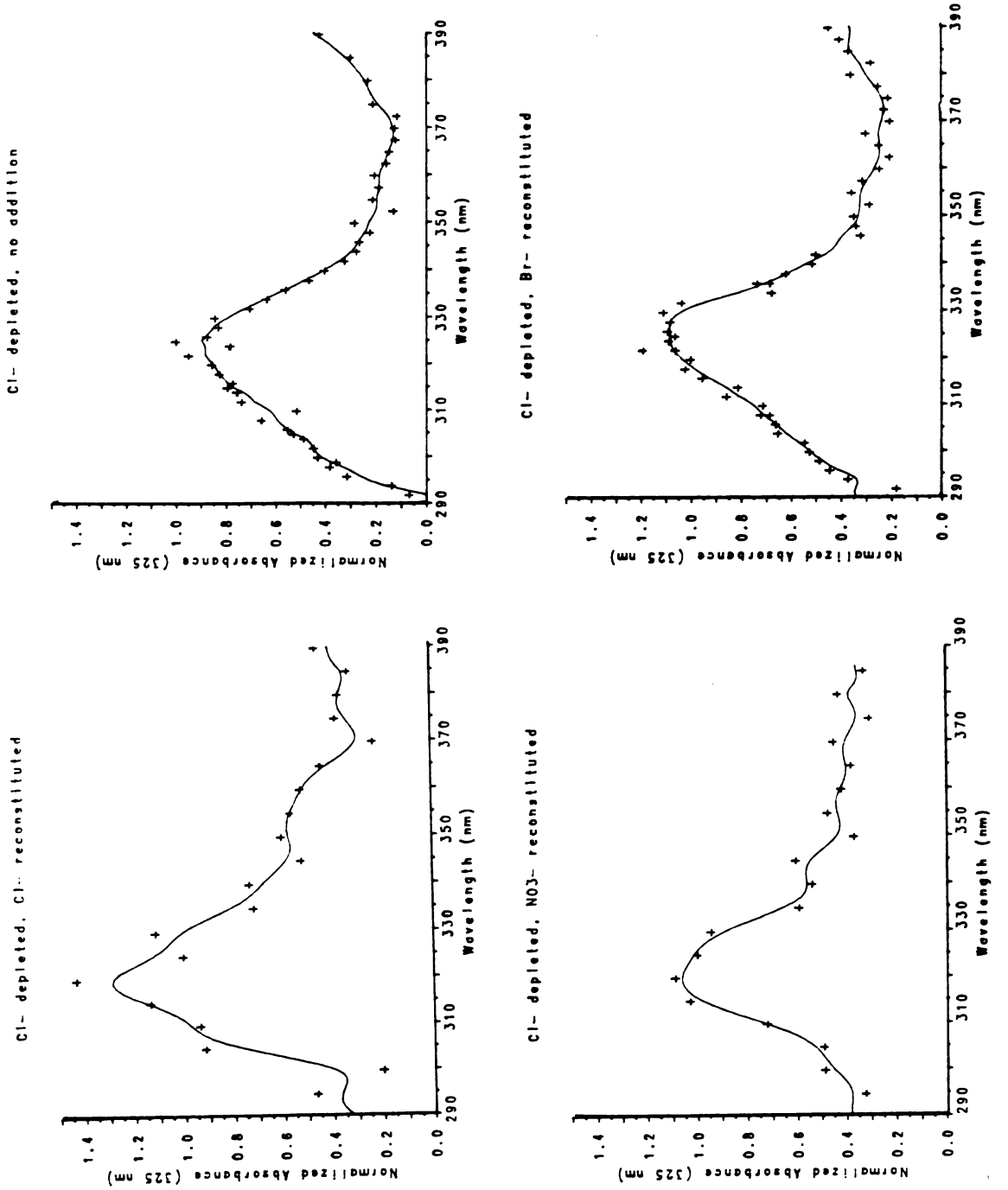
Cl- depleted, no addition
Cl- depleted, Cl- reconstituted
Cl- depleted, Br- reconstituted
Cl- depleted, NO3- reconstituted
Normalized Absorbance (325 nm)
Wavelength (nm)
0.0
0.2
0.4
0.6
0.8
1.0
1.2
1.4
290
310
330
350
370
390

FIGURE 5.9

Comparison Between Two First Flash Difference Absorption Spectra.

Replot of the data reported by Dekker (1985) for the first flash in O_2 evolving Photosystem II membranes, '+', and a replot of the data given in Figure 5.2, 'o'. Both sets of data are normalized at 325 nm. The conditions used by Dekker differed in that he used only 5 *u*M ferricyanide, no ferrocyanide, and 5 mM $MgCl_2$. The concentration of DCMU also differed, 10 *u*M, but this should have no secondary effect. The other differences noted may be significant, see text for further discussion.

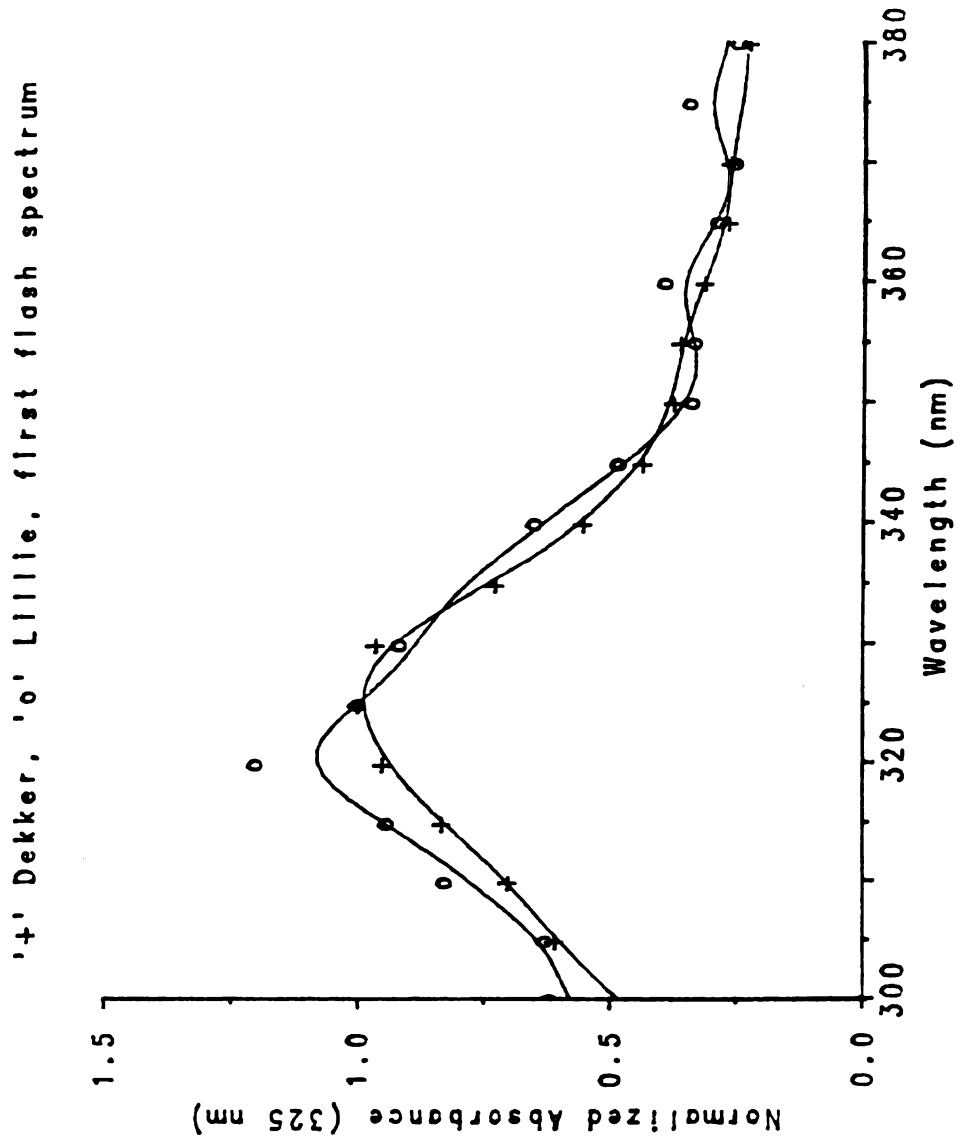
'+' Dekker, 'o' Llllle, first flash spectrum
Normalized absorbance (325 nm)
1.5
1.0
0.5
0.0
300
320
340
360
380
Wavelength (nm)

FIGURE 5.10

Comparative Plots for the S2/S1 Difference Spectra Between O2 and X-substituted, X- = {Cl-, Br-, NO3-, OH-}.

Each plot contains the normalized (325 nm) first flash absorption spectrum obtained in untreated O_2 evolving Photosystem II membranes, '+', the same spectrum obtained in X^- reconstituted Photosystem II membranes, 'o', and the difference between the two, '.'. In order, a) no substitution, OH^- reconstitution, b) Cl^- reconstitution, c) NO_3^- reconstitution, and d) Br^- reconstitution. See text for further discussion.

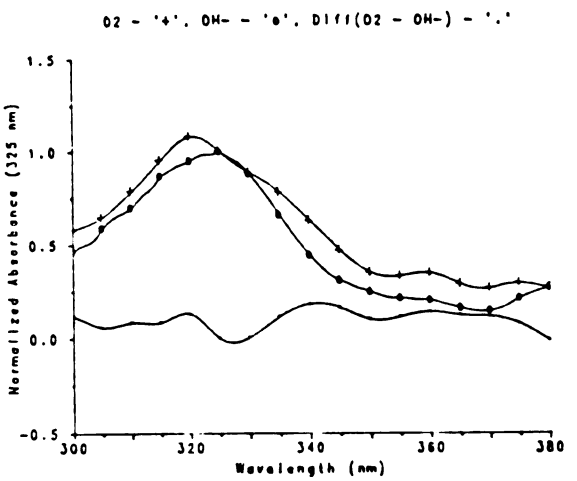
O2 - '+', OH- - 'e', Diff(O2 - OH-) - '.'
Normalized Absorbance (325 nm)
1.5
1.0
0.5
0.0
-0.5
300
320
340
360
380
Wavelength (nm)

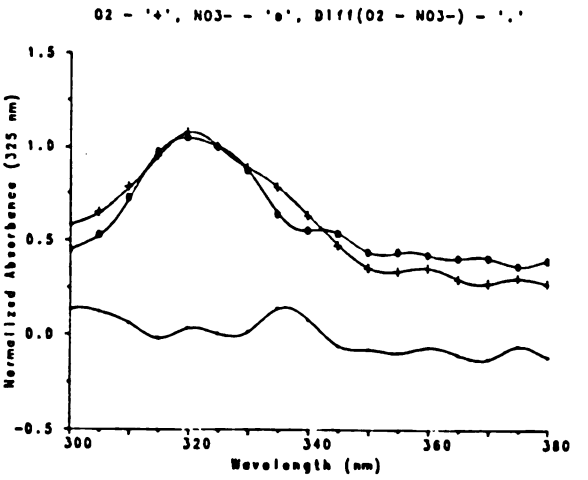
O2 - '+', NO3- - 'e', Diff(O2 - NO3-) - '.'
Normalized Absorbance (325 nm)
1.5
1.0
0.5
0.0
-0.5
300
320
340
360
380
Wavelength (nm)

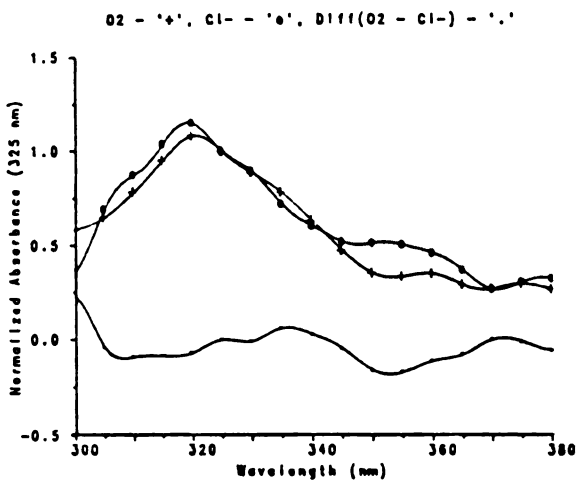
O2 - '+', Cl- - 'e', Diff(O2 - Cl-) - '.'
Normalized Absorbance (325 nm)
1.5
1.0
0.5
0.0
-0.5
300
320
340
360
380
Wavelength (nm)

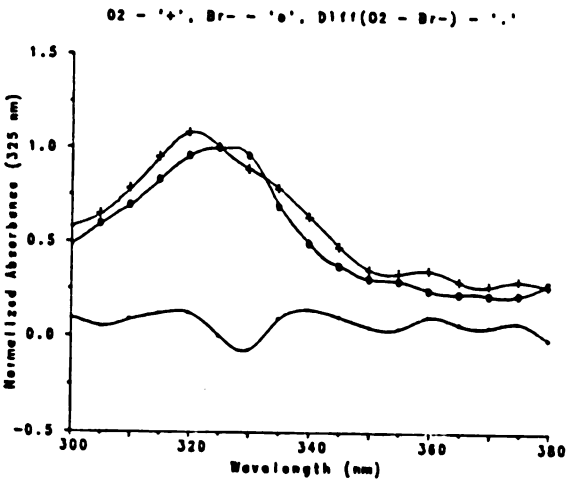
O2 - '+', Br- - 'e', Diff(O2 - Br-) - '.'
Normalized Absorbance (325 nm)
1.5
1.0
0.5
0.0
-0.5
300
320
340
360
380
Wavelength (nm)

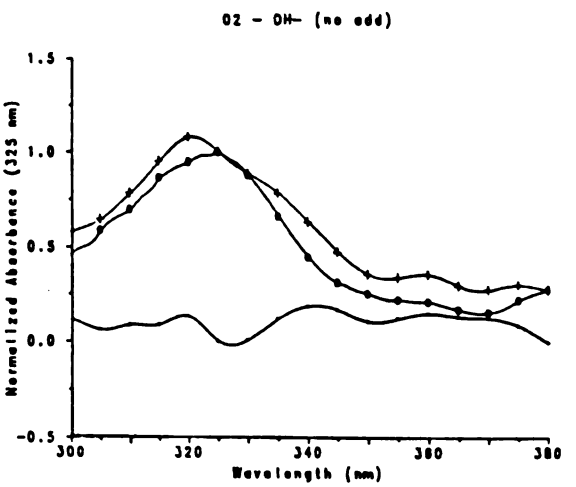
O2 - OH- (no add)
Normalized Absorbance (325 nm)
1.5
1.0
0.5
0.0
-0.5
300
320
340
360
380
Wavelength (nm)

REFERENCES

Akabori, K., Imaoka, A., and Toyoshima, Y. (1984). FEBS Letters, **173**, 36-40.

Åkerlund, H.-E., Jansson, C., and Andersson, B. (1982). Biochimica et Biophysica Acta, **681**, 1-10.

Beck, W. F. (1988). "Ligand-Exchange and Oxido-Reduction Reactions of Water Analogs with the Manganese Tetramer Complex of Photosystem II," Ph.D. Thesis, Yale University.

Berthold, D. A., Babcock, G. T., and Yocum, C. F. (1981). FEBS Letters, **134**, 231-234.

Blough, N. V. and Sauer, K. (1984). Biochimica et Biophysica Acta, **767**, 377-381.

Brudvig, G. W. and Crabtree, R. H. (1986). Proceedings of the National Academy of Sciences, USA, **83**, 4586-4588.

Cammarata, K. V. and Cheniae, G. M. (1987). Plant Physiology, **84**, 587-598.

Damoder, R. Klimov, V. V., Dismukes, G. C. (1986) Biochimica et Biophysica Acta, **848**, 378-391.

Dekker, J. P. (1985). Ph.D. Thesis, "Electron Transfer in the Oxygen - Evolving System of Photosynthesis," p48.

Dekker, J. P., Van Gorkom, H. J., Brok, M., and Ouwehand, L., (1984a). Biochimica et Biophysica Acta, **764**, 301-309.

Dekker, J. P., Van Gorkom, H. J., Wensink, J., and Ouwehand, L. (1984b). Biochimica et Biophysica Acta, **767**, 1-9.

de Paula, J. C. (1988). Personal communication regarding experiments he had performed and were being continued in Professor Brudvig's laboratory.

de Paula, J. C. and Brudvig, G. W. (1985). Journal of the American Chemical Society, **107**, 2643-2648.

Dismukes, G. C. and Siderer, Y. (1981). Proceedings of the National Academy of the Sciences, USA, **78**, 274-278.

Dismukes, G. C. and Siderer, Y. (1980). Febs Letters, **121**, 78-80.

Franzén, L.-G., Hansson, O., and Andreasson, L.-E. (1985). Biochimica et Biophysica Acta, **808**, 171.

Ghanotakis, D. F. and Yocum, C. F. (1986). Photosynthesis Research, **10**, 483-486.

Ghanotakis, D. F., Topper, J. N., Babcock, G. T., and Yocum, C. F. (1984a). FEBS Letters, **170**, 169-173.

Ghanotakis, D. F., Babcock, G. T., and Yocum, C. F. (1984b). FEBS Letters, **167**, 127-130.

Grann, T. (1986). FEBS Letters, **206**, 9-14.

Imaoka, A., Akabori, K., Yangi, M., Izumi, K., Toyoshima, Y., Kawamori, A., Nakayama, H., and Sato, J. (1986). Biochimica et Biophysica Acta, **848**, 201-211.

Joliot, P. (1966). Biochimica et Biophysica Acta, **126**, 587-590.

Kessissoglou, D. P., Kirk, M. L., Bender, C. A., Myoung, S. L., and Pecoraro, V. L. (1989). Chemical Communications, submitted.

Kok, B., Forbush, B., and McGloin, M. (1970). Photochemistry and Photobiology, **11**, 457-475.

Kretschmann, H., Dekker, J. .P., Saygin, O., and Witt, H. .T. (1987). Biochimica et Biophysica Acta, **932**, 358-361.

Lavergne, J. (1987). Biochimica et Biophysica Acta, **894**, 91-107.

Lavergne, J. (1986). Photochemistry and Photobiology, **43**, 311-317.

Mabad, B., Cassoux, P., Tuchagues, J.-P., Hwang, Y., and Henrickson, D. N. (1985). Journal of the American Chemical Society, **107**, 2801-2803.

Metz, J. G., Wong, J., and Bishop, N. I. (1980). FEBS Letters, **114**, 61-64.

Metz, J. G. and Seibert, M. (1984). Plant Physiology, **76**, 829-832.

Metz, J. G., Pakrasi, H. B., Seibert, M., and Arntzen, C. J. (1986). FEBS Letters. **205**, 269-274.

Miyao, M. and Murata, N. (1985). FEBS Letters, **180**, 303-308.

Miyao, M. and Murata, N. (1984a). FEBS Letters, **168**, 118-120.

Miyao, M. and Murata, N. (1984b). FEBS Letters, **170**, 350-354.

Miyao, M. and Murata, N. (1983). Biochimica Biophysica Acta, **725**, 87-93.

Ono, T. and Inoue, Y. (1987). FEBS Letters, **227**, 147-152.

Ono, T. and Inoue, Y. (1984). FEBS Letters, **168**, 281-286.

Ono, T., Zimmermann, J. L., Inoue, Y., and Rutherford, A. W. (1987). "Progress in Photosynthesis Research," Volume 1, 653-656 (Biggins, J., ed.), Martinus Nijhoff Publishers, Dordrecht, The Netherlands.

Renger, G. and Weiss, W. (1986). Biochimica et Biophysica Acta, **850**, 184-196.

Saygin, O. and Witt, H. T. (1985). Photobiochemistry and Photobiophysics, **10**, 71-82.

Shen, J.-R., Satoh, K., and Katoh, S. (1988). Biochimica et Biophysica Acta, 936, 386-394.

Velthuys, B. R. (1981). "Proceedings of the 5th International Photosynthesis Congress," Vol 2, "Photosynthesis II. Electron Transport and Photophosphorylation," 75-85, (Akoyunoglou, G., ed.), Balaban International Science Services, PA.

Vincent, J. B. and Christou, G. (1987). Inorganica Chimica Acta, 136, L41-L43.

Vincent, J. B. and Christou, G. (1986). FEBS Letters, 207, 250-252.

Waggoner, C. M. and Yocum, C. F. (1987). "Progress in Photosynthesis Research," Volume 1, (Biggins, J., ed.), 685-688, Martinus Nijhoff Publishers, Dordrecht, The Netherlands.

Yachandra, V. K., Guiles, R. D., McDermott, A., Cole, J. L., Britt, R. D., Dexheimer, S. L., Sauer, K., and Klein, M. P. (1987). Biochemistry, 26, 5974-5981.

Yachandra, V. K., Guiles, R. D., McDermott, A., Britt, R. D., Dexheimer, S. L., Sauer, K., and Klein, M. P. (1986a). Biochimica et Biophysica Acta, 850, 324-332.

Yachandra, V. K., Guiles, R. D., McDermott, A., Britt, R. D., Dexheimer, S. L., Sauer, K., and Klein, M. P. (1986b). Biochimica et Biophysica Acta, 850, 332-342.

APPENDIX A

Flash Absorption Spectrometer Computer Interface

A.1. Introduction

Note

This Appendix is a modification of the original documentation concerning the FASCI. As such the purpose of the document was to be instructive in the uses and capabilities of FASCI instead of justifying particular design considerations. Additionally, the reader will note that there are areas of overlapping coverage between this Appendix and Chapters 2 and 3, but in terms of technical detail this Appendix should be more complete.

FASCI is a computer interface package which interfaces a PDP-11/xx computer, operating under the RSX-11M/MPLUS operating system, to the Babcock Laboratory's Flash Absorption Spectrometer. This document is written to provide enough information to operate the spectrometer and take meaningful data. Some of the more conventional (i.e, commonly encountered) problems will be discussed. Hardware and/or software malfunctions are not covered, and the user is referred to the hardware schematics and Marty Rabb.

It is assumed that users of the FASCI spectrometer have a basic understanding of double beam and single beam absorbance spectroscopy and familiarity with the computer operating system. It is NOT necessary to be a programmer to use the interface; however, an understanding of the mathematical and graphical tools available is essential.

The interface package was designed, and the spectrometer built by Dwight Lillie of the Babcock Research Laboratory in partial fulfillment of the requirements for his doctoral project in photosynthesis in the Department of Chemistry at Michigan State University. All components built or designed at Michigan State were done so by Lillie unless stated otherwise. This documentation was written June, 1987 shortly before leaving M.S.U.

A.2. Overall description

The FASCI spectrometer consists of several component systems:

Optical,

Electronic, analogue,

Electronic, digital,

Electronic, timing,

Computer, hardware.

Computer, software,

A.2.1. Optical System

The stability of the optical system ultimately determines the resolution and reproducibility of the FAS. Current setup allows dO.D. of 0.0005 and 0.005 for simple changes and kinetic resolution respectively.

A.2.1.1. Probe light source.

This is a 75W Xenon Arc Lamp from Photon Technology with an optical feedback system. The optical feedback system uses a separate photodiode that receives its input from a fraction of the light generated by the Xenon Arc Lamp. A beam splitter is used to divert the output fraction into the photodiode. A current is

generated by the photodiode, it is amplified, and used in the feedback control of the lamp.

A.2.1.2. Iris.

This is a pin actuated, hand operated iris from Melles Griot and it is used to control the quantity of light reaching the entrance slits to the monochromator.

A.2.1.3. Electronic shutter and computer control.

This is a mechanical shutter from Uniblitz that is controlled electronically. The power supply and computer control for the shutter were designed at Michigan State and it can be operated either manually or automatically from a computer.

A.2.1.4. UV-VIS monochromator.

The monochromater is an Instrument SA H-20, with fixed interchangeable slits of 0.5, 1.0, and 2.0mm giving an optical bandwidth of 2.0, 4.0, and 8.0nm respectively. Two ion-etched concave holographic gratings for the UV and near-IR, as well as a normal concave holographic grating for the UV-VIS region.

A.2.1.5. Quartz focusing optics.

These optics are used within the sample compartment (next item) to focus the probe light emerging from the monochromater through the sample cell and onto the Photomultiplier Tube.

A.2.1.6. Sample Compartment.

The sample compartment was built by the machine shop of the Chemistry Department at Michigan State University. It serves a structural role in that it holds the monochromater, the sample cell(s), and the detector at fixed distances. It also serves to protect the sample cell from ambient light while a sample may be equilibrating before an experiment.

A.2.1.7 Optical Filter holder.

A filter holder was constructed by the machine shop to protect the detector against the light caused by the laser during sample excitation. It was designed for space minimization between sample cell location and PMT and can easily accomodate more than one filter to be held with thin plastic spacers between each. It was also built with mounting slots for a mechanical shutter (next item).

A.2.1.8. Mechanical shutter.

The mechanical shutter fits between PMT mounting and the sample compartment for blocking light from PMT entrance while allowing the sample compartment to be exposed to light.

A.S.1.9. Photodetector Unit.

This unit consists of a housing for a detector, a mounting platform inside the housing for the detector, and the detector itself. The housing is bolted on the sample compartment behind the sample cell so that its surface is flush with the plate it is mounted onto. Two types of detectors are supported, one is an EMI 9558-QB photomultiplier tube and the other other is an EG&G FND-100 photodiode. The photomultiplier tube is used for work from 250 to ~700 nm and

the photodiode is to be used from 700 to ~900 nm. Each detector has its own mounting platform because the requirements differ for each.

A.2.2. Electronics, analogue

The analogue electronic system interfaces with the optical system at the PMT, and processes the analog signal from the PMT into a form suitable for the Analog-to-Digital converters (ADC). The various components involved are:

A.2.2.1. Detector Amplification Circuits.

The photodiode produces current that is converted to voltage by using a resistor. An op-amp (Burr Brown 3551) is used to match impedances and to send the signal through 6" of cable to reach the PMT post-amplifiers. The EMI 9558-QB requires a divider chain to take advanatage of the secondary photo-electron multiplication effect. The divider chain determines the maximum allowable current (up to the limit of the PMT itself) that can be extracted from the dynodes. The current available in the divider chain must be maintained at levels greater than 20 times that of the maximum current drawn from the dynodes via secondary electron emission. On the other hand, too high of a current flow will increase the temperature of the resistors and wires that make up the divider chain. This heat increase will increase the temperature of the dynodes, thereby lowering the potential required for secondary emission and a noiser and less predictable output will ensue.

A.2.2.2. Photodector Post Amplifiers.

This is a two-amplifier (Burr Brown 3551, 50Mhz GBP) package we designed that is arranged in a current-follower with an inverting amplifier

configuration. A current offset control allows a balance current to adjust the output around the zero crossing threshold.

A.2.2.3. Signal Amplifier.

The signal amplifier serves three functions: it provides a fixed and user adjustable signal amplification, it provides a user adjustable time-constant, and it provides two signal outputs. The two signal outputs contain the original signal, possibly amplified, and the original signal with the D.C. component(s) subtracted out.

A.2.2.4. 3 Fourth-order Active filters.

A set of fourth-order active filters were constructed and used to process the analog signal between the amplifiers and the ADC. These were used because the frequency cut off point is considerably sharper than with simple passive or active first order filters. These are adjusted to provide minimal filtering s that no digital sampling is performed on the analog signal containing frequencies higher than the nyquist frequency.

A.2.2.5. ADC pre-amplifiers.

The ADCs each have a pre-amplifier that adjusts the incoming analog signal so that the digitizing window is filled. The pre-amplifier for the slow ADC usually has a unit gain because the background signal has already been adjusted to give ~10 V.

A.2.3. Electronic, digital

The digital electronic component system provides an interface to the analog electronic system via the two ADCs, and provides an interface to the

computer hardware. It effectively includes the digital transmission, handshaking, and other required components. The component list:

A.2.3.1. Analog to Digital Converter and Storage.

This system consists of the electronics necessary to convert, store, and retrieve an analogue signal. The analogue signal is presumed to have already been split into two signals: a D.C. offset analogue signal that contains the transient information, and the unprocessed analogue signal for baseline information.

Two converters are used:

FAST/ULTRA-FAST Converter (FADC)

SLOW Converter (SADC)

The FADC converter is used to sample the D.C. offset analog signal after having been amplified by the ADC preamp for collection of the transient signal. The SADC converter is used to sample the non-offset analog signal for collection of the baseline. Each converter is connected to 1024 bytes of 8 bit memory. Additional circuitry exists to initialize and sequentially read out of memory upon activation of data request lines.

A.2.3.2. Signal Transmission via parallel cable.

Sixteen bits of data, 8 bits for the FADC, 8 bits for the SADC, and 2 bits for handshaking are sent along 32 conductor parallel cable. Properly, the number of conductors in the cable should be double the number of signal lines so that every other conductor would be ground. This would minimize groundtalk between the communication lines; unfortunately, not enough 40 conductor cable was readily available so the convention of every other conductor being ground

was violated for the 2 bits of handshaking. Generation of these signals are handled by the ADC.

A.2.3.3. Signal Reception.

This component set comprises those electronics responsible for shaping transmission information into a suitable form for transmission through many meters of media, the transmission documentation, and reception of the data.

A.2.3.4. Computer handshaking.

This set provides signal transformation of the handshaking generated by the ADC into what is appropriate for the parallel board used by the DEC 11/xx computer. In the current case a DRV-11J, a simple input/output parallel port board, is used.

A.2.4. Electronics, Timing

This system consists of TTL pulses generated by the computer and sent out to the appropriate device. All devices under computer control are controlled via simple pulses. Generally, while there may be one or more pulses used to control function there is at least one pulse which forces a device to 'clear,' i.e., return to default state. The appropriate components are given below in the following sections.

A.2.5. Codar Timing Board.

This board generates up to 16 pulses, each of which, except for the first, is triggered to begin a delay countdown by the 'firing' of the previous pulse. Each countdown is 16 bits, and programmable over the range of 250 ns to 16 s.

A.2.6. Pulse Enable.

This is a programmable mask for the timing pulses. The timing board has no provision for software selection of enabled output lines when the timers are wired in a cascade configuration. The addition of a separate set of enable lines allows a Boolean 'mask' to be created via software that fulfills this need. The output port of a DRV-11J is used.

A.2.7. Signal Transmission.

Signal Transmission occurs via a 32 conductor cable. Unlike the earlier situation, the convention of every other conductor being a ground is followed.

A.2.7.1. Signal Reception and distribution.

This system handles appropriate line termination and distribution of the signals to a panel with 15 BNC connectors. Every device to be controlled in this manner requires a 120 ohm resistor to properly terminate the input signal line.

A.2.8. Computer, hardware

The computer uses the hardware discussed in the following sections.

A.2.7.2. Codar Timing Board.

See the previous section for a discussion of this.

A.2.7.3. Parallel Port.

The output pulses emitted when a timer is finished are required to trigger the next timer in the sequence, but the pulses need to be disabled from being sent to the final output devices. The parallel port, a DRV-11J, is used to provide

16 parallel lines for masking the timers' output. See the previous section on 'pulse enable.'

A.3. Miscellaneous Hardware

A video display terminal is needed for user interaction. A video display terminal, either the one used for user interaction or another separate one, is required for graphics display. Synchronous data plotting requires either a Hewlett- Packard plotter or a dot matrix printer capable of raster graphics. If the plotting is to be done while unattended then a dot matrix printer iks suggested. This situation will occur frequently when a continuous set of experiments are being performed. At the completion of one experiment, the data plotting for the experiment can be initiated, and the user can then begin another experiment without having to wait for the completion of the plotting.

Storage of collected data requires some form of storage that is mounted and accessible. The preferred device is a fast, hard disk, but also acceptable devices include mag tape or another computer system accessible over an ETHERNET. The problem with the last two as the principal storage device is access time - especially in the middle of an experiment.

A.4. Computer software

Two primary tasks are responsible for working together to use all of the other systems in a useful manner. Other support tasks also exist to provide additional functions such as ADC calibration, data massaging, graphics, etc.

The two primary tasks are divided into a user interface and a instrument interface, and communicate with each other through a well defined software interface. While more detail will occur later; it is enough to mention here that the instrument interface is not dependent upon the user interface per-se. Another

task(s) could interface to it following the correct protocol and thus allow the experiment to take on new functionalities. High level access has been provided on the user interface end so that construction of a new user interface should not be too onerous of an undertaking.

Original documentation and design specifications referenced a third task, the Graphics Display Processor (GDP). It still exists and can be used but because of its drain on system resources it is not routinely used and the current software will require a recompilation with the support for the GDP turned on. For the lifetime of this project the functionality provided by the Nicolet 1074 and its display oscilloscpoe should serve adequately.

The next section will be wholly concerned with what's required to conduct an experiment. The various screens the user is presented with during the course of execution will be examined. The following section will then discuss some of the software design philosophies that were employed. The last section will discuss building the various tasks.

A.4.1. Preliminary - some requirements before starting.

The two tasks responsible are known as 'UPLODR.TSK' and 'FAS.TSK.' Both UPLODR.TSK and FAS.TSK are privileged. UPLODR.TSK must be installed (default task name is assumed), and a recommended priority of no lower than 140 (out of 255) is recommended. FAS.TSK doesn't have to be installed, but if it's not installed then the user must be a privileged user in order to activate it. Currently, UPLODR.TSK is installed at boot time from LB1:[1,54] via the GTBINS.CMD file which is run by STARTUP.CMD. A flying install is done on FAS.TSK, located in LB1:[1,54], via CCL. The necessary command is located in LB:[1,5]SYSCCL.CCL, and is typically activated by typing 'FASCI.'

It is a good idea for the user to be privileged because if a problem develops and the software doesn't synchronize or falls out of synchronization then a lockup could occur. If a lockup occurs then no other tasks can be loaded, KILL will not be able to run (unless its priority at install time is raised above UPLODR's), and a privileged user would have to come in and ABOrt UPLODR and/or FAS.

A file, FASCALIB.FIL;1, MUST BE AND IS EXPECTED TO BE located in LB:[1,1]. This file contains calibration information about the ADCs, if the file is not there then it will have to be regenerated by the program ADCCAL.TSK.

A.4.2. Starting

If all of the above is correct, and it should be, then the interface is activated, as mentioned above, by typing 'FASCI.' The screen should clear (if the terminal is either a VT100 or a VT52 and the type is set correctly), a message that UPLODR is running should appear, and a series of lines validating that dynamic memory buffers were successfully created and read and write access has been guaranteed. The screen should again be cleared off, a menu written, and a prompt of the form 'FASCI > ' on the left side of the screen roughly 2/3 of the way down.

a) Failure to Start

If only a part of this sequence has occurred and then stopped; wait for roughly ten seconds. If nothing else has still happened, one can assume the software de-synchronized and a lockup may have occurred. Abort the tasks in the order: UPLODR first and then FAS.

A.4.3. Execution

Continuing to describe an experiment in this serial fashion becomes not only difficult but confusing as well. As can be seen in the next section there are several options the user should specify to define the experiment. User can choose them in the order and manner desired; some of the option ranges depend on values already chosen for other selections.

Therefore, each of the option will be discussed in turn. Meaning of the option descriptor, invocation of the option, other dependencies, etc. will be discussed for each where appropriate. It shall be left to the user to determine what needs to be specified and the order in which they are specified.

A.4.4. Execution Screen Display

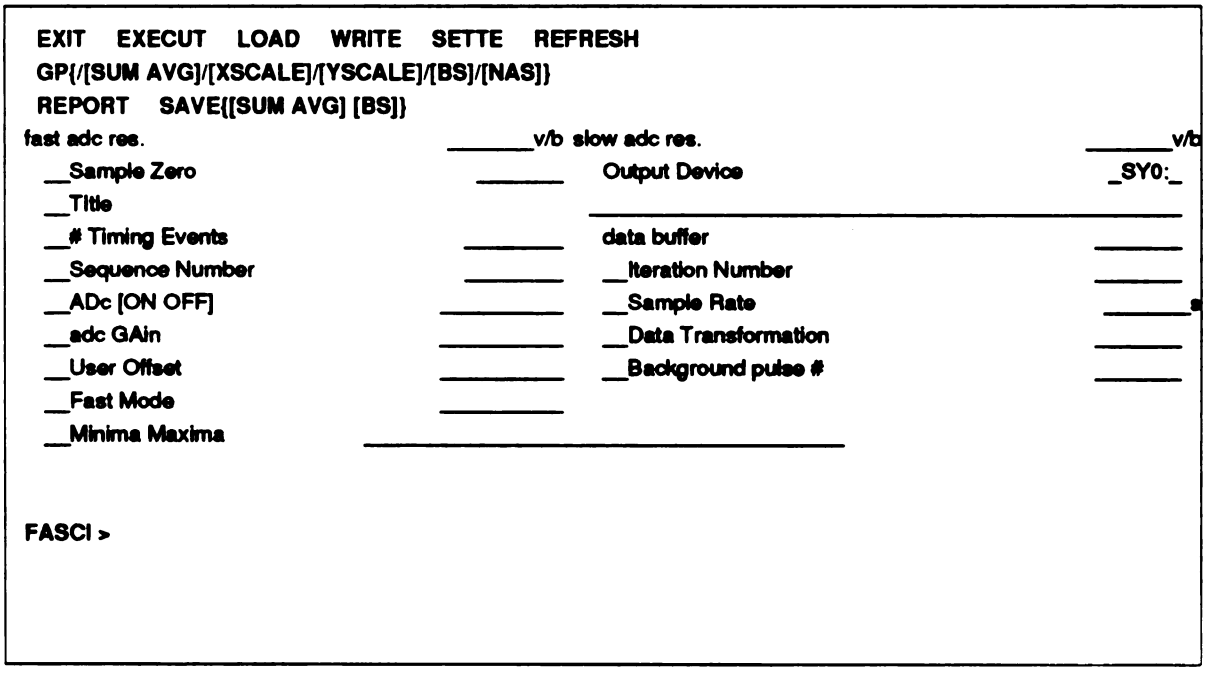

A.4.4.1. Execution Screen Display General Description

The above is a reasonable facsimile to the primary execution screen that user deals with most of the time. The first three lines of words are 'executable' commands. Each executable command is separated from another by several

spaces. Some of the commands have options that can be attached as well, these are shown as being options by the braces, {...}. Valid options are the words within the braces. In some cases one option selection may exclude another option selection, and these are then grouped inside of the brackets, [...]. An example above is the SAVE command. The data can be saved in an averaged, AVG, mode, or in a summed, SUM, mode. These two selections are obviously (to me anyways) exclusive and grouped within the same bracket. Unfortunately, not a terribly great amount of attention was paid to remaining syntactically similar; hence, GP (Go Plot) options are delimited by a slash, and SAVE options are delimited by spaces.

The two columns contain a field descriptor, field space, and often something written in the field space. In cases, where the field descriptor also doubles as a command (these commands are known as 'configuration commands'), the command will consist of a two character tag. The two characters are known by the letters in caps in a descriptor. Thus, the command for '# Timing Events' is TE<cr>. The command for 'Data Transformation' is DT<cr>.

Additional information needed will be prompted for. In some cases (pointed out below) the command expects its argument on the line of the two character tag.

A.4.4.2. Execution Screen Display Configuration Commands

fast adc resolution. *This is not a settable option.*

This is a value that reflects the resolution in terms of bits per volts (b/v) for the fast adc. This value is modified when the adc GAin selection is modified.

slow adc resolution. *This is not a settable option.*

This is a value that reflects the resolution in terms of bits per volts (b/v) for the slow adc. As the slow adc has only one gain, this value is not usually modified during execution of FAS.

SZ - Sample Zero. *This is a settable option.*

This allows definitions of what raw data point constitutes a 'time zero.' The FADC collects 1023 points. If the conversion rate is 1Mhz, 1 point per 1 micro-second (*us*), and the exciting flash is generated 200 *us* after the FADC begins converting then the 'time zero' is 200. If the conversion rate is 1Mhz, 1 points per 2 *us*, the 'time zero' is still 200. The number for the Sample Zero refers to the raw data point.

OD - Output Device. *This is a settable option.*

This allows definition of the physical definition the data is written to when saved. Unfortunately, when the file is closed, the lun associated becomes reassigned to SY0:, and this option needs to be reselected each time.

TI - Title. *This is a settable option.*

This allows user to select a title to be associated with plots that are generated, or data files that are saved.

TE - # Timing Events. *This is a settable option.*

This allows definitions of the number of events that controlled by FASCI. If the sequence of events follows something like:

Open Shutter

Trigger, FADC

Trigger, laser

Close Shutter

Then there are only 4 timing events.

Data Buffer. *This is a settable option.*

This allows user to 'turn off' the storage data buffer which is used to dynamically store processed data. When a scan is being iterated, for the particular sequence being executed, data is read out of the buffer, added to the data just collected, and written back to the buffer. This data buffer is created anew at the beginning of each EXECUT command, and is sized to be no larger than the number of sequences in the current scan. Optionally turning off the data buffer allows memory to be conserved if needed.

SN - Sequence Number. *This is a settable option.*

This defines number of sequences in an iteration cycle. This option must be set BEFORE the timing pulses are configured.

A sequence is the group of pulses defined to be generated when an experiment is running. If one is looking at steady state flash turn over experiments then only 1 sequence is required. If one is looking at a four flash oscillation, and wants an additional four flashes to confirm an oscillatory pattern then a total of 8 flashes are to be generated before beginning to loop around and continue averaging. 8 sequences are thus to be chosen for sequence number.

IN - Iteration Number. *This is a settable option.*

This allows definition of the number of times a sequence group will be iterated.

SD - Sequence Delay. *This is a settable option.*

This defines the amount of time (in units of integer seconds) which elapses between any two sequences when the number of sequences are greater than one. If there is only one sequence number then the sequence delay should be set to the iteration delay value.

Time range is from 3 to 16000 s when Fast Mode is DISABLED. When Fast Mode is ENABLED then the time range is from 1 to 16000 s; however, there

are some qualifications. Total number of sequences cannot exceed 8; see the description on Fast Mode for more details.

Chosing delay times between sequences is usually no problem for lower time delays of 5 s or greater. Between 3 and 5, though, care must be taken in the configuration of the timing pulses, consideration must be given to the number of users logged on, etc. Remember that after every sequence 1023 points must be converted from raw 8 bit binary values to 32 bit floating point numbers in either transmission or absorption format. Choosing too short of a value is usually manifested by 'TIMING or DATA OVERRUN' error type messages. Meaning that not enough time is available for processing before more data becomes available.

ID - Iteration Delay. *This is a settable option.*

This defines the amount of time (in units of integer seconds) which elapses between any two sequences when the number of iterations are grater than one.

Time range is from 3 to 16000 s.

AD - ADc [ON OFF]. *This is a settable option.*

This is an obsolete option and is disabled.

DT - Data Transformation. *This is a settable option.*

This allows user to define how the data is processed. More detail is given in the next section; though, it is briefly described here. Data can be transformed into Raw Transmission (summed or averaged Volts) or into Relative Absorbance (summed or averaged). Raw transmission simply involves converting the 8 bit binary value into a voltage. Relative absorbance, though, requires baseline information.

Prompts will appear for the following types of information:

Raw or Transmission

Sample and Hold Active (SHA) or Not

If SHA is active then get baseline duration (in raw units of points)

Data zeroed or not.

The SHA is used to lock a baseline for sampling. The baseline information is usually from when the conversion is started to just before the laser goes off. The length of time is given in raw sample points.

UO - User Offset. *This is a settable option.*

This allows user to define the amount (volts) the baseline has been offset from 0.0v. This is useful to provide more of a dynamic range, and enhanced signal-to-noise. If a background voltage (related linearly with voltage) is 10, and dV is expected to be 0.01; then, if the background voltage is 20, the dV will be 0.02. This results in a doubling of the signal fed to the FADC.

BK - BacKground pulse #. *This is a settable option.*

This allows user to specify that the first sequence (implies that Sequence Number is already set and is in the range [1,31]) is a 'background.' Prompt for the pulse # which turns on the excitation. On the first sequence of each iteration that pulse will be prevented, and the data recorded will be considered a background.

Specifying this option increases the number of sequences by one, and is indicated in the Sequence Number field by a '(+)' at the end of the field. This cannot be set if Sequence Number was not already defined, or the 32 sequences were already defined.

All data structures which are manipulated by the user, whether it be the dynamic data holding the last scan or the saved file, will have one more field than

originally specified. In place of the first sequence's y-axis data will be the background.

FM - Fast Mode. *This is a settable option.*

This allows user to specify a shorter sequence delay than 3 s for a limited number of sequences. Minimum time is now 1 s, and still in units of integer seconds. Achievement of this short of a time delay is by delaying data processing until all sequences in an iteration are completed. This means that the Iteration Delay time has to be increased enough to handle the additional time required for processing.

A.4.4.3. Execution Screen Display Executable Commands

These commands actually cause something to happen. This something can be anything from running a scan, to plotting the data, to saving it, to spawning off a command to the system, etc.

]EXIT. I would think this does the obvious - shuts down the interface.

EXECUT. This begins the scan. Some potential error conditions are caught and this command is aborted; sometimes not, though.

LOAD. Complement of the WRITE option. Allows user to load in a saved configuration command file. Not all of the variables from the previous configuration are saved. More than one configuration file can exist.

WRITE. Complement of the LOAD option. This allows user to save most of the current configuration in a file of choice. The first real data sequence, thus, is #2. If user wants to plot the second sequence then #2 has to be specified. User can write more than one configuration.

SETTE. This command causes entry into another menu which allows user to define the configuration used for the timing pulses. See below, "Configuration Display Screen for Timing Pulse Generation."

REFRESH. This command refreshes the screen display; occasionally things get a bit cluttered and/or out of place.

GP. Allows user to generate plots of up to six sequences at a time from the previous scan. Graphic devices supported are usually some subset of the MULPLT devices, and can be determined in a like fashion by typing:

GP? <cr>

This command results in the graphic devices supported, the referent number of the graphic device, and the internal number of the graphics device to be printed. Supposing that graphic device #1 was a tektronix graphics terminal and that sequences 1,2,4, and 32 were to be plotted on this graphic device then the following sequence would be entered:

GP1,1,2,4,32 <cr>

The first '1' is the graphic device number, and the following 4 numbers are the sequences to be plotted. Additional options, in the form of switches, may also be specified. As mentioned previously, options specified within a pair of "[...]" are mutually exclusive, and non-exclusive options are delimited from one another by "/." The examples below are given in the form:

GP{/...}/OPTIONn,m <cr>

or

GP{/...}/OPTION n,m <cr>

The "...{/...}..." refers to other options that may or not be present on the command line. .../OPTION"... is the option being explained. Order of occurrence in the command line is NOT significant.[1]

---

[1]the main difference in the two examples (above) is the separation of the device and sequence(s) specifications from the body of the command switches. In the case of where a switch will end with a numeric value it would be difficult (impossible) to separate out the end of the switch's numeric value from the beginning of the device number.

[SUM AVG]

GP{/...}/AVG1,2 - plot the average of sequence *2* on device *1*.

[XSCALE]

GP{/...}/XSCALE:rrr 1,2 - plot the sequence *2* on device *1*, and scale the x-axis by *rrr*.

[YSCALE]

GP{/...}/YSCALE:rrr 1,2,30 - plot the sequences *2* and *30* on device *1*, and scale the y-axis by *rrr*.

[BS] [2]

GP{/...}/BS n,m - plot the sequences *2*

If "GP?" is typed, the binary file option shows up, but choosing this result causes the resulting graphics file to be processed in a special way.

SAVE. Allows user to save the results from the last scan. Again options are available in a switch selectable form. When a scan is saved all of the sequences in the last scan is saved, and, unlike other options where the user can specify the input/output file names, the name for the saved scan file is determined by FAS.

Often when data files from an instrument are saved the user will come up with unique names like:

FOO1.DAT

FOO2.DAT

FOO3.DAT

and the names may or may not be relevant to the scan(s) completed. FAS automatically generates a name based on the date and the elapsed time after

---

[2]Only valid if BacKground pulse # was given.

midnight. This name, therefore, is unique (for a year at any rate), and cannot be confused with another "FOOx.DAT"-type of filename. The naming and internal structure of the saved data files are discussed in a later section.

The available switches are:

[SUM AVG]

SAVE/AVG - data in the sequences are saved in an AVERAGED mode. This is the default.

[BS]

SAVE/BS - sequences in the saved data file have the base-line (as contained in sequence 1) subtracted. The default is NOT BS.

REPORT. This command causes the results of the last scan to be printed on the terminal.
.page

A.4.4.4. Configuration Display Screen for Timing Pulse Generation

A screen for displaying the timing pulse configuration is brought up when the user specified "SETTE."

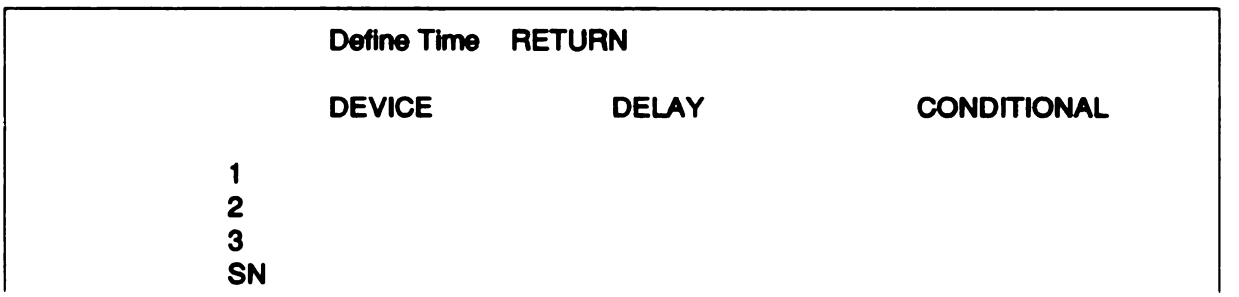

Only two commands exist for this screen (it is entirely possible that the top line does not agree with what comes up in FAS, if that's so then what's said here overrides what the program has displayed!).

A.4.4.5. DT - Define Time

Allows user to define the timing parameters for a single pulse. A prompt will come back after

DT<cr>

prompt:

Pulse #, Name, Time(s,m,u),{c_enable, beg, inc)

This is asking for the above elements to be given in a single line.

Pulse # - just the pulse being defined. Number cannot be any higher than # of timing events defined in previous screen.

Name - allows user to associate a name with the pulse, like "laser", "shutter", "die",..

Time (s,m,u) - specifies the elapsed time (real number) and the units of the number before the pulse is triggered. A time of 1.0s would cause a delay of 1 second before the pulse is triggered. A time of 12.5u would cause a delay of 12.5*u*s. And a time of 0.01m would cause a delay of 0.01 milliseconds. The screen display is updated after every DT command, and sometimes the value entered is changed. 0.01m would be (probably) modified to be 10.0u. The minimum time allowable is 0.25u (250ns), and the maximum is 16.0s (16s).

{c_enable beg,inc} - this is optional. Allows user to specify a "conditional pulse." Normal pulses are fired every sequence and every iteration. Conditional pulses can have their start time and sequence increment fired every time. A command

DT1,SILLY,1.0U,CE_5,6

would cause pulse # 1 to be fired conditionally; first occurrence of the pulse would be the 5th sequence of each iteration, and the next

occurrence would be after 6 sequences had elapsed (the 12th). A command

DT10,SILLY,5.S,CE,1,1

would cause pulse #10 to be triggered on the first sequence of each iteration, wait a sequence, and fire on the 3rd, wait, fire on the fourth, etc.

A.5. ERRORS AND SUGGESTED RECOVERY METHODS

A.5.1. Failure to start UPLODR fully

A.5.1.1. Aborting UPLODR and/or FAS.

The MCR command only allows abortions of NAMED tasks. If FAS was invoked on user's terminal, call it TT5:, by the user typing 'RUN LB1:[1,54]FAS' then FAS's running name is 'TT5.' If run via CCL then its running name is 'FAST5.' The appropriate abort commands would be, in order, 'ABORT TT5' and 'ABORT FAST5.' UPLODR is installed under the name UPLODR, and can then be aborted via the same name. This is not a trivial point. KILL.TSK, unless installed at a higher priority than UPLODR's (nominally 140 or 150) will not be able to get in a 'kill' these errant processes!!).

A.5.1.2. Other Cases

Otherwise Normal Error Messages result in unexplainable looping. This behaviour prevents graceful recovery. Some errors can be detected, and the software does recover somewhat gracefully with appropriate error messages.

A.5.2.. Interface at computer end not powered up.

UPLODR detects this, generates an error message that informs the user this possibility should be checked out, and exits. Once the condition is remedied (i.e, the power turned on), the user should make sure neither task is active from the terminal, and attempt to restart.

If power was already on, then either power routing on the board(s) on the panel has failed, a chip has gone down, or something similar. UPLODR generates this message when it is unable to clear the DRV-11J input port, so the interrupt generation circuitry should be checked out first.

A.6. DATA TRANSFORMATION

This is only included because it is important to understand how data is transformed from 8-bit binary numbers relating to digitized voltage coming out of the back end of a PMT to difference absorbance values.

Until recently, researchers typically reported optical changes in units of

$$dA \sim\sim dI/I \sim dV/V$$

where I is the original light intensity upon the PMT face which is equivalent to the voltage generated, V. dI is the small change of light intensity induced by the photochemistry resulting from 9excitation, and this is also equivalent to dV, the change in voltage coming out the PMT. dA is the change in absorbance.

Formally, though:

$$dA = \log ((Voff + dV)/Voff)$$

where Voff is the voltage detected BEFORE excitation, and dV is the change of voltage detected from Voff.

The thinking has been that as dV/V is so small, 10^{-3}, that it's roughly equivalent to dA. If treatment of the data warrants this, then a potentially complicated problem becomes tractable. When signals are small, as they are in photosynthesis, it is necessary to average many scans, and the equations look like:

$$dA\ (avg) = dA(tot)/N = SUM[dA(i)]/N$$
$$= SUM[log((Voff(i)+dV(i))/Voff(i))]/N$$

where dA(avg) is the total absorption change averaged over N scans. dA(i) is the absorption change of the ith scan. SUM[...] represents the summation sign over the quantity in "[]." Voff(i) is the offset voltage for the ith scan, dV(i) is the small voltage for the ith scan.

The above, however, is difficult to do in real-time, and requires two channels over which data is collected. If the approximation :

$$dA(avg) \sim (SUM[dV(i)]/Voff(avg))/N$$

can be employed then Voff may be read off from a voltmeter at the beginning and end of the scan, averaged, and used in the above equation. This is simple, and only requires one data channel the computer has to worry about in real-time.

If the basic approximation, instead of being:

$$dA \sim dV(i)/Voff$$

were

$$dA \sim dV/Voff - 1.0$$

the results would then be within the correct order of magnitude, and for small (10^{-3}) changes or smaller, within experimental error. the results would have an error of 10^{-4}.

FASCI has two data channels available and can perform the full blown calculation; however, tests run with the 11/23 (the processor FASCI was developed on) show that the intrinsic log function ran 10 times slower than an equivalent Taylor series expansion which was accurate to 10^{-5}. The same performance ratio holds true for the 11/73 processor, though the latter is so much faster the intrinsic log function could be put back in. A test case for this is given in LOGTST1.FTN.

A.7. STRUCTURE OF THE SAVED DATA FILES

This section discusses the philosophy behind the name used for the data files, and the structure by which they're written to disk.

A.7.1. Data File Names

As mentioned earlier, saved scan sets are given semi-unique names (unique till the following year at any rate). These names are constructed from the data and the time after midnight. An extension of ".FDF" (Flash Data File) is added to further identify the file uniquely as being constructed from FASCI.

Within each data file is a header (see below), and in the header is a SCANID field. This SCANID contains the first 9 characters of the filename and provides a degree of association in that fashion.

Plots which are directed to the line-printer are generated so that a SCANID is written out on the plot itself, and also on the accompanying parameter file.

In this fashion data files which are generated (both internally in the header and externally in the name itself), plots which are also derived from the same data set by FASCI, and the parameter files which are written out are associated fairly uniquely, i.e., chance for replication until the following year is slim.

A.7.2. Structure of the Data File.

The data file has two parts :

Header, 'PL' data tag

DATA, 'RD' data tag

As can be guessed by now, this file is in the binary MULPLT format. The header contains information relating to the date and time of the scan, SCANID, title of the scan (if one was given), configuration of the scan, timing configuration, number of iterations and sequences, etc. Additionally, and quite important, information relating as to how the data was saved (summed or averaged, base-line zeroed or not, background subtraction) is also present and can be pulled out to be examined.

The data field consists of the data tag, the x-value (in micro-seconds), and then all of the sequences. If being plotted by MULPLT later, the format command to access the x data and the first sequence would be :

FM#1,2

To access the x data and the 3rd sequence (if at least that many sequences were specified):

FM#1,4

If a background subtraction was performed, then the first sequence data (#2) is the background shot. The first sequence of data containing the kinetic data would be #3.

A.8.3. Examination of the data file directly

Provisions have been made to examine separately the header. BINDMP.TSK (made up from BINDMP.FTN and BINDMP.CMD, there may be additional files associated) will dump out the header of the saved scan file (it will also work with data files collected by PERKIN).

A.8. GRAPHICS DEVICE 0 SELECTION

FASCI has been designed to take advantage of both 1) the RASTER processing feature (from the MULPLT package), and 2) the batch environment of RSX-1MPLUS to facilitate generation of graphics-hard copy while not interrupting real-time experiments.

It is possible to run an experiment, save the data, send a graphics image to a file, and continue running another experiment immediately. Meanwhile, a batch job will have been started running at low priority which will reproduce the plot on the printer specified, print the parameter file, delete the graphics file (fairly large) and the parameter file (not large, but it gets to be annoying to have a lot of them around).

This is all done by selecting "GP0,..." in the Go Plot command. Syntax for specifying the sequences to be plotted are identical to the other GP commands.

A.8.1. Method

Getting this accomplished is simple. Buried somewhere in FASCI is a subroutine that gets called. This subroutine executes the command file "RASQUE.CMD." RASQUE.CMD builds a batch file, "RASTER.BAT" that, after successfully built, will be submitted to BAP0 (the batch processor for RSX-11M+). When the batch job, controlled by RASTER.BAT, is completed, the result

of the job is written to a file RASTER.LOG. Unfortunately, LOTS of these will acrue in user's area unless periodically purged.

Several files either have to be present in the user's area, or are generated by RASQUE.CMD and/or RASTER.BAT (depending on version of RASQUE.CMD). These files are:

ALLP.CMD - command file which runs under the indirect command processor at low priority. It's purpose is to allocated the printer to the batch job. This is to keep other print jobs from intervening between the plot and the parameter file.

DEALLP.CMD - command file which deallocates the printer.

SEPARATE.TXT - a file which contains a line of '*' to separate one plotting set (defined by a plot and its parameter printout) from another.

FORMFEED.TXT - a file which contains the <FF> character to force a formfeed.